NTNU – Trondheim
Norwegian University of
Science and Technology

An under-excavation model for The Leaning Tower of Pisa

Maria Kristiansen

Civil and Environmental Engineering
Submission date: June 2012
Supervisor: Thomas Benz, BAT

Norwegian University of Science and Technology
Department of Civil and Transport Engineering

NORWEGIAN UNIVERSITY OF SCIENCE AND TECHNOLOGY
DEPARTMENT OF CIVIL AND TRANSPORT ENGINEERING

Report Title: An under-excavation model for the Leaning Tower of Pisa	Date: 10.06.2012 Number of pages (incl.): 102			
	Master	X	Project	
Name: Maria Kristiansen				
Professor in charge/supervisor: Tomas Benz				
Other external professional contacts/supervisors: Martino Leoni				

Abstract:

The Leaning Tower of Pisa is a complex case and has due to its nature been analyzed for decades through both manual and numerical testing. Resent FEM analyses have still not succeeded in modeling all of the stabilizing measures that have been performed on the Tower foundation and are important in relation to the numerical recreation of the measured Tower deformation. One of these is the under-excavation procedure and a new approach to this procedure has been created and modeled in simplified FEM analyses. The new method is implemented in the constitutive Anisotropic Creep Model and has been tested and optimized to make it applicable in a full 3D model of the Tower.

Testing performed has shown to be especially sensitive to the choice of mesh refinement, and also to the chosen tube size and in order to obtain accurate extraction values a finer mesh must be used or tube measures must be increased. The new under-excavation procedure has so far not been implemented in the full 3D model of the Tower. This model is complex and thus time demanding and is so far using the internal Soft Soil Model in PLAXIS.

Keywords

1. numerical analysis
2. volume strain
3. mesh refinement
4. soft soil creep method (SSCM)

NTNU
Faculty of Engineering Science
and Technology
Department of Civil
and Transport Engineering

MASTER THESIS

(TBA4900 Geotechnical Engineering, Master Thesis)

Spring 2012
for
Maria Kristiansen

An underexcavation model for the Leaning Tower of Pisa

BACKGROUND

Pisa's landmark, the Leaning Tower of Pisa was re-opened for public in 2001 after its foundation was stabilized using various measures including the method of underexcavation: Some 40 extraction holes were drilled below the tower. The method of underexcavation is currently believed to have majorly contributed to the current apparently stable situation. Different prognoses for future development exist, ranging from a permanent stable situation to scenarios where the evolution of the leaning instability may only have been retarded for a few years.
Numerical models are frequently applied to gather a thorough understanding of the tower's past behaviour and also give a prognosis for future developments. Numerical models of the Leaning Tower of Pisa, however, face a number of challenges which - if not tackled adequately - may lead to biased quantitative results. Besides the constituted material behaviour, a major challenge is the consideration of all stabilization measures over time. The underexcavation, for example, is conducted in a soil layer that settled some 3 meters in history. In a classical FEM analysis, the underexcavation can therefore hardly be defined in the reference configuration. This problem has never been adequately addressed before.

TASK DESCRIPTION

The aim of the thesis is to implement and test a new approach to model the underexcavation of the Leaning Tower of Pisa in a classical large strain FEM analysis. The underexcavtion shall be modelled through a dedicated material model that applies volume strains in the location of the extraction tubes. The dedicated material model shall be based on a time dependent creep model that was previously demonstrated to give reasonable results in back calculating the Leaning Tower of Pisa problem. Before applied to the boundary value problem, the model shall be thoroughly tested and evaluated.

The objectives of the thesis are defined as follows:

1. To summarize the history of the Leaning Tower of Pisa
2. To summarize the underexcavation process
3. To implement/ enhance a constitutive model that can be used to model the underexcavation.
4. To validate the implementation in FEM
5. To indicate requirements for the use of the model
6. To perform a full 3D analysis of the Leaning Tower of Pisa
7. To conclude on the calculation results

It is acknowledged that the given task is a research driven task and that due to unforeseen computational costs and issues not all objectives may be fulfilled in the given timeframe.

Professor in charge: Prof. Thomas Benz

Department of Civil and Transport Engineering, NTNU

Date: 06.06.2012

Professor in charge

Preface

This thesis is written in connection with the completion of my Master's degree in Civil and Environmental Engineering, at the Norwegian University of Science. The content is intended for readers with basic geotechnical background and whom are familiar with numerical analysis.

The reason why this topic was chosen was that I wanted to work on numerical analyses, and what could be better than to get the chance to work on a complex task such as the Leaning Tower of Pisa. It has been an educational and exciting process though also a test of patience as time has been a persistent dilemma. Had I not had good guidance along the way time could have become an even greater issue. I would therefore like to thank my teaching supervisor Tomas Benz for providing me with support throughout this process and for having given me the opportunity to work on his idea. I would also like to thank my Italian teaching supervisor, Martino Leoni for giving me an important introduction to the subject and for his cooperation throughout the working period.

Abstract

The Leaning Tower of Pisa is a complex case and has due to its nature been analyzed for decades through both manual and numerical testing. Resent FEM analyses have still not succeeded in modeling all of the stabilizing measures that have been performed on the Tower foundation and are important in relation to the numerical recreation of the measured Tower deformation. One of these is the under-excavation procedure and a new approach to this procedure has been created and modeled in simplified FEM analyses. The new method is implemented in the constitutive Anisotropic Creep Model and has been tested and optimized to make it applicable in a full 3D model of the Tower.

Testing performed has shown to be especially sensitive to the choice of mesh refinement, and also to the chosen tube size and in order to obtain accurate extraction values a finer mesh must be used or tube measures must be increased. The new under-excavation procedure has so far not been implemented in the full 3D model of the Tower. This model is complex and thus time demanding and is so far using the internal Soft Soil Model in PLAXIS.

Sammendrag

Det skjeve Tårn i Pisa er et komplekst tilfelle som på bakgrunn av sin særegne historie har blitt analysert i årtier, både manuelt og numerisk. Til nå har man ikke klart å modellere stabiliserende tiltak som har blitt gjort i forbindelse med opprettingen av tårnet på en tilfredsstillende måte. Dette gjelder blant annet jord utgravingen som ble utført under tårnet og det er for dette tiltaket utviklet en ny metode som er blitt modellert i forenklet FEM-analyse. Metoden er implementert i materialmodellen for anisotropisk kryp og er blitt testet og optimalisert for å gjøres anvendbar i en 3-dimensjonal modell av tårnet.

Optimaliseringsarbeidet viser at jordutgravingssprosedyren er svært ømfintlig i forhold til valg av nett og størrelse på utvinningsrør og resultatene tilsier at metoden er avhengig av fint nett eller store rørdimensjoner dersom den skal fungere nøyaktig. Jordutgravingsmetoden er så langt ikke blitt implementert i 3D modellen av tårnet. Sistnevnte modell er kompleks og således tidskrevende og den bruker så langt den innebygde material modellen for fingradert jord.

Content

Figures

Tables

Boxes

1 Introduction

During the last part of the 19th century and the beginning of the 20th, there have been made several attempts to create numerical models of the leaning Tower of Pisa and the underlying ground. The goal has been to replicate the Tower movement in order to understand why it is deforming, save it from severe deformation and to predict future deformation after stabilization.

The most recent numerical model of the Tower has been developed by Prof. M. Leoni (2006) and it is a refined version of Leoni and Vermeer's model (2002). Modeling the Leaning Tower in Pisa is challenging as the case in question is an old construction that has been inflicted by several operations and rescue attempts. These has to be modeled in an accurate and correct way in order to obtain satisfying results and even though the latter model has developed procedures that are working well there are still some features of this numerical model that are not replicated in a satisfying way.

The four most important features of the numerical model that should be explored further is the modeling of the top soil behavior as the Tower starts moving, the excavation of the Catino, the incorporation of small strain stiffness into the constitutive model and the under-excavation.

Grasping all of the listed subjects would be a time challenging affair, requiring much more time than what has been available for this thesis. Thus the content of this thesis focuses on the under-excavation and the implementation of a new approach on modeling this process. Different aspects of the new procedure has been tested and optimized with the aim of being able to implement it into a large strain FEM analysis of the leaning Tower of Pisa.

In the following chapters a full review of the under-excavation procedure, the real and the numerical is given together with results from testing. An introduction to the full 3D Tower model is given in the final chapters together with a summary of the work, but as an introduction the first chapters deals with the history of the Tower in order to give the reader a clearer insight to the case in question and to create an

understanding of the complexity involved in making a numerical model of the leaning Tower of Pisa.

2 Construction history

The construction of the Tower began in 1173 and due to two long breaks it went on for 176 years. These breaks were most likely caused by war, but other possibilities have also been discussed (Burland, Jamiolkowski, & Viggiani, Stabilizing the leaning tower of Pisa, 1998). The first break came in 1178, and by that time construction work had only reached the 4th order of the final Tower, which is illustrated in Figure 1.

The second break was in 1278 after having reached the 7th order of the finished Tower. Completion with the rise of the bell Tower was first achieved in 1360 and although completion would have taken almost $\frac{1}{16}th$ of the time had it not been for the two shutdowns, these have actually proven to have been crucial for the Tower existence (Burland, Jamiolkowski, & Viggiani, The stabilization of the leaning tower of Pisa, 2003). Had they built the Tower, giving it no time to consolidate, the weight of the Tower would have caused an undrained bearing capacity failure in the underlying soil and the Tower would have been history already after the first construction phase.

As will be stated later the Tower moved most during construction, but also after completion there have been multiple interventions causing further and severe tilting of the Tower. As described e.g. in Leoni and Vermeer's report (2006) one of the first operation which had severe impact on the Tower started in 1838 and involved the building of the Catino, a trench around the Tower with a depth of 1 meter on the north side and 2 meters on the south side. This trench was built to unveil the original foundation, which had sunk into the ground due to heavy settlement and rotation. On the south side the ditch was dug below the groundwater table, which resulted in an inflow of water. In 1934 this inflow was stopped when it was decided to make the walls and floor of the Catino and the Tower foundation watertight. Cement grout was injected into the foundation mass through several steel pipes which were i.a. inserted through the Catino floor and the walls and floor were made impermeable by covering them with an impervious membrane (Leoni & Vermeer, 3D creep analysis of the Leaning Tower of Pisa, 2002).

In the beginning of the 20th century the first out of 16 committees was appointed by the Italian government to start an investigation of the Tower movement. This appointment was done in connection to a similar Tower to the one in Pisa falling over in 1902. The latest Committee was engaged at the end of the 20th century and this team was also formed in the light of a similar Tower, the civic Tower in Pavia, collapsing with no warning in 1989. “Pavia’s belfry was perfectly perpendicular, collapsing simply because of weakened, centuries-old masonry” (Smart, 2010). This type of collapse could also strike the Pisa Tower, especially as the facade on the Pisa Tower was under more stresses due to the tilting. This created great concerns for the Tower of Pisa and as is written by Burland *et al* (1998) the Italian Government reacted immediately by appointing a multidisciplinary International Committee to safeguard and advice on the stability of the Tower of Pisa.

One of the Committee’s first countermeasures was to construct a pre-stressed concrete ring around the base of the Tower in 1993. This was made to work as a base for counterweights that were later being placed on the north side in order to bring the Tower back to a temporary safe position. With the casting of this ring the Tower experienced its most critical rotation ever, as much as 5.5°. At the same time, due to the heavy rotation, the masonry walls of the Tower were subjected to very high stress which made the Committee worry not only about the hazard of overturning, but also about masonry collapse. Considering both impending threats the Tower was in 1993 closed for the public and it was kept closed for the 12 following years.

The counterweights were placed in four stages with a total weight of 600 t. This made the Tower tilt northwards and reduced the overturning moment (Burland, Jamiolkowski, & Viggiani, 2009).

In 1995 a need for more counterweights arose. Ironically enough these had to be installed as a countermeasure to an operation that was performed in order to be able to remove the counterweights, as they were infecting the aesthetic of the building.

This operation was to be permanent and included the installation of 30 micro piles north of the Tower. These piles were to be installed in a concrete ring situated around the Tower foundation. To install this ring it was necessary to excavate beneath the

Catino and thus below the ground water table, and in order to gain control over the water it was decided to use local ground freezing in an area between the Catino floor and the foundation. Before freezing was initiated investigation of the Catino floor revealed an 80 cm thick underlying layer of concrete conglomerate. It appeared to originate from 1838, and one became concerned about this layer being connected to the Tower foundation. Drilling proved that there was no connection and thus ground freezing was initialized and the concrete ring and micro piles were installed. (Burland J. B., 1998).

Unfortunately, to everyone's surprise it was discovered that there was actually a connection between the conglomerate slab and the Tower foundation (Burland J. B., 1998). Grouting tubes, which were installed through the Catino floor and thus the conglomerate layer during the impermeabilization of the Catino in 1934 had not been removed, they had only been cut and left in the structure making it a rigid connection (Leoni & Vermeer, 3D creep analysis of the Leaning Tower of Pisa, 2002). The disturbance which followed the installation of the micro piles was therefore transferred to the Tower foundation and the Tower started to accelerate its southwards rotation. (Leoni & Vermeer, 3D creep analysis of the Leaning Tower of Pisa, 2006). To counter this reaction additional weights were applied, rather 400 tons additionally and the whole operation was abandoned.

After the latter attempt all following safety measures made up till 1999 were suppose to be temporary while a new method was devised. The next main attempt on long time stabilization had to be examined by thorough analysis because the Tower was close to failure and one needed to come up with a method that would not be harmful to either the Tower masonry or the foundation. After having tested the effect of several stabilizing measures the method of under-excavation was in 1998 accepted as a long time stability measure. (Burland, Jamiolkowski, & Viggiani, 2009).

After severe testing, i.a. running the under-excavation procedure on a small scale model of the Tower, a preliminary extraction was performed underneath the real Tower to monitor its response. In connection to this a safeguard structure was constructed to prevent the Tower from overturning. This limited soil extraction was a success and in February 2000 the full excavation was carried out.

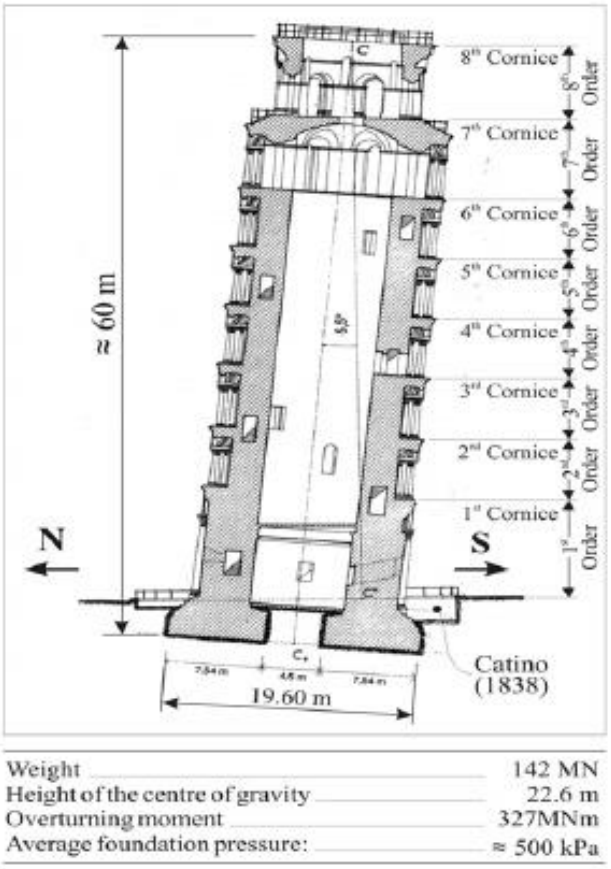

Figure 1: Cross-section of the Tower (Burland, Jamiolkowski, & Viggiani, 2009)

During excavation lead ingots were removed from the north side of the Tower and in the middle of February 2001 the cast concrete ring was also removed. Further the augers used for extraction were pulled out of the ground and the operation was over in June 2001.

The last major measure against future rotation commenced in 2002. It was observed that the water table in horizon A was rapidly and noticeably fluctuating and It was actually repeatedly observed that peaks of water level resulting from intense rainfalls lead to immediate irreversible rotation of the Tower southwards (Burland, Jamiolkowski, & Viggiani, The stabilization of the leaning tower of Pisa, 2003). In order to remove this negative effect a drainage system was installed to control the water table. This system still exists and consists of three wells. These are all installed north of the Tower and are each connected to five tubes reaching the drainage layer beneath the Catino. For a better description of this system see Burland *et al* (2009).

Summing up the above is Table 1 with the main happenings that should be included in a potential numerical model.

Table 1: Historical overview including main events

Year	Happening
1173 – 1178	Construction of the foundations and the first levels, H = 29 m.
1178 – 1272	Constructions pause of 94 years.
1272 – 1278	Construction of next four levels, H = 51 m.
1278 – 1360	Constructions pause of 82 years.
1360 – 1370	Completion of Tower with bell chamber, H = 58 m.
1838/1839	Construction of the Catino and the placing of an 80 cm thick conglomerate layer.
1934	Impermeabilization of the Catino floor and foundation mass.
1993 (May)	A pre-stressed concrete ring (1000 t) is constructed around the base of the Tower, at plinth level.
1993 (July)	Inclination of the Tower reaches 5.5 degrees. Applications of counterweights of 600 t, on the north side on top of the concrete ring. This was done in 4 phases.
1994 (January)	Last lead ingot (counterweight) of the first series is placed.
1995	Ground freezing and installation of micro piles. Installation of a second series of counterweights on the north side of the Tower.
1999 (February-June)	First soil extraction (preliminary under-excavation) under the north side of the Tower.
2000-2001	Second soil extraction (final under-excavation) completed in February 2001.
2002 (April/May)	Implementation of a water drainage system on the north side of the Tower.

3 Facts about the Tower and the underlying soil

The leaning Tower of Pisa - the Campanile is the bell chamber of the cathedral in Pisa and is one of four monumental buildings on the “Cathedral Square” or more proper - the Piazza del Duomo - which is depicted in Figure 2. It was originally built for touristic purposes even though the design was for it to be completely vertical. (Towerofpisa.info, 2012) The Tower has a foundation diameter of 19.6 meters and is close to 60 meters high. The weight of the Tower is 141.8 MN and it has the shape of a hollow cylinder with an inner diameter of 4.5 meters. The inner and outer surfaces are faced with marble and the annulus between these facings is filled with rubble and mortar (Burland, Jamiolkowski, & Viggiani, The stabilization of the leaning tower of Pisa, 2003), (Potts, 1993).

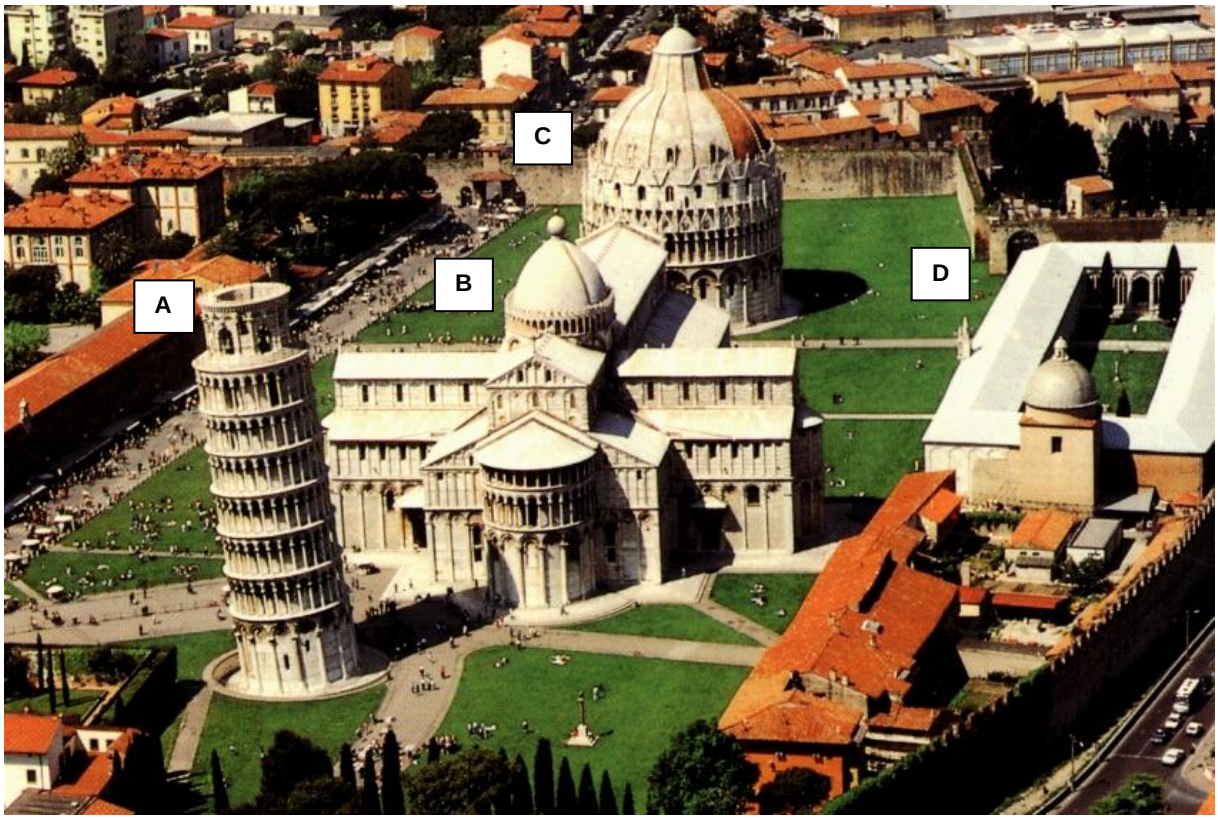

Figure 2: The Cathedral Square in Pisa. A: The leaning Tower. B: The Cathedral. C: The Baptistery. D: The cemetery (Viaggi)

3.1 The underlying soil

The soil underneath the Tower can be divided into three distinct layers – horizon A, B and C, which is illustrated In Figure 3. Horizon A is approx. 10 meters thick and consists mainly of variable silts and clays. The mass is estuarine deposits and is laid down under tidal conditions. The ground water is between 1 and 2 meters below the ground surface (Burland, Jamiolkowski, & Viggiani, Stabilizing the leaning tower of Pisa, 1998).

Horizon B is approx. 40 meters thick and can be divided into 4 sub-layers based on clay stiffness. The topmost layer is generally called the Pancone clay and is of soft sensitive clay. The next sub-layer is stiffer clay, while the third sub-layer is sand. The shallowest sub-layer consists of normally consolidated clay. Horizon C consists of dense sand which extends to considerable depth (Potts, 1993).

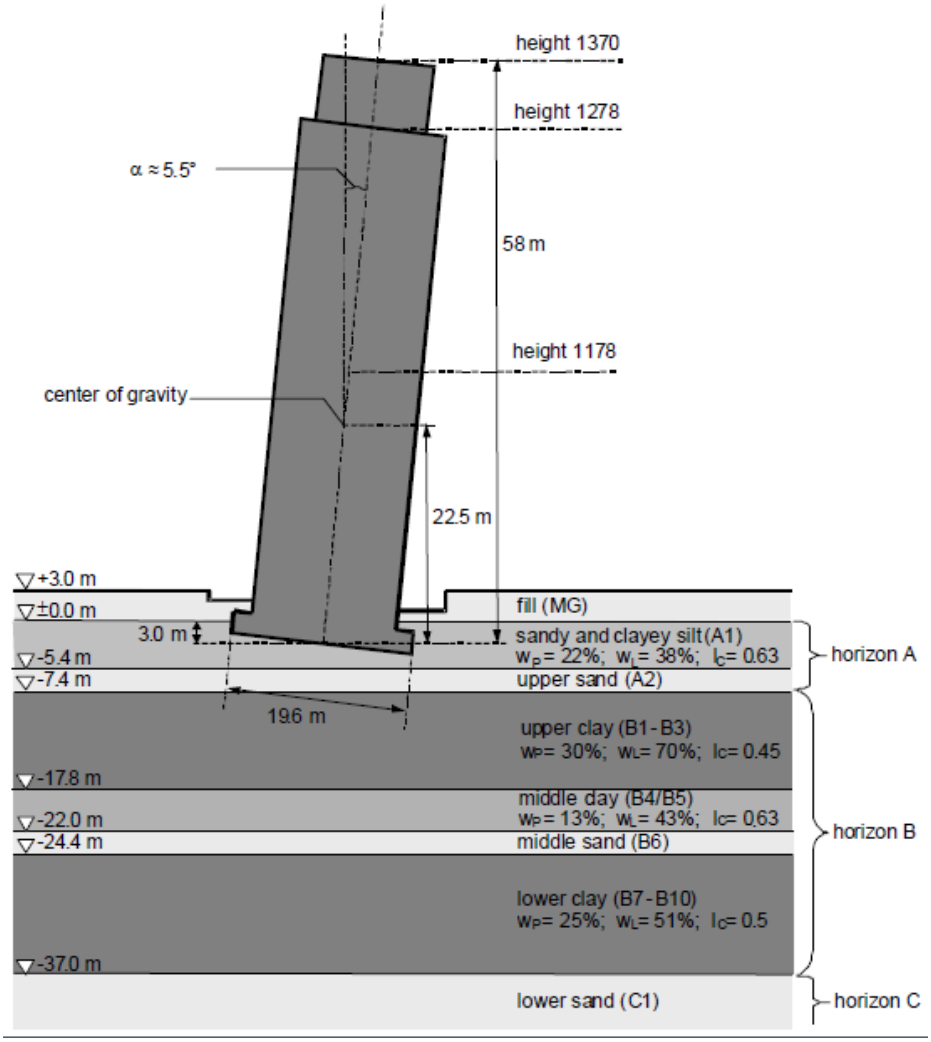

Figure 3: Geology of the subsoil beneath the Tower (Leoni & Vermeer, 3D creep analysis of the Leaning Tower of Pisa, 2002)

4 Previous movement

In present time there is a mutual understanding that the Tower is moving much less now compared to what it was doing during construction. According to Burland (1998) the magnitudes of movement are actually about three orders of magnitude less now than what was experienced during construction. Still there is movement and it is important to recognize that the Tower will reach a critical state again. This is why it is necessary to compute models that are able to predict the future movement of the Tower.

4.1 Before 1911

There are no building journals to obtain from the building period of the leaning Tower of Pisa so there exist no written evidence on how much the Tower was tilting during construction. Still there is visual proof of the Tower having been adjusted for the progressive inclination and as explained by Potts *et al* (1993) this can be found by inspecting the Tower construction. For instance one can observe corrections made in relation to the construction of the bell chamber; where on the north side there are 4 steps from the seventh cornice and up to the bell chamber, while on the south side there are only 6 steps.

Burland and Viggiani based their modern reconstruction of the inclination history on careful measurements of the relative inclinations of the masonry courses. This work lead to the launching of two theories; one, suggesting that the masons aimed to bring the centre line of the Tower back above the centre of the foundation when completing each storey and two, that the masons tried to restore the horizontality of the construction by adjusting the floors of the Tower and building perpendicular to this new level (Burland & Viggiani, 1994).

Based on the latter theories Burland and Viggiani were able to compose a time/load line for the rotation of the Tower. The curve, shown in Figure 4 is their reconstruction of the rotation history of the Tower. It shows that during the first construction phase and the subsequent pause, the Tower had a northwards rotation and in 1272 it reached an inclination of about 0.2° north. When recommencing construction work the Tower started to rotate southwards and at the point when construction reach the

6th cornice it was basically vertical. In 1278, having reach the 7th cornice of the Tower, it had an inclination of 0.6° to the south (Burland, Jamiolkowski, & Viggiani, Stabilizing the leaning tower of Pisa, 1998) and for the following years with construction pause this inclination increased moderately up to 1.6°. It was first with the construction of the bell Tower in 1360-70 that the inclination aggravated drastically.

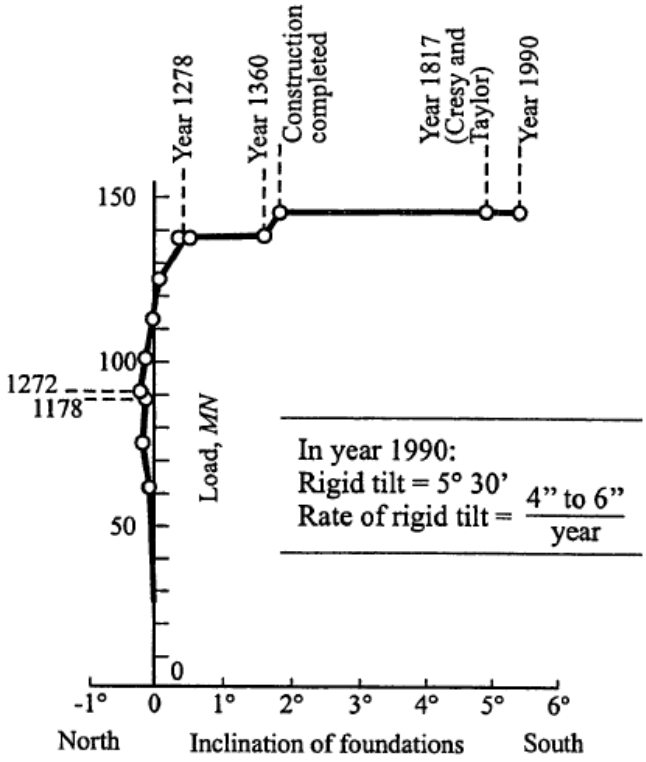

Figure 4: Illustration of the rotational progression of the leaning Tower of Pisa (Burland, Jamiolkowski, & Viggiani, The stabilization of the leaning tower of Pisa, 2003)

4.2 After 1911

1911 was the start-up year for precise and regular measuring of the Tower behavior. Through these results it has in later years been possible to understand how vulnerable the Tower is in relation to ground movement. Even the slightest disturbance to the foundation or the underlying ground has resulted in increased southwards rotation. Figure 5 shows how the Tower has destabilized throughout the last century and what has caused this movement.

What can be seen from the curve is that there are obvious jumps that interrupts the linear time-tilt line. As explained in Burland *et al* (1998, p. 95) the first jump in the curve is due to the work perfomed in 1934 when there were drilled 361 holes into the foundation masonry as is dicribed in Chapter 2. In 1966 some soil and masonry boring created a small tilt. Then in the late 1960's - early 1970's groundwater lowering influenced the Tower, but this time it was reduced to its previous state as the pumping of water reduced. Finally, in 1985 there was carried out more work on the foundation masonry which again lead to increased tilting.

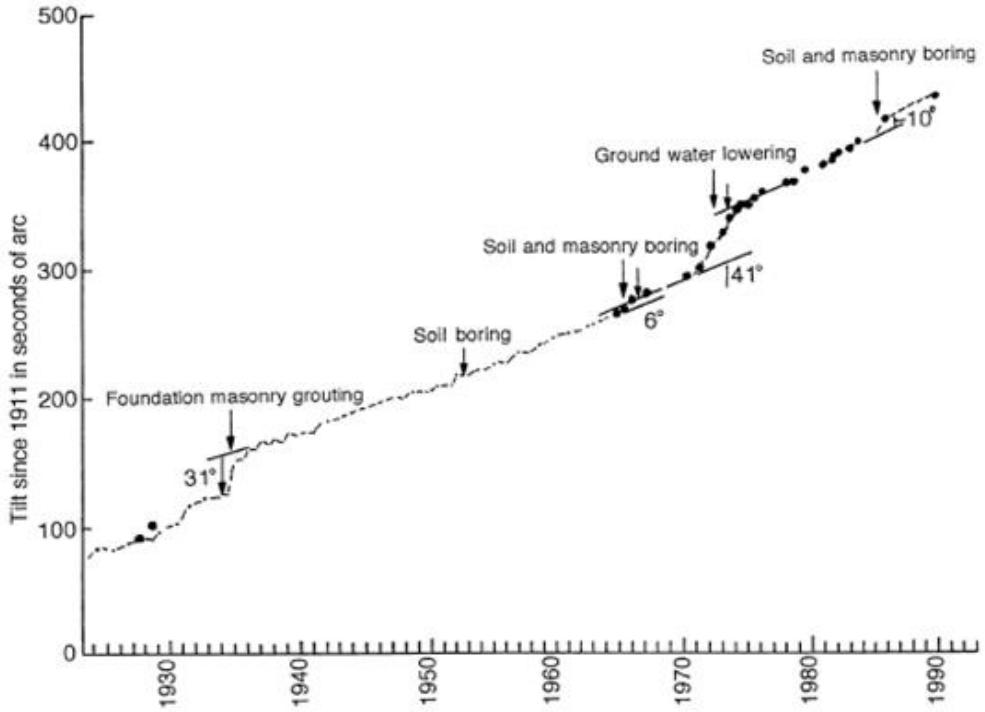

Figure 5: The history of tilt from 1911 and onwards (Burland, Jamiolkowski, & Viggiani, Stabilizing the leaning tower of Pisa, 1998)

The events that are described in the figure are, except from the grout filling in 1934, not listed in the historical overview on page 7. This is because they did not lead to distortions in line with what was experienced during and immediately after construction and as one can see from Figure 5 the tilt is given in arcseconds[1] instead of degrees . Still despite the insignificanse of these events, they show that the Tower

[1] One arc second equals 1/3600 degrees
[2] As the regarded soil configuration is made in 2D, depth is made 1 meter
[3] See Eq. 3
[4] This value would expectedly be more accurate than values from the coarser mesh refinements and

is extremly sensitive to ground and foundation disturbance and that even the smallest influence is recognized. This is knowledge that was vital for the work on devising plans on how to stabilize the Tower in the 1990’s and that is important to be fully aware of when making future predictions.

5 Understanding the Tower behaviour

The measurments performed after 1911 were in the later part of the century studied closely in order to understand the behaviour of the Tower. Previous theories claimed that the inclination was a result of low bearing capacity in the Pancone clay, but after close study of measurements and extensive testing (Burland, Jamiolkowski, & Viggiani, The stabilization of the leaning tower of Pisa, 2003), (Potts, 1993) this statement was disproven. Testing showed that the inclining Tower was affected by leaning instability - “a phenomenon controlled by the stiffness of the soil rather then by its strength” (Potts, 1993). Leaning instability occurs when a tall building, having reached a certain critical height, experiences an overturning moment that is greater than or equal to the foundation moment resistance. This overturning moment comes from an increase of inclination which can be minimal (Potts, 1993). This means that “No matter how carefully the structure is built, once it reaches the critical height the smallest perturbation will induce leaning instability” (Burland, Jamiolkowski, & Viggiani, 2009).

The extenxive test work was performed with both physical and numerical models of the Tower. One of the most important tools for discovering the true stability issue of the Tower was a numerical model developed in the 1990s by proffessors D. Potts and J. B. Burland. Based on available measurements of the Tower-movement and predictions of the inclination history, as explained in Chapter 4.1, this numerical model was able to simulate previous motion and predict the responce of future stabilization work. An example drawn from this work is shown in Figure 6; by using constant undrained shear strength and varying shear stiffness it is made clear that soil of high shear stiffness withstands greater loading and is much more resistant to rotation compared to soils of low stiffness. The curve also show that for a certain critical weight, the rotational deflection is great for less stiff soils - much greater then for stiff soils. (Burland, Jamiolkowski, & Viggiani, The stabilization of the leaning tower of Pisa, 2003).

Another case the numerical model was set to investigate was the present strenght of the Pancone clay. Computed results showed: “that the seat of the continuing long-

term tilting of the Tower lies in Horizon A and not within the underlying Pancone clay as has been widely assumed in the past" (Potts, 1993). This meant that during the last construction break the clay had had a long time to consolidate and in this period it increased strength eliminating almost all zones of contained failure from previous construction (Potts, 1993). This discovery played a very important role in the work on evaluating the effect of different stabilization measures, expesially the counterweight solution.

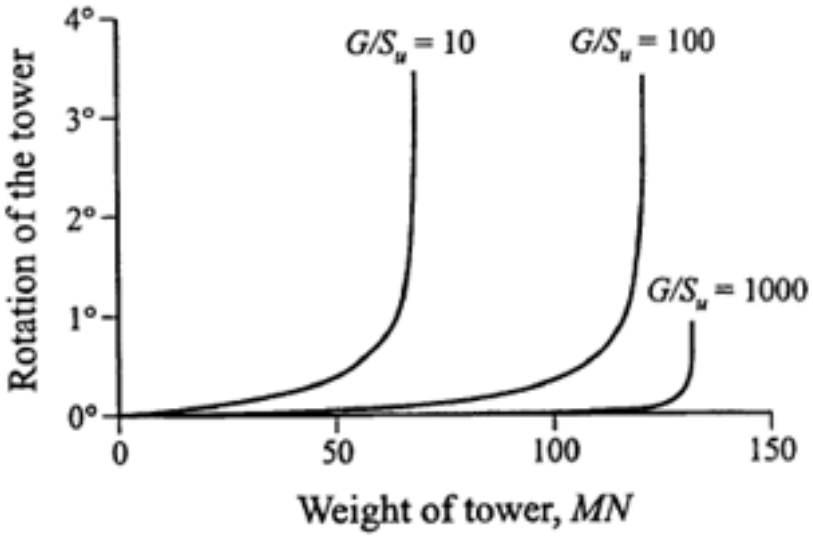

Figure 6: Rotation-load curve (Burland, Jamiolkowski, & Viggiani, The stabilization of the leaning tower of Pisa, 2003)

With the knowledge on why the Tower had started to tilt in the first place and its seat of rotation, one later discovered new factors causing the Tower to rotate. Careful observations of the change of inclination over many years showed that there was a distinct seasonal pattern to this movement (Burland, Jamiolkowski, & Viggiani, Stabilizing the leaning tower of Pisa, 1998). It was discovered that the Tower inclination was influenced by ground water fluctuation in horizon A, caused by heavy rainstorms. One also discovered that the Tower inclination was influenced by air temperature. As has been described earlier the contribution from ground water fluctuations was subsequently removed by implementing a drainage system for the Tower in 2002. This system was able to control the ground water and thus decrease the inclination.

6 Under-excavation 1999-2001

The rescue operation which was performed during year 1999-2000 involved the removal of small soil volumes from underneath the elevated part of the foundation. The procedure was performed in two stages; first a preliminary excavation, testing the effects of the procedure on the Tower, and last a complete, final excavation as the preliminary test was proven to be successful. The preliminary under-excavation consisted of 12 perforations taken down to horizon A with an inclination of 26° to the horizontal surface, as shown in Figure 7 and Figure 8. A total amount of 7 m^3 of soil was extracted in which 71 % was excavated north of the Tower and 29 % below the Tower foundation.

The final under-excavation consisted of 41 holes, now with less inclination of only 20° because one wanted to avoid penetration of the Pancone clay due to the tubes being elongated. Extraction tubes had a diameter of 0,168 meters, were installed with a distance of 0.5 meters and were made parallel and symmetrical to the axis of maximum inclination. An overview of this is shown in Figure 9 and Figure 10 were one also can observe that it for the full excavation also was prepared some lateral holes for extraction of soil just below the floor of the Catino. This was done with a view of protecting the Catino from cracking as the Tower started tilting backwards, but these holes were not used in the end. The total amount of soil extracted gave a volume of 37.668 m^3, where approx. 60 % was taken from below the Catino - outside the perimeter of the Tower foundation (Squeglia & Viggiani, 2005).

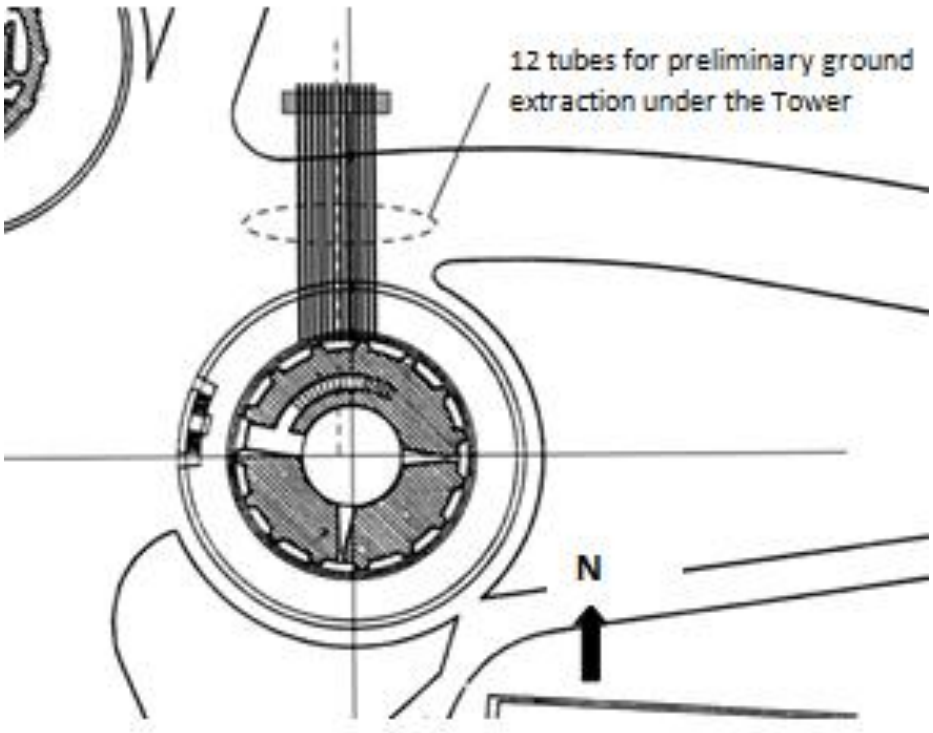

Figure 7: A plane overview of the preliminary under-excavation with 12 pipes inclined 26 degrees to the horizontal. The line cross symbolizes the axis of maximum inclination (Squeglia & Viggiani, 2005)

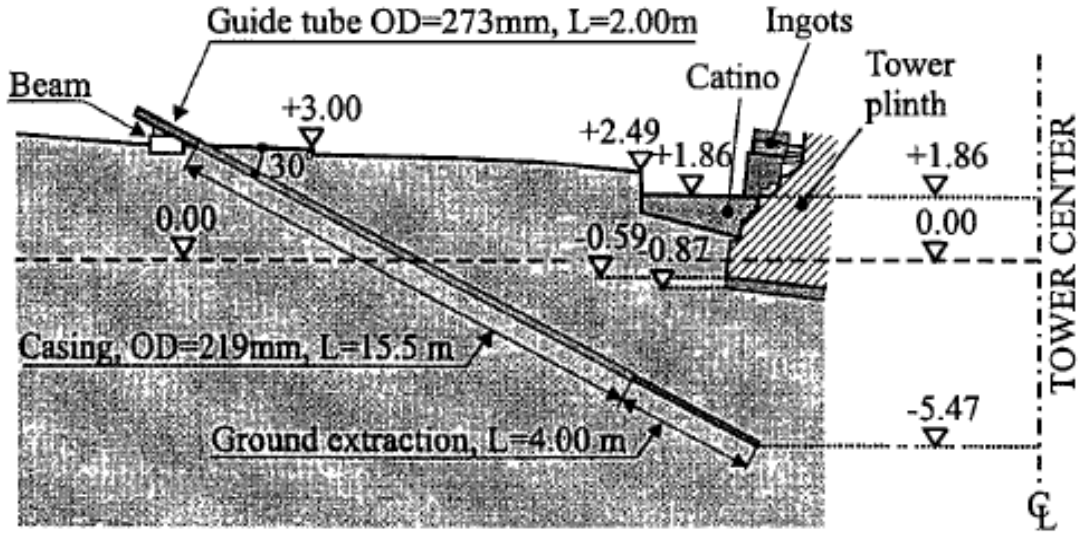

Figure 8: vertical section of the preliminary soil extraction (Burland, Jamiolkowski, & Viggiani, The stabilization of the leaning tower of Pisa, 2003)

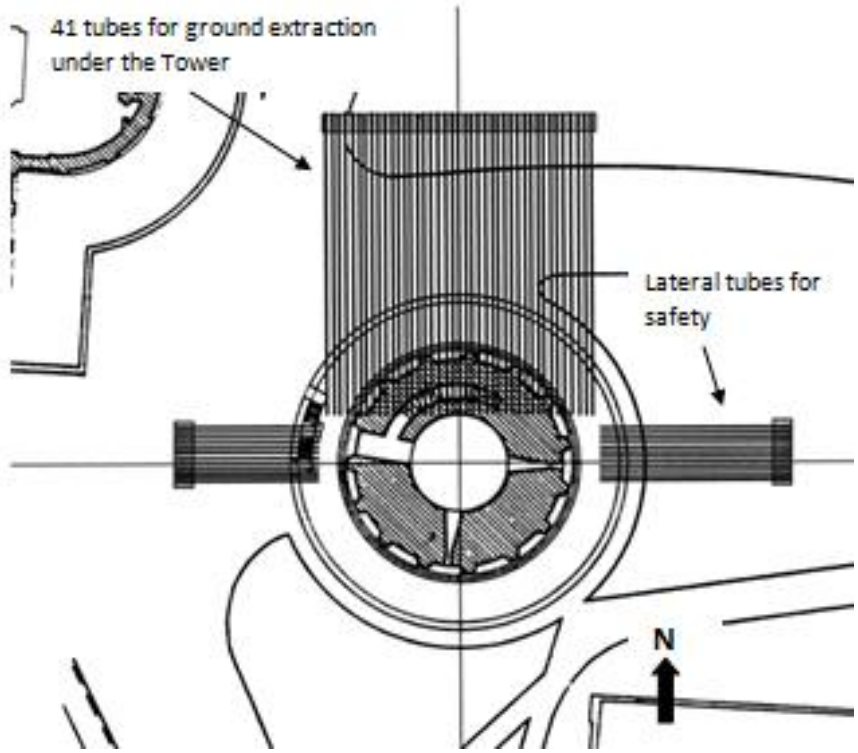

Figure 9: A plane overview of the full under-excavation. The line cross symbolizes the axis of maximum inclination (Squeglia & Viggiani, 2005)

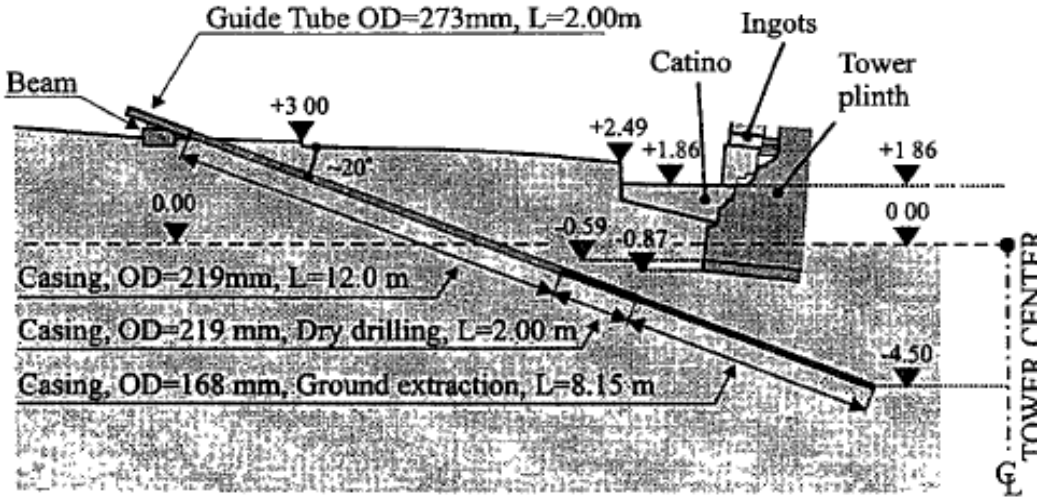

Figure 10: vertical section of the final soil extraction (Burland, Jamiolkowski, & Viggiani, The stabilization of the leaning tower of Pisa, 2003)

The amount of volume that was removed from underneath the Tower is schematized in Appendix A-1 and A-2. As will be discovered later by the reader; due to time limitations for this thesis, testing has only been performed regarding the final under-excavation. But because future calculations most likely will consider also the preliminary under-excavation it is implemented in the documentation of this thesis as well.

The tables in Appendix A-1 and A-2 give the total amount of soil extracted for each tube and the location of each tube for both preliminary and final excavation. The total volume, which is summarized in the bottom row in both tables, does not agree with the total sum of each column, which is in bold writing in each section. This is just because each number has been rounded and one cannot see the decimal value of the number in each box. The total volume is the sum of the real number, with decimals, in each box.

Each column in the form represents a tube and from each section one can read how many times soil was extracted at this depth and how much was last removed. The reference point, from which the distance in the form is taken, is by the tube casings, at the point where the tubes cut into the ground. This is approx. 18.4 m straight north of the Tower, as shown in Figures 7-10

7 Finite element analysis

7.1 Constitutive models

The first finite element analysis that was performed for the case of the leaning Tower of Pisa was developed by Burland and Potts and is previously mentioned in Chapter 5. It was carried out on a finite element package developed at the Imperial College using a form of the modified cam clay model with fully coupled consolidation for soft soils (Potts, 1993).

Later analysis were performed with the finite element software PLAXIS and analyses were performed with the soft soil creep model (SSCM) as it was proven that creep effects played an important role in relation to the inclination of the Tower. (Leoni & Vermeer, 3D creep analysis of the Leaning Tower of Pisa, 2006) Resent numerical models of the Tower have been improved further by the application of a new constitutive model - the anisotropic creep model (ACM), which accounts for the anisotropy of natural soils in addition to creep (Leoni & Vermeer, 3D creep analysis of the Leaning Tower of Pisa, 2006). This model is not a part of the internal material model assortment, but it can be implemented as a user defined material model.

As the ACM has shown to give reasonable results in back calculating the leaning Tower of Pisa (Leoni & Vermeer, 3D creep analysis of the Leaning Tower of Pisa, 2006) one wants to be able to keep this material model for future analysis. The new approach to the under-excavation has therefore been implemented in the ACM code so that this model can be used to its full potential in the future. Temporarily the anisotropic abilities have been disabled and a preliminary goal has been to make the under-excavation routine run with the SSCM.

Testing has been divided into two parts. The first part only considers the under-excavation procedure and different tests have been performed in order to optimize the procedure. Testing has disregarded creep entirely and considered only elastic deformation. The second part has been an analysis of the full Tower model with the accurate load and soil conditions. This analysis has been performed with the internal SSCM in PLAXIS and has been a step in the process of implementing the under-excavation procedure into the real boundary value problem.

In the following a short introduction to the isotropic creep model is made and also a few hints are given on how the ACM differs from the SSCM and why it would be beneficial to implement the anisotropic features in future models of the Tower.

7.2 Soft soil creep model

The ACM is a development of the isotropic soft soil creep model (SSCM) which in its turn is a refinement of the soft soil model. All three mentioned models are soft soil models and referring to Vermeer & Neher (1999) soft soils are considered to be near-normally consolidated clays, clayey silts and peat. These soils have a common characteristic in that they are extremely compressible and the soft soil oedometer stiffness (E_{oed}) is linearly stress-dependent (Neher, Wehnert, & Bonnier). The high compressibility is well illustrated in the oedometer test where one finds that normally consolidated clay behave 10 times softer than normally consolidated sand (Vermeer & Neher, A soft soil model that accounts for creep, 1999)

The SSCM takes into account time-dependent deformation occurring under a constant effective stress – which is the definition of creep (Leoni & Vermeer, 3D creep analysis of the Leaning Tower of Pisa, 2006). The creep implementation assumes the usual decomposition of total strains into elastic and plastic components. In terms of time dependent volumetric strain, $\dot{\varepsilon}_V$ this becomes as shown in Eq. 7.1 where the superscript 'e' denotes elastic strain and the superscript 'c' denotes plastic strain – creep. The dot above the symbol represents time differentiation.

$$\dot{\varepsilon}_V = \dot{\varepsilon}_V{}^e + \dot{\varepsilon}_V{}^c \qquad \textbf{Eq. 7.1}$$

For three-dimensional creep the plastic strain component can be found by Eq. 7.2 where μ* is the creep index, τ represents the time of each load step in the oedometer test, λ* is the modified compression index and κ* is the modified swelling index. The mentioned parameters can be found through standard oedometer tests, as is illustrated in Figure 11 and Figure 12.

$$\dot{\varepsilon}_V{}^c = -\frac{\mu^*}{\tau}\left(\frac{p^{eq}}{p_p{}^{eq}}\right)^{\frac{\lambda^*-k^*}{\mu^*}} \qquad \textbf{Eq. 7.2}$$

$$p'^{eq} = p' + \frac{q^2}{M^2(p')}$$ **Eq. 7.3**

The ellipses of the modified cam clay model are taken as contours for volumetric creep strain rate in the three dimensional SSCM. The point where the ellipse intersects the p'-axis when it is drawn through a current stress is called p^{eq} and is found by Eq. 7.3. The superscript 'eq' stands for equivalent and a diagram of the p^{eq}-ellipse is found in Figure 13. In Eq. 7.3 the p' represents the effective mean stress, q is the deviatoric stress and M is the slope of the so called "critical state line" which is the found by Eq. 7.4.

$$M = \frac{6sin\varphi}{3-sin\varphi}$$ **Eq. 7.4**

The second ellipse that is depict in Figure 13 is the normal consolidation surface in the p'-q plane and the intersection point with the p'-axis of this ellipse is p_p^{eq}, which is the pre-consolidation stress for three-dimensional conditions.

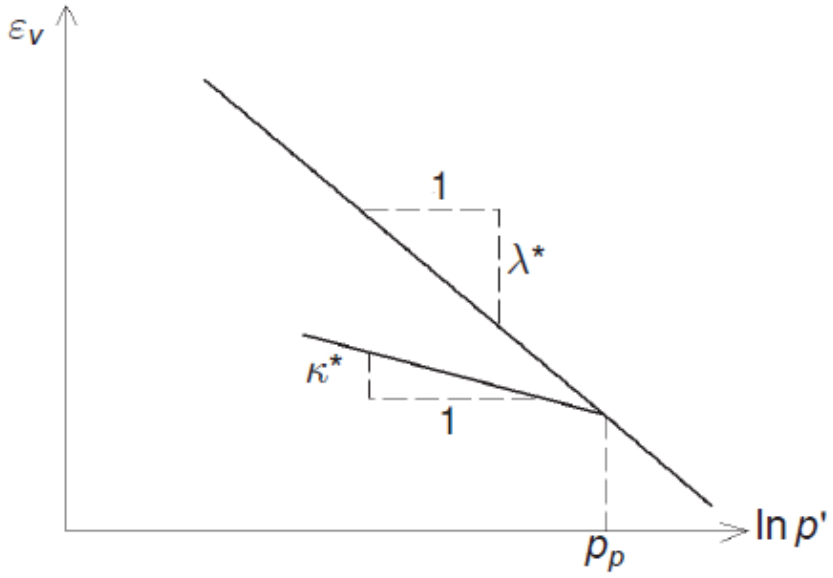

Figure 11: Logarithmic relation between volume strain and mean stress showing unloading reloading lines (Brinkgreve, Swolfs, & Engin, Plaxis 3D Reference manual, 2012).

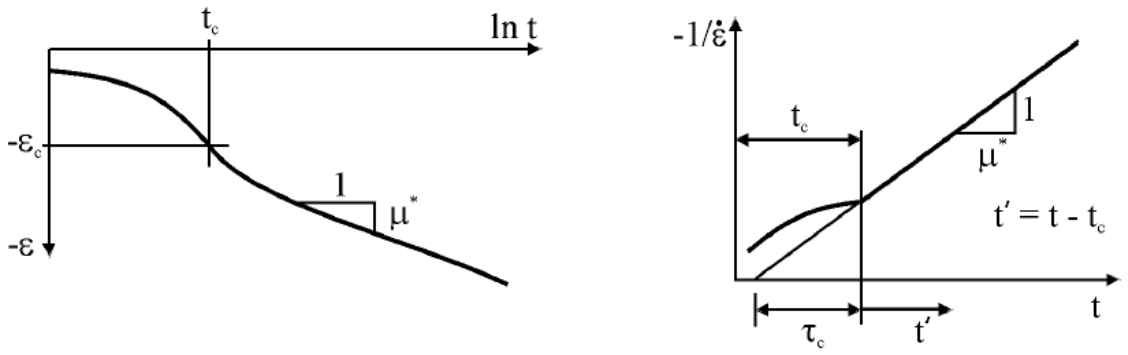

Figure 12: Curves showing consolidation and creep behavior in a standard oedometer test, where the modified creep index can be found in two different ways. (Leoni & Vermeer, 3D creep analysis of the Leaning Tower of Pisa, 2002).

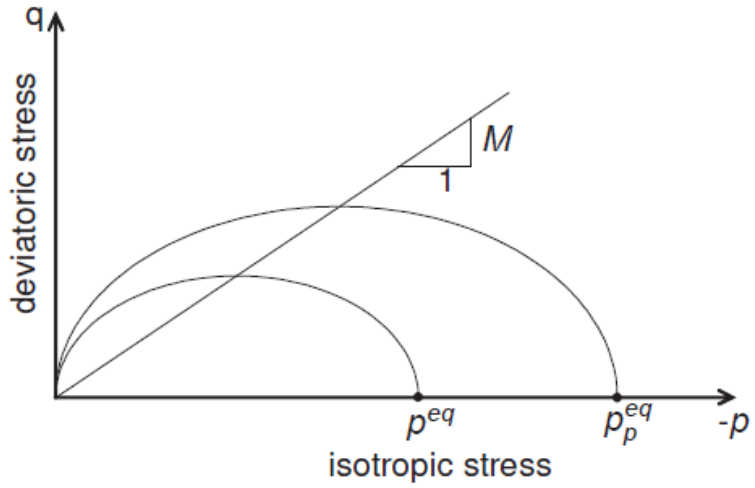

Figure 13: Diagram of p^{eq} ellipses in the p-q plane (Brinkgreve, Swolfs, & Engin, Plaxis 3D Reference manual, 2012).

The SSCM is an isotropic model meaning it assume symmetrical ellipses to the isotropic p'-axis and this is illustrated by the dashed circle in Figure 14. According to M. Leoni *et al* (2008) models based on isotropy generally works well on remolded and reconstituted soft soils. On natural soils however, they can often be inaccurate because: "natural soils tend to exhibit anisotropy that is related to their fabric, that is, the arrangement of particles. This affects the stress–strain behavior of the soils in terms of viscous behavior and deformations, and therefore needs to be taken into

account" (Leoni, Karstunen, & Vermeer, Anisotropic creep model for soft soils, 2006). The anisotropy is developed through deposition and one-dimensional consolidation due to the soil self-weight. The resulting effect, which violates earlier assumptions of isotropic yield surfaces, is skewed yield surfaces in the p' – q plane which from experiments have been observed for a wide range of soft soils (Leoni & Vermeer, 3D creep analysis of the Leaning Tower of Pisa, 2002).

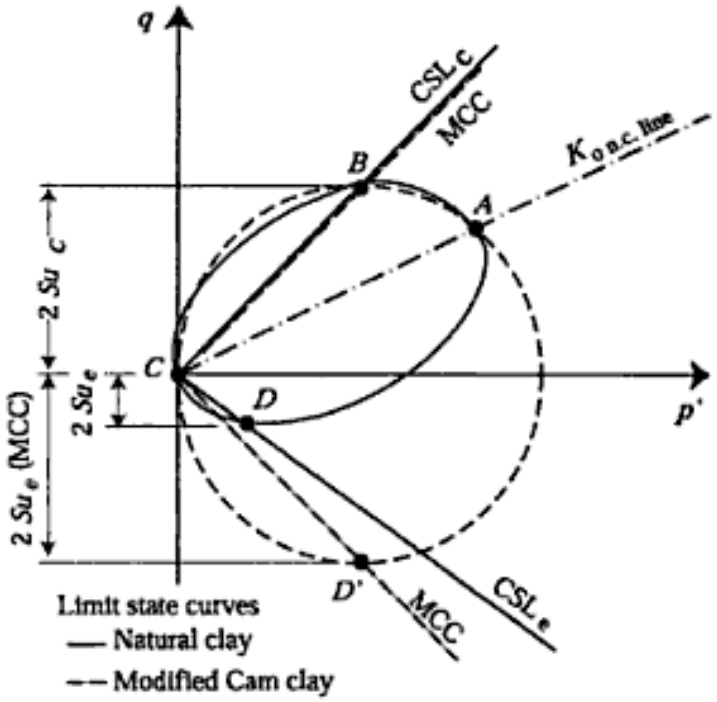

Figure 14: Anisotropic limit state curve defined for natural clays and isotropic limit state curve defined for Modified Cam clay (Leroueil, 2001)

The anisotropic creep model is also a time dependent creep model, but it is different in the way that it accounts for destructuration and anisotropy by using a rotational component and a destructuration component of hardening, in addition to volumetric hardening (Nordal, 2011). The skewed yield surface which is used in the ACM is shown in Figure 14 by a solid line.

7.3 Soil parameters

The first part of testing involving optimization of the under-excavation routine has only considered elastic deformation and not creep or anisotropy. Soil layering has been disregarded since the under-excavation procedure is only performed in the second uppermost layer beneath the Tower. Thus the only soil parameters that have been considered are the friction angle, the cohesion and the earth pressure coefficient of this layer. These parameters have been given values identical to those used by Leoni(2006) for the second layer of his full 3D analysis of the Tower implying a friction angle of 34 degrees, cohesion of 1.0 kPa and a approximately K_0-value of 0.5.

In the second part of the test program, involving the full 3D analysis of the Tower model, internal constitutive models have been used for the soil layers; the Soft soil creep model for soft soils and the Mohr-Coulomb model for the man made fill and sands. The Soft soil creep model has been assigned to materials: A1N, A1S, B1-5 and B7-10 while the Mohr-coulomb model has been assigned to materials: MG, A2 and B6. All of the above are undrained materials and they are explained further in in Chapter 3.1.

The chosen soil parameters are also basically the same as the ones used by Leoni(2006) and a overview of the different soil parameters used for different soil layers is given in Appendix B-1. In Appendix B-2 a description of the available parameters in the user-defined ACM is also given.

8 Optimizing of the new under-excavation method

8.1 Previous method

Previously the numerical simulation of the under-excavation has been performed by reducing the volume of finite elements under the foundation on the north side, as emphasized in blue in Figure 15 (Leoni & Vermeer, 3D creep analysis of the Leaning Tower of Pisa, 2006). Doing it this way one has not been able to extract the correct amount of volume and at the same time obtain the inclination that has been observed for the Tower. This is problematic and is probably caused by the inaccurate placement of the extraction area since: “results have been very sensitive to the choice of the area in which soil is being extracted” (Leoni & Vermeer, 3D creep analysis of the Leaning Tower of Pisa, 2002).

The reason it has been hard to obtain an accurate position of the tubes is that the user is not allowed to prescribe volume strain during calculation in PLAXIS. As the Tower starts inclining the mesh is deformed and when it is time for the under-excavation it is not given that the elements that have been predefined for extraction are in the right place.

8.2 New method

The new approach for the under-excavation seizes previous drawbacks and uses the exact placement of the extraction tubes in the procedure. The routine is implemented in the user defined ACM (Fortran) code which means that the elements that needs to be decreased are not marked manually as before. The new routine works on stress point level checking each gauss point’s coordinates if it is inside the area for extraction. If it is so the gauss point is made elastic and it is assigned volume strain that is carried out when it is time. If the point is not found to be inside the extraction area it is applied the creep material. How the procedure is built up in a more detailed way is described in the subsequent sections starting with the definition of the tubes.

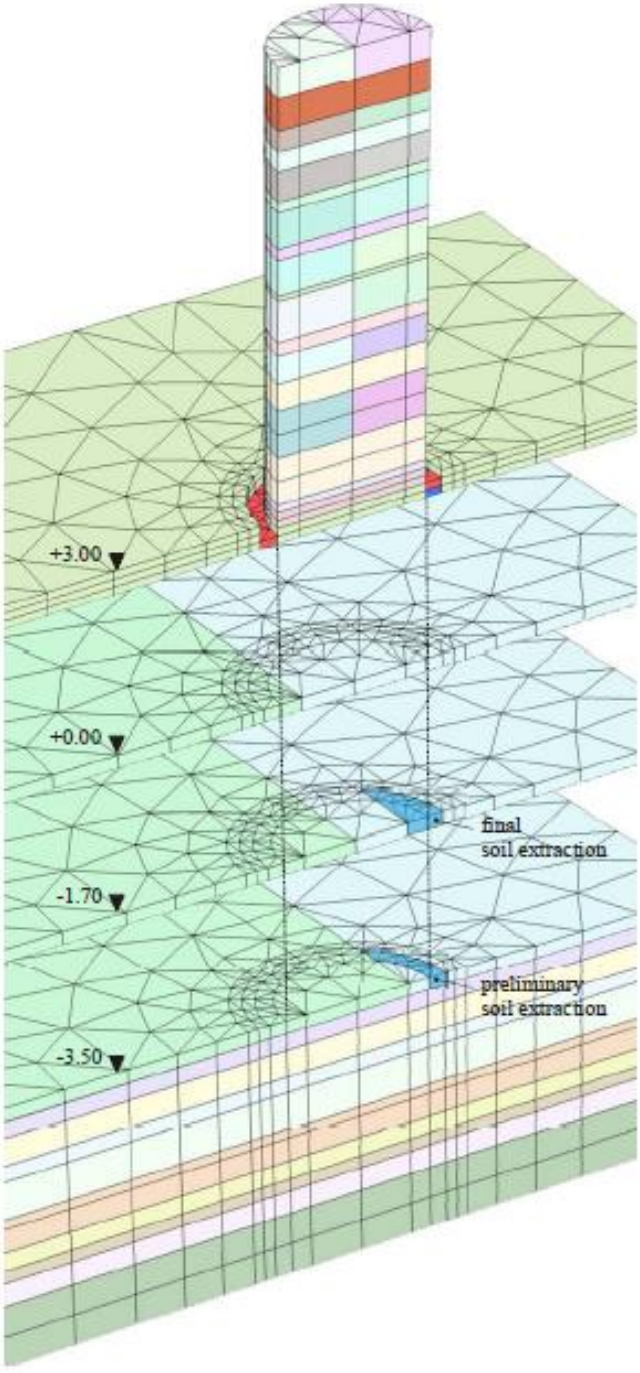

Figure 15: previous model showing elements used for soil extraction (Leoni & Vermeer, 3D creep analysis of the Leaning Tower of Pisa, 2006)

8.2.1 Tube definition

The fictitious extraction tubes are defined in a separate volume_strain.DAT file that is called by the code which PLAXIS accesses through the temporary folder on the computer. This file is created by the user and includes coordinates and measures for each excavation tube that is to be used. Each line in the file represents one tube and is made up by 9 input variables: $\lfloor x_0\ y_0\ z_0\ x_1\ y_1\ z_1\ r_{tube}\ r_{elastic}\ \varepsilon_V \rfloor$. The first part represents the x, y and z-coordinates for the starting point and the end point of the tube. The second part represents the radius of the tube, the elastic radius and the volume strain, which is to be applied gauss points that are found to be inside the tube volume. The exact amount of tubes is posted at the top of the DAT file as is illustrated in Box 1. This box also shows an extract of the file, listing the three first of the total 41 tubes. The complete list is found in Appendix C-1.

```
41
-10. -19.7 -2.2 -10. -23.5 -5.6 0.474 0.474 0.5
-9.5 -19.3 -2.0 -9.5 -23.5 -5.6 0.452 0.452 0.5
-9.0 -18.8 -1.8 -9.0 -23.5 -5.6 0.432 0.432 0.5
```

Box 1: Extract of the DAT file where the excavation tubes are defined

The part of the ACM code that treats the under-excavation procedure with localization of gauss points and application of volume strain is found in IDTask 1 and is reproduced in Box 2. The procedure is made up by basic vector calculus and is described in a less codified way in Appendix D-1.

```
      !VOLUME STRAIN ADD ON - Check if Gauss Point falls in volume
      StVar0(34) = 0.
      do i=1,nVolume
        xAB(1)= VolDef(i,4)- VolDef(i,1)
        xAB(2)= VolDef(i,5)- VolDef(i,2)
        xAB(3)= VolDef(i,6)- VolDef(i,3)
        xAC(1)= x          - VolDef(i,1)
        xAC(2)= y          - VolDef(i,2)
        xAC(3)= z          - VolDef(i,3)
        xAB_Norm= Max(Sqrt(xAB(1)**2+xAB(2)**2+xAB(3)**2),1d-6)
        xAC_Norm= Max(Sqrt(xAC(1)**2+xAC(2)**2+xAC(3)**2),1d-6)
        xAB_xAC = xAB(1)*xAC(1)+xAB(2)*xAC(2)+xAB(3)*xAC(3)
        xCosTeta= xAB_xAC/xAB_Norm/xAC_Norm
        xSinTeta= Sqrt(1-xCosTeta**2)
        xDist   = xSinTeta*xAC_Norm
        if (xDist             .LE. VolDef(i,8) .AND.
     +      xAB_xAC           .GE. 0.          .AND.
     +      xAC_Norm*xCosTeta .LE. xAB_Norm         ) then
          if (StVar0(34) .EQ. 0.) then
            StVar0(34)  = -1.d-8                    !elastic region
          end if
          if (xDist  .LE. VolDef(i,7)) then
            VolPoi(i,1) = VolPoi(i,1) + 1
            StVar0(34)  = StVar0(34) + VolDef(i,9) !volume strain
          endif
        endif
      enddo
```

Box 2: Code extraction showing the part where stress points are located and appointed volume strain. The parts that are emphasized in yellow consider the overlap of tubes.

8.2.1.1 Tube overlap

The part of the depict code that has been emphasized in yellow is the part that is not described in the appendix and it is the part which considers overlap of tubes.

In reality the total soil volume that was extracted in 2000 was a sum of several minor extractions carried out in the same tube hole, as depicted in Appendix A-2. In the numerical model it has not been feasible to imitate reality and the total volume is extracted in only one operation, meaning that the total volume extraction procedure is performed once for each gauss point that is found to be within the extraction area. Unfortunately, if one is to use the original tube radiuses this means that the total extracted volume per tube has to equal or be less than the volume of the tube. Each tube only has a diameter of 0.164 m and with tube lengths of maximum 5 meters one finds a total volume that is much less than what was actually excavated. So in order to extract a correct amount of soil the solution has been to increase the numerical tube radius. A challenge with this solution is that the distance between each tube is

only 0.5 m. By using an increased tube radius some tubes intersect. This is then solved by the emphasized implementation in the volume strain procedure that distinguishes between gauss points that have already been given volume strain, and points that have not. The appointed volume strain is stored in StVar0(34), and could then be a sum of several appointments if a point is found to be within several tubes.

8.2.2 Volume strain activation

The localization of actual gauss points and distribution of volume strain is done in phase 1 of the calculation and every time a new phase is started. The actual volume strain procedure needs to be activated and this can be done in any phase where the points have been located.

The activation part of the code is found in IDTask 2 and here it is stated that the volume strain procedure should run if *time0* is greater than or equal a certain value. *time0* represents the start time of a phase interval and throughout testing the certain value has been made 0 since the only time consuming phase has been the under-excavation phase. How this part is made when the under-excavation procedure is implemented in the full 3D model is described in Chapter 9.1.1.

From the latter part of the code one can also read that the gauss points that are being volume strained are maid elastic. This is done because it is assumed that making them elastic will give better convergence and to avoid risking failure which can be the consequence if the point is made plastic. In the case of failure, developed volume strain might come out of hand, which is unfortunate because then the procedure will become very inaccurate.

```
!VOLUME STRAIN ADD ON - Modify strain increment
!if(time0 .GE. 0.) then
   if (StVar(34) .GT. 0.) then
     dMStage = Sig0(9)-Sig0(8)
     dEpsVol(1:3) = StVar0(34)/3.*dTime !Volume change step = 1
     dEpsVol(4:6) = 0.
     dEps = dEps - dEpsVol
     Props(6) = 0.495
   endif
   if (StVar(34) .NE. 0. .AND. dTime .GT. 0.) then
     ElastFlag = .TRUE.
     Props(26) = 1.
   endif
!endif
```

Box 3: Code extraction showing the part where the volume strain procedure is activated. The part that is emphasized in yellow is the appointed Poisson's ratio, which is changed in order to make the tube incompressible.

Another part in the code that is important to clarify is the part which is emphasized in yellow in Box 3. As one can see the void ratio, Props(6) is set to 0.495. This is done in order to gain control over volume strain that develops during extraction. The goal is to lock the volume of the tube to the prescribed one and with a Poisson's ratio of 0.5 the material is made incompressible and thereby the tube is "untouchable". For numerical reasons it is necessary to use a Poisson's ratio value that is not exactly 0.5 and thus the value of 0.495 is chosen. If a value less than 0.495 is used then the resulting change in effective stress due to the volume strain procedure will lead to additional volume strain.

In addition to the implemented part mentioned in the latter, one needs also to implement a similar addition in the specification of the stiffness matrix as a change in Poisson's ratio affects the stiffness. The stiffness matrix is defined in IDTask 3/6 and this addition part is emphasized in yellow in Box 4.

```
  Call GetELParam2 (Props,Stress, G, xNu)
  if (StVar0(34) .GT. 0) xNu = 0.495
  Call Dmatr (G, xNu, Del, IsUndr)
```

Box 4: Code extraction with the additional Poisson's ratio implementation in the specification of the stiffness matrix emphasizing in yellow.

8.2.3 2D versus 3D calculations

When going from PLAXIS 2D to PLAXIS 3D it has been discovered that the ACM-code needs to be different for 2D- and 3D-calculations. In the original code σ_{yy} is defined as the vertical stress; Sig0(2) and σ_{xx} and σ_{zz} are defined as the horizontal stresses; Sig0(1) and Sig0(3). For 3D calculations σ_{yy} is no longer the vertical stress, but the horizontal stress and without changing the code one obtains inaccurate $K0_{NC}$ - values. Therefore it has to be clarified in a separate code for 3D analysis that Sig0(3) is the vertical stress and Sig0(2) the horizontal stress.

Changes that have been made to the code as it is used for 2D-calculations, in order to get it to function well also for 3D-calculations is given in Table 2 and the location of the changed part in the code is given in the leftmost column.

Table 2: Overview of the modifications that needs to be done in the ACM code when changing from 2D to 3D analysis.

Loc.	**ACM code for PLAXIS 2D**	**ACM code for PLAXIS 3D**
Task1 case1	Sig0(2)=Props(16) !030609_01	Sig0(3)=Props(16) !030609_01
Task1 case1	SigPOP(2)=SigC(2)*Props(9)+Props(10)SigPOP(1)=(SigC(2)*Props(9)+ Props(10))*xK0nc SigPOP(3)=(SigC(2)*Props(9)+ Props(10))*xK0nc	SigPOP(3)=SigC(3)*Props(9)+Props(10) SigPOP(1)=(SigC(3)*Props(9)+ Props(10))*xK0nc SigPOP(2)=(SigC(3)*Props(9)+ Props(10)) *xK0nc
Task1 case1	Sig0(2) vertical stress unchanged Sig0(1)=-(SigPOP(1)-Props(6)/ (1.-Props(6))*(SigPOP(2)-SigC(2))) Sig0(3)=-(SigPOP(3)-Props(6)/ (1.-Props(6))*(SigPOP(2)-SigC(2)))	Sig0(3) vertical stress unchanged Sig0(1)=-(SigPOP(1)-Props(6)/ (1.-Props(6))*(SigPOP(3)-SigC(3))) Sig0(2)=-(SigPOP(2)-Props(6)/ (1.-Props(6))*(SigPOP(3)-SigC(3)))
Task1 case1	Sig0(1)=Sig0(2)*xK0nc Sig0(3)=Sig0(2)*xK0nc	Sig0(1)=Sig0(3)*xK0nc Sig0(2)=Sig0(3)*xK0nc
case 16	ParamName = 'Sig0(2)'	ParamName = 'Sig0(3)'

8.3 Results from testing

In order to optimize the volume extraction procedure several numerical simulations have been executed using both the 2D (2010)and 3D (2011) package of the finite element software PLAXIS.

2D-calculations have been run on a 2.27 GHz Intel Core i3 processor equipped with 4 GB RAM and on a 32 bits system. 3D-calculations have been run on a 2.83 GHz Intel Core Quad processor equipped with 8 GB RAM on a 64 bit system.

For 2D-testing a simplified soil area of 10x10 meters has been used and for 3D-testing a soil volume of 25x30x7 m^3 has been created, as is shown in Figure 16. Both

soil geometries have been assigned the ACM with parameters as stated in Chapter 7.3. The mutual calculation procedures involve two phases in addition to the initial phase. A vertical load of 100 kPa has been activated in phase 1, which is a simplification of the Tower load, and the soil excavation procedure has been activated in phase 2. The chosen *calculation type* has been K0 procedure in order to obtain a homogeneous constant stress field and both soil weight and groundwater has been neglected for simplicity reasons. Default calculation settings have been used except from the *arc-length control* which has been switched off in order to reach accuracy conditions and *the desired maximum* and *minimum* which has been set to 6 and 3 for 2D-calculations and 15 and 2 for 3D-calculations in order to avoid severe divergence during calculation.

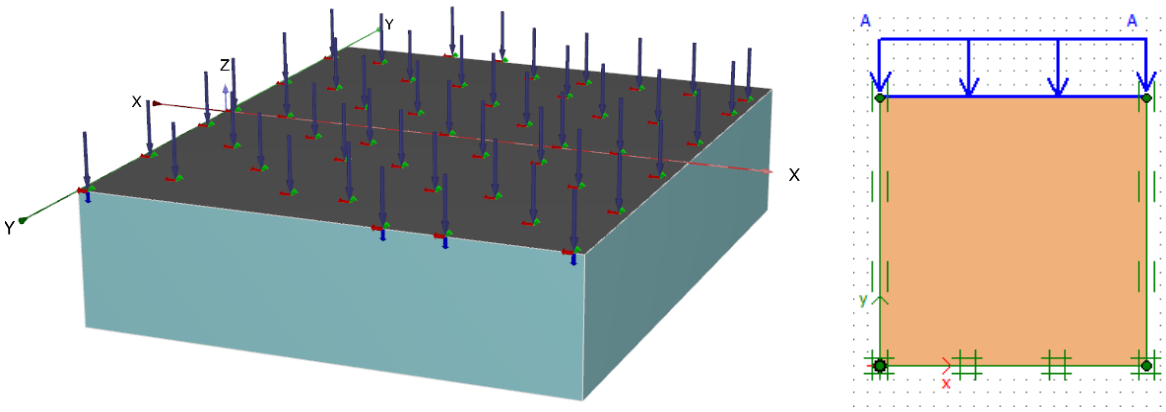

Figure 16: An illustration of the geometry in PLAXIS 3D on the left and PLAXIS 2D on the right.

8.3.1 Cluster effect and the importance of the selected number of nodes

In the previously used method for under-excavation predefined clusters with applied volume strain has been created. Since this has not given optimal results the new method does not require predefinition of clusters. The effect of not geometrically assigning areas for volume extraction has been tested and results show that it is beneficial to withdraw volume from a predefined cluster, as can be seen in Table 3.

For this part of the testing two different soil geometries has been defined, one consisting of only one large cluster and another identical to this but with an internal

1x10 m^2 cluster predefining the area for soil extraction. For both cases the tube radius was made equal the elastic radius of 0.5 m and given a volume strain of 0.5 - giving a required volume extraction of 0.5 m^3. Required extraction value should then equal the obtained value from analyses if the procedure is to be 100 % accurate.

In Table 3 results from testing performed both with a tube cluster definition and without are given. These show that for both 6-noded and 15-noded elements it is beneficial to use a tube cluster. This is as expected because, as can be seen from Table 5, when a cluster has not been defined several elements are intersected by the tube definition routine, meaning that not all stress points from these elements are found to be inside the tube. If these stress points represents volumes that are not inside the tube then the change of volume becomes inaccurate. Opposite when a cluster has been defined the relevant elements are isolated and whole elements are used in the volume strain routine, so that all stress points belonging to these elements are assigned volume strain and the correct amount of volume is extracted.

Table 3: Obtained volume change for analysis using different element types and different soil geometry configurations.

Assigned cluster	Type of element	No. of soil elements	No. of nodes	Average element size (m)	Obtained volume change (m^3)	Deviation from correct value (m^3)
Yes	6-noded	162	361	0.7857	4.990	0.01
No	6-noded	162	361	0.7857	4.278	0.722
Yes	15-noded	162	361	0.7857	4.990	0.01
No	15-noded	162	361	0.7857	5.17	0.17

What can also be seen from Table 3 and Table 5 is that there is an obtained accuracy difference using 15-noded elements instead of 6-noded elements in which the 15-noded elements obtain the most accurate result. This is not surprisingly as more stress points are available with the 15-noded element.

The *obtained volume*[2] *change* in the table is found by using equation 8.1 where ε_V is the volume strain assigned each stress point, V is the original volume of these stress points and ΔV is the volume change for each stress point.

$$\varepsilon_V = \frac{\Delta V}{V} \qquad \textbf{Eq. 8.1}$$

When finding the total volume change per tube, volume change per stress point needs to be summarized. In this context the numerical integration of area elements, shown in Eq.8.2 (Brinkgreve, Swolfs, & Engin, Plaxis 2D Scientific Manual, 2011) applies for both 6-noded and 15-noded elements and represents the total area contained by *k*-stress points. $F(\xi_i, \eta_i)$ is a function of the position factors ξ_i and η_i and multiplied with w, which is the weight factor of the integration points they represent the exact area held by stress point *i*.

$$\sum_{i=1}^{k} F(\xi_i, \eta_i) w_i \qquad \textbf{Eq. 8.2}$$

$$\sum_{i=1}^{k} F(\xi_i, \eta_i, \zeta) w_i \qquad \textbf{Eq. 8.3}$$

The weight factor of the integration points for 6-noded elements is 0.333 and the volume is equally divided between the stress points. For 15-noded elements *w* holds three different values for the 12 stress points and these are listed in Table 4.

The volume of each element is found in the *Mesh* drop-down menu of PLAXIS Output. The overview of which elements have been assigned volume strain is found in the *User-defined parameters* table in the *Stresses* drop-down menu.

[2] As the regarded soil configuration is made in 2D, depth is made 1 meter

Table 4: weight factors for the 12 gauss points in 15-noded elements (Brinkgreve, Swolfs, & Engin, Plaxis 2D Scientific Manual, 2011).

Element stress points	w
1-3	0.050845
4-6	0.116786
7-12	0.082851

Table 5: Tube definition with and without a soil cluster and performed both with 6-noded and 15-noded elements.

	6-noded elements	15-noded elements
Without cluster	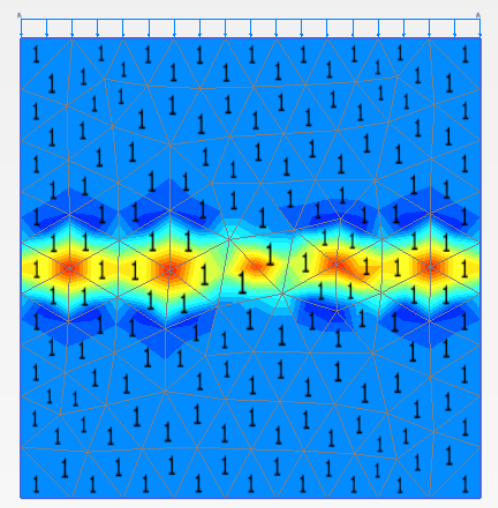	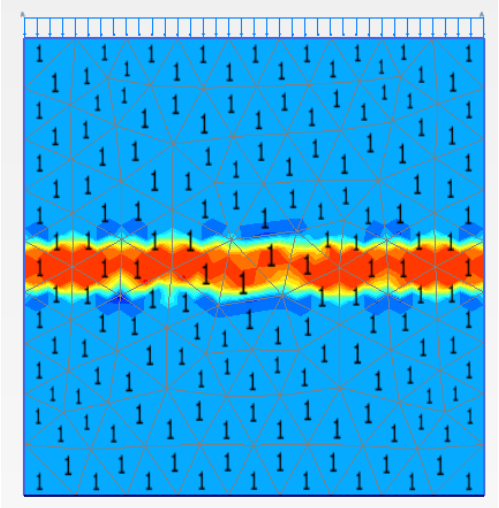
With cluster	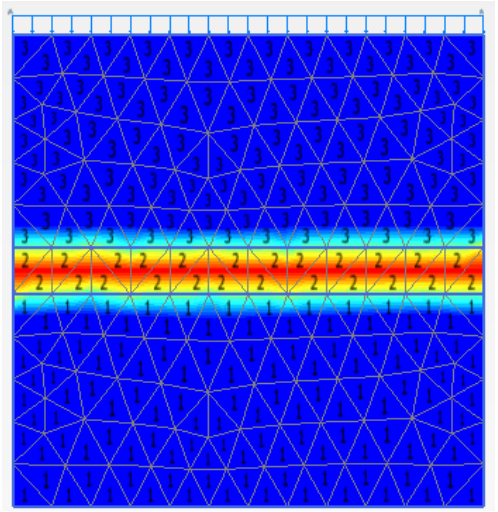	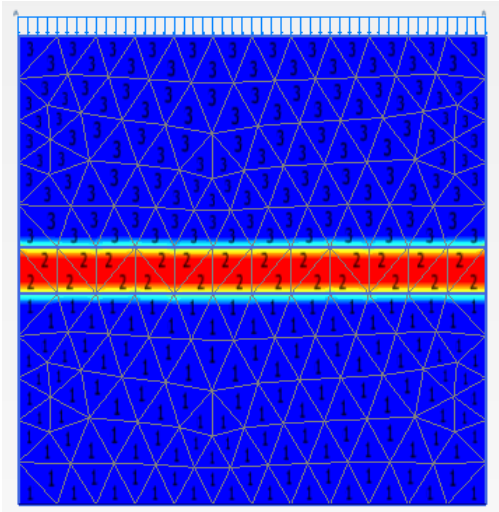

8.3.2 Elastic radius size

In the volume strain file one have to specify the elastic radius where the soil is supposed to react elastic when being extracted. What has been tested in this context is if it is beneficial for the calculation procedure to make the elastic radius larger than the tube radius, this because it was initially guest that it would be so.

For a tube radius of 0.084 meters and a volume strain equal 1, five different values of the elastic radius have been tested: 0.084, 0.094, 0.1, 0.94 and 1.4. Results gave that the calculations performed with an elastic radius greater than the tube radius needed more time to finish than the calculation performed with the elastic radius equal the tube radius. For the test using an elastic radius of 1.4 meters the calculation was not even able to finish as accuracy conditions were not reachable.

8.3.3 Choice of value for the over-relaxation factor

The technique of over-relaxation is often used in order to improve the iteration procedure of PLAXIS in the form of reducing number of iterations used for convergence. An illustration of this is given in Figure 17 a and b which show a case where it is beneficial for the iterative process to use an over relaxation factor greater than 1.

The degree of over relaxation is controlled by the over relaxation factor, ω which can be between 0 and 2 (Vermeer & van Langen, Soil collapse computations with finite elements, 1989). A factor of 1 means that there is no over relaxation, as is illustrated in Figure 17 a. Values above 1 means there is over relaxation, as is illustrated in Figure 17 b, and values below 1 means there is under-relaxation. By default the factor is 1.2 in PLAXIS.

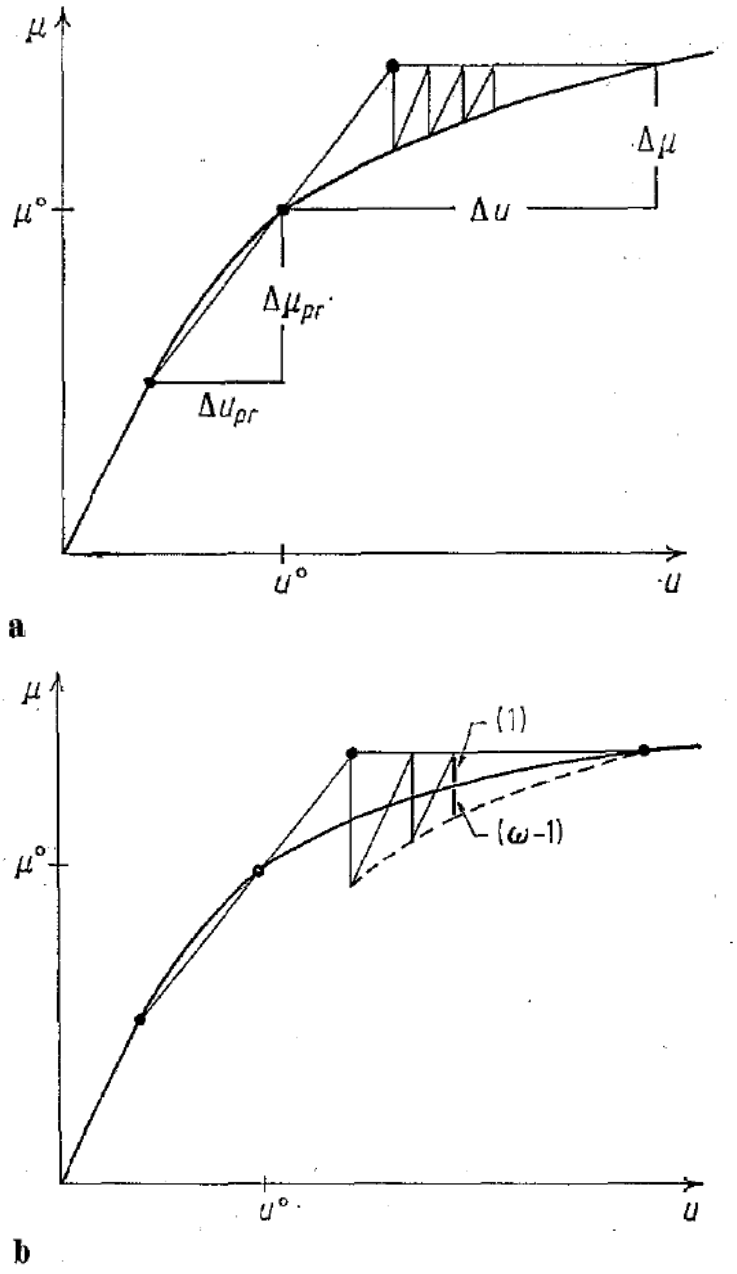

Figure 17: Load-displacement curves illustrating in a: a over relaxation factor of 1 and in b: a over relaxation factor greater than 1.

Time has been the main challenges throughout the work on implementing the volume strain procedure in the ACM. Complex analysis using a very high amount of elements is time consuming and in order to decrease the time consumption in the best possible way the over relaxation factor has been assessed.

The different over relaxation factors have been tested with PLAXIS 3D with tube radiuses equal the elastic radius of 0.084 meters and a volume strain of 0.5. Results from this part of the testing are shown in Table 6.

As can be seen in Table 6, it is time beneficial for this calculation to use a high over-relaxation factor because then the total amount of steps needed for calculation is low. Using a factor that is too high has the opposite effect because then the calculation is not able to converge and the kernel encounters severe divergence problems.

Table 6: Results from calculations performed on a 2.83 GB processor using different over relaxation factors and $\varepsilon_V = 0.5$

Over-relaxation factor	**0.5**	**1.0**	**1.2**	**1.3**	**1.4**	**1.5**	**1.8**
Realized end time	1.0 days	1.0 days	1.0 days	1.0 days	1.0 days	1.0 days	-
Mesh	Coarse	Coarse	Coarse	Coarse	Coarse	Coarse	Coarse
Total amount of steps	1404	715	708	717	370	370	Severe divergence

8.3.4 Mesh refinement

One of the main goals for this thesis has been to develop a method for under-excavation that is more accurate then earlier methods. The number of elements and the element size is an important aspect in relation to accuracy, because if the geometrical features, which in this case are 41 tubes, are much smaller than the average element size, the mesh resolution will not be able to adequately capture them and the results become inaccurate.

In order to clarify the effect of mesh refinement, analysis with different refinements have been run and results from these have been compared based on reached levels of volume extraction. The total volume extracted in 2000 was 37.699m^3 and it is necessary to obtain an equivalent value by numerical analysis if this is to be used as an adequate tool.

Table 7 displays obtained volume change for different mesh refinements and these numbers have been found in the same way as was described in Chapter 8.3.1, but now Eq. 8.3, which is the numerical integration over volumes, has been used with function F now being a function of a third position factor, ζ.

The basic soil elements of the 3D finite element mesh are the 10-noded tetrahedral elements. These elements hold 4 stress points with integration point weight, *w* of 0.25 so each stress point is assigned ¼ of the element volume (Brinkgreve, Swolfs, & Engin, Plaxis 3D Reference manual, 2012).

Table 7: Obtained volume change for analysis using 5 different mesh refinements.

Mesh refinement	Nr. of soil elements	Nr. of nodes	Average element size (m)	Obtained volume change (m^3)	Deviation from correct value (m^3)	Efficiency[3] (%)
Very fine	109694	157128	0.2188	37.514	-0.155	100
Fine	44246	64812	0.3445	39.647	1.978	95
Medium	16493	24989	0.5642	36.660	-1.009	97
Coarse	5035	8030	1.021	40.041	2.372	94
Very coarse	2317	3877	1.51	44.093	6.424	85

Table 7 indicates that it is necessary to use a fairly fine mesh in order to obtain an accurate volume extraction, but one does not have to use the finest mesh refinement available since both the fine and medium refinement attain good results. This is time beneficial.

In Appendix E-1 an illustration accompanying Table 7 is given of how decisive the choice of mesh is. From these figures it becomes clear that choosing a coarse mesh can result in fairly inaccurate tube locations. This is very unfortunate when tube

[3] See Eq. 3

location is particularly determining for the results on the rotation of the Tower, as described by Leoni (2006).

8.3.4.1 Graphical versus true output

The output displayed in Appendix E in general, is output of the state variable 34, which contains prescribes volume strain. What is important to be aware of in this connexion is that PLAXIS gives graphical output only on nodal point level and not on gauss point level. It calculates based on gauss point input, but for the graphical output the volume strain input assigned each gauss point is distributed to a nearby nodal point. A consequence of this is that the graphical value of StVar0(34) can be of a much smaller value than the real input value. An example of this is shown in Figure 18 where the true value of StVar0(34) is 0.5 and the displayed value in PLAXIS Output is only 0.3020.

Figure 18: Illustration on how the graphical value of StVar0(34) is different from the real input value which is used for calculations. Here for 41 tubes with radius = 0.084 and a mesh consisting of 109694 elements and 157128 nodal points.

The tests described in the latter were run with prescribed tube radiuses adjusted for a volume strain of 0.5. The element size effect has also been tested using the true tube radius for the 41 tubes which is 0.084 meters.

Table 8 compares the number of elements appointed volume strain for the calculation using true radiuses and for calculation using adjusted radiuses. It is made clear that the tube section with the true tube radiuses involves geometry features that are not well captured by the mesh resolution and far fewer elements are used in the volume strain procedure. The total volume extracted when using adjusted radiuses is 37.514 m^3 which is approx. 100% accurate, while when using true radiuses it is only 1.959 m^3 which is only 5 % accurate.

Table 8: Total number of soil elements appointed volume strain for different meshes and two different tube sections

Average element size	Elements appointed volume strain using a tube section with true tube radiuses, r = 0.084	Elements appointed volume strain using a tube section with adjusted radiuses, r varies
0.2188	**156**	**1209**
0.3445	**65**	**487**
0.5642	**19**	**104**
1.021	**6**	**91**
1.51	**4**	**67**

An illustration of how many fewer elements were appointed volumetric strain when using true tube radiuses is shown in Appendix E-2. Eventhough the accuracy is far below the desirable level one can still see how it is drastically increased through each increase in number of finite elements.

8.3.4.2 Result efficiency and up-scaling procedure

How well the numerical analysis is able to capture the correct volume for extraction based on the average element size used, can be assessed by viewing the efficiency of the different mesh refinements. Efficiency is found by using Eq.3

$$Efficiency = \frac{\Delta V_{wanted}}{\Delta V_{extracted}} \qquad \textbf{Eq. 8.4}$$

Here ΔV_{wanted} is the theoretically correct volume that should be extracted from the tube whit the given ε_V and $\Delta V_{extracted}$ is the volume which is actually extracted in the FEM analysis.

For the results shown in Table 9 only one tube has been analyzed and illustrations are found in Appendix E-3. This is done in order to see how well the accuracy of the tube section accompanies the accuracy of each single tube. The middle tube in the tube section has been used with the enlarged radius of 0.3454 meters adjusted for a volume strain of 0.5. The length of this tube is 5 meters and thus has a volume of 1.874 m^3. Wanted volume change is 0.937 m^3 and from the results one can see that by using both an average element size of 0.2188 meters and 0.3445 meters one obtain the same accuracy as was done when using the whole tube section. This vaguely indicates that when the resulting accuracy from using 41 tubes is good, this is a result of 41 accurate tubes and not a sum made up by inaccurate tubes that accidentally compliments one another into something that seem accurate.

Table 9: Obtained soil extraction for different mesh refinements, using one tube.

Mesh refinement	Nr. of soil elements	Nr. of nodes	Average element size (m)	Obtained volume change m^3)	Deviation from correct value (m^3)	Efficiency (%)
Very fine	109694	157128	0.2188	0.9463	0.009	99
Fine	44246	64812	0.3445	0.9835	0.046	95
Medium	16493	24989	0.5642	0.4589[4]	-0.478	49
Coarse	5100	8115	1.015	1.051	0.114	87
Very coarse	2317	3877	1.51	1.469	0.532	57

What Table 9 can also be used for is to upgrade the efficiency result by up scaling the tube radius which includes decreasing the volume strain. If one for instance focuses on the mesh including an average element size of 1.015 meters, this only gives an obtained accuracy of 87 %. If one wants to keep the average element size but increase the efficiency, for instance to 95 %, this is feasible if the up-scaling procedure is run. This procedure assumes that the relationship between the tube radius and the efficiency value is proportional and Eq. 4-6 applies.

$$r_2 = \frac{r_1 \times Eff_{wanted}}{Eff(r_1)} \qquad \textbf{Eq. 8.5}$$

$$V_{tot} = {r_2}^2 \times \pi l \qquad \textbf{Eq. 8.6}$$

$$\varepsilon_V = \frac{V_{tube}}{V_{tot}} \qquad \textbf{Eq. 8.7}$$

[4] This value would expectedly be more accurate than values from the coarser mesh refinements and it is probably incidental that the stress points are arranged in such a way that much too less volume is extracted.

Results from the recalculation with the average element size of 1.015 meters are given in Table 10.

Table 10: Values used in the calculation of Eq. 5-7 and values obtained by these equations.

Already known:	r_1 (previous radius)	0.3454 m
	Eff(r_1) (previously obtained efficiency)	87 %
	Eff_{wanted} (wanted efficiency)	95 %
	l (length of tube)	5 m
	V_{tube} (volume of the tube using r_2)	2.234 m^3
Obtained by Eq. 5-7:	r_2 (new radius)	0.3771 m
	V_{tot} (volume extracted)	0.937 m^3
	ε_V	0.42

Writing the new tube radius and volume strain in the volume strain_DAT file and running the analysis again gives a new efficiency of 94% which is close to the wanted value of 95 %.

9 3D-calculation of the Tower

The latest model of the Pisa Tower has been modeled by M. Leoni and is a development of the 3D full Tower model that was presented by Leoni and Vermeer in 2006.

The latter model only considered half of the symmetrical Tower cylinder in order to reduce the computational time. The new model is circular and the modeled Tower geometry resembles the true geometry in a much more detailed way as is illustrated in Figure 19.

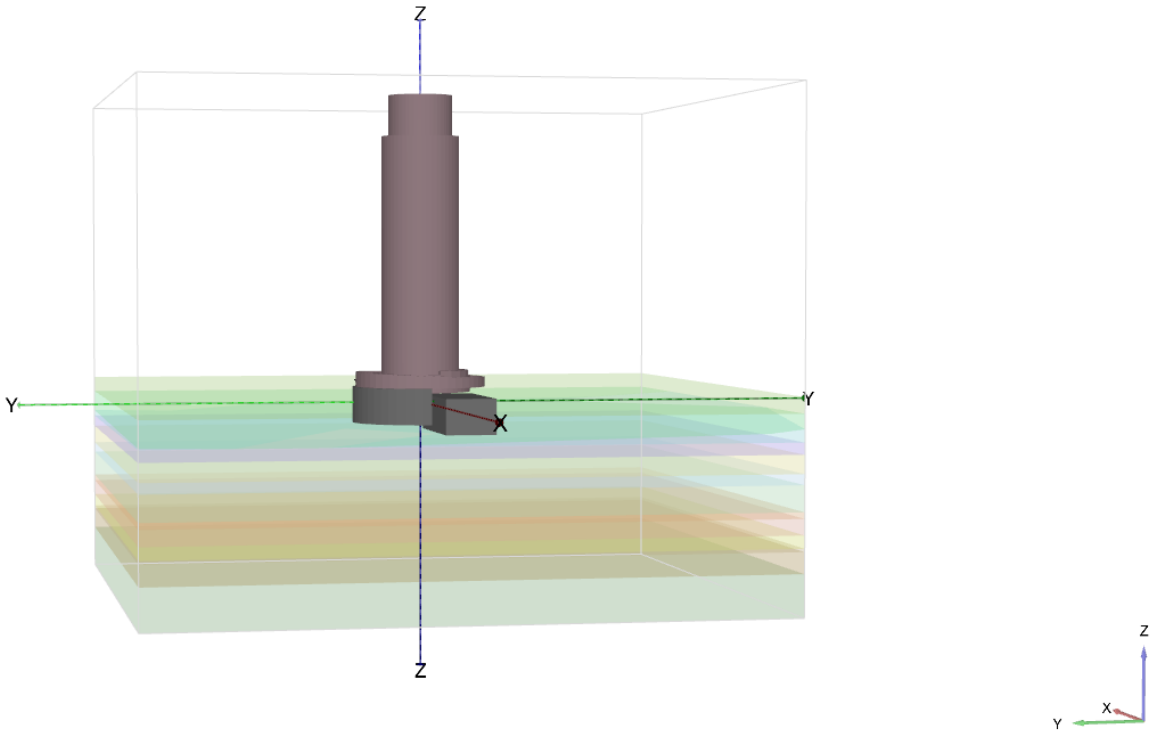

Figure 19: Illustration of the Tower made for full 3D analysis

The soil layering of the new model is the same as before, with one exception; previously the silty sub-layer in Horizon A was separated into a north part and a south part by a sharp transition which has not been satisfying. In this model the transition has been made more smoothly due to the use of the borehole application in

PLAXIS 3D. This application makes it possible to enter layer information that is not connected to a specific cluster, but a defined point. For the areas which have not been appointed a material the program assigns material by interpolating between the given points making this smooth transition between the layers. A table showing the soil layering and the location of boreholes for the final Tower model is enclosed in Appendix F-1.

The full Tower model analysis has been performed on a 2.40 GHz Intel Core Quad processor equipped with 8 GB RAM on a 64 bit system and it has proven to be a very time demanding process which has not been able to finish within the time boundaries of this thesis. When this work is being printed the analysis has been running for three weeks and the calculation has only reached phase 12. The part of the construction that has been calculated is illustrated in Figure 20 and attained results from the calculated parts are given in Appendixes G-1 to G-5. The results added in the appendix is the excess pore pressure situation for phase 12, the vertical and horizontal effective stress situations for phase 12, total vertical displacement, incremental vertical displacement for phase 12, total volumetric strain, incremental volumetric strain for phase 12 and total displacements of each phase.

What one needs to be aware of in relation to viewing the results is that when the analysis was stopped it was discovered that results are given for a load situation that is not entirely correct. The foundation and the first construction phase have been executed at the same time, which gives a basic stress condition for the first construction phase that should differ from the case where the foundation is constructed first and then followed by a consolidation phase – which is the real case. Also no stress points had been chosen before the calculation and thus the yielding results displayed in the appendix are somewhat amputated. Had there been time, these mistakes would have been corrected, but as the calculation was kept active for as long as possible, they were not discovered in time.

What can though be concluded by watching the results in Appendix G-5 is that the Tower is responding in a realistic way as it is rotating in the right direction which is to the north. As is described in Figure 4, in Chapter 4.1 the Tower was inclining northwards up until the 6th cornice was built. What are not as realistic are the

generated settlements underneath the Tower. They are too large and must be examined in future analyses.

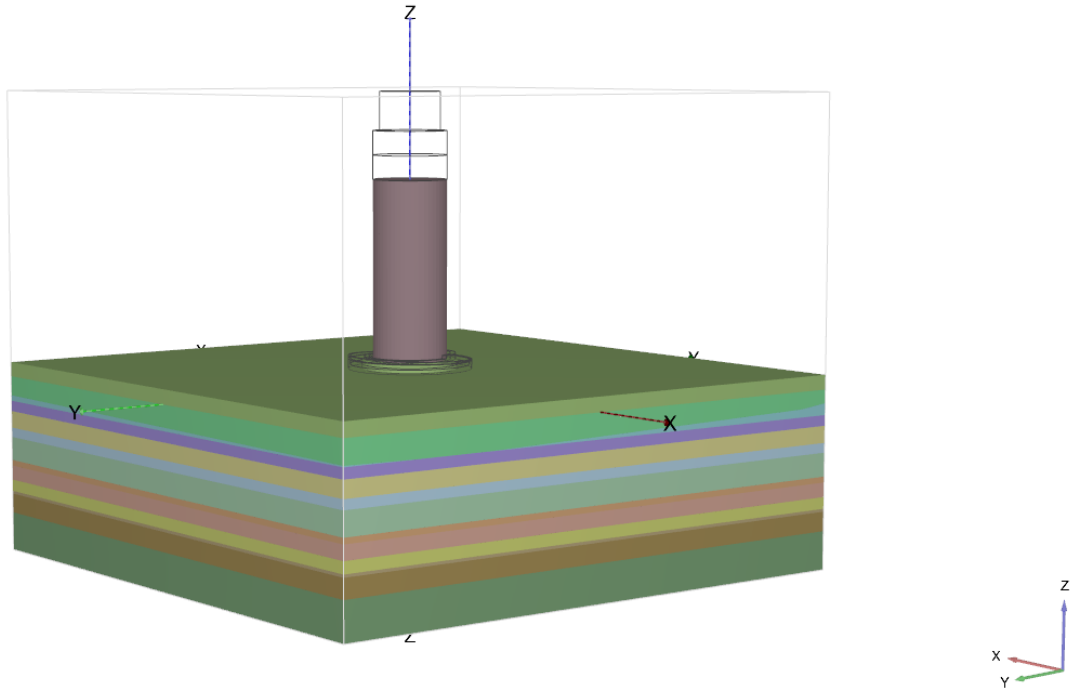

Figure 20: Illustration of how far analysis of the full 3D model of the Tower had come before had to be stopped.

9.1.1 Future work

Considering that the full 3D Tower model with internal material models was not able to finish within the time limits of this thesis an obvious mission would be to finish the calculation of this model. Stronger computers are available and so one should try to run the calculation on a stronger processor to see if this can reduce the computational time. If this is successful one should try to implement the external SSCM and compare these results. Next step would be to keep the external material model and implement the new under-excavation method to see how this affects the Tower behavior.

At the moment an accurate completion of the under-excavation procedure is not obtainable. The reason for this is that it has become clear during testing that the new

under-excavation method only works well when the soil geometry at the beginning of the under-excavation phase has not been deformed and is the same as the reference configuration. This will not be the case when the routine is implemented in the Tower model; by the time the under-excavation is activated the geometry has changes about 3 meters compared to the reference geometry and it is therefore important that the coordinates of the stress points are updated when the mesh is set to update. This is not a function in the existing version of PLAXIS and therefore the procedure will not function as accurate as one would expect. This shortcoming has been reported to PLAXIS and the updated coordinates of the stress points will be implemented in the next released version of PLAXIS 3D

Through testing the true time aspect has not been considered. As the procedure is to be implemented in the full Tower model it needs to be adjusted time vise in order to run correctly. Since it is only the final excavation that is being considered in this thesis the total excavation time is one year, as it was carried out between February 2000 and February 2001. The phases that should be run in a full 3D analysis of the Tower are listed in Appendix F-2. Summing up the previous phases before the under-excavation one finds that the starting time for the under-excavation is day 301829 and end time is day 302194 - after construction commencement. Thus *time0* is 301829 and *dtime* – which is the time interval - is 365 days. The volume change step is still equal 1. The new version of the code, which is previously shown in Box 3, is emphasized in yellow in Box 6 and should be include in the code for the full 3D-model of the Tower.

```
!if(time0 .GE. 301829. AND. Time0 .LT. 302194.) then
   if (StVar(34) .GT. 0.) then
     dMStage = Sig0(9)-Sig0(8)
     dEpsVol(1:3) = StVar0(34)/3.*dTime/365. !Volume change step = 1
```

Box 5: Time confinement adjusted for use in the real boundary value problem.

Finally one should also evaluate the part of the code where the stress points are located and assigned volume strain. Up until now the procedure has been run from the first phase. One should consider adjusting this frame and postponing the search to a later phase.

10 Summary

The prime goal of this thesis has been to test a new approach to model the under-excavation of the Leaning Tower of Pisa in a classical large strain analysis and if time implement the procedure in a Full 3D-model of the leaning Tower. In order to reach that goal testing has been performed in two phases; an optimization part and a full Tower analysis part.

Tests executed in order to optimize the under-excavation procedure have used a simplified case of soil geometry and loads, and results from these tests show that the method is sensitive to the choice of mesh refinement. Tests conducted with large average element sizes of 1.021 meters and 1.51 meters have only been able to capture 85-94% of the true amount of volume extraction, as for average element sizes of 0.5642 meters, 0.3445 meters and 0.2188 meters the procedure has been able to extract 95-100%.of the exact volume. This is though dependent on the size of the tube configuration in use. The new method does not honestly reproduce the course of the true under-excavation process and each tube has been enlarged compared to the original size. In relation to what is mentioned above the tube modification has proven to be beneficial as it is geometrically larger than the true configuration and thus easier to capture with the available element size. Results show that when using true tube radiuses and smallest average element size one can only obtain an accuracy of 5 % in terms of extracted volume, while when using true radiuses and the same average element size the obtained volume extraction is approx. 100 % accurate. It has in this context also been shown that the accuracy of the tube configuration is a result of the accuracy provided by each tube as each tube obtains similar accuracy as the tube configuration in relation to different mesh refinements.

The previous used method for soil extraction has been performed by applying certain elements volume strain. This procedure is cluster based, but since the new approach is not the effect of not using area boundaries has been tested. Results from 2D-simulations indicate that it is more time demanding to run the volume extraction in an undefined area. Also there is a small accuracy difference as one with a predefined geometrical extraction area is able to extract with 100 % accuracy while with an undefined area one is only able to obtain 97 % accuracy. Further it is made clear that

element type is an important factor in relation to accuracy. This statement is based on results from the comparison of 6-noded elements and 15-noded elements with no geometrically defined extraction area. Using an average element size of 0.7857 meters the soil extraction performed with 15-noded elements obtained total volume extraction accuracy of 97 % while the 6-noded elements obtained an accuracy of 86 %. Considering these results it is evident to draw lines to the utilization of 10-noded elements in the 3D-version of PLAXIS and to indicate that some of the accuracy is lost by switching to the 3D-version and that it will be necessary to use a finer mesh in order to obtain the same accuracy as for analysis using 15-noded elements.

A way to reduce the mesh refinement without having to sacrifice the result accuracy can be to increase the tube radius and thus decrease the volume strain. This has been tested and what has been proven is that by using this up-scaling procedure one is able to increase the accuracy of the obtained volume extraction for a coarse mesh analysis by 8 %. This has so far only been proven for a single tube and needs to be assessed further since the tube section has been applied dissimilar radiuses.

As the procedure is to be implemented in a complex model, different features have been assessed in order to decrease time losses were it is possible. Herein the over-relaxation factor has been considered and from these tests it has been found that a high over-relaxation factor of 1.3-1.5 is beneficial for the calculation performance. In the same context the value for the prescribed elastic tube radius has been examined and results show that it is most beneficial to give the elastic radius the same value as the tube radius and not to increase it as was firstly assumed.

Last but not least the full 3D-Tower model has been analyzed, but as the model was not available until the last months of this work it did not finish calculating in time. What can be seen from the results so far is that the tower is inclining in the right direction and it is experiencing too much settlement. As this work has not been completed yet it is up to future explorers to finish it and further implement the external soft soil creep model and run the full Tower model with the implemented under-excavation procedure.

11 References

Brinkgreve, R. B., Swolfs, W. M., & Engin, E. (2011). Plaxis 2D Scientific Manual. I R. B. Brinkgreve, W. M. Swolfs, & E. Engin, *Plaxis 2D 2010* (ss. 615-679). The Netherlands: Plaxis bv.

Brinkgreve, R. B., Swolfs, W. M., & Engin, E. (2012). Plaxis 3D Reference manual. I R. B. Brinkgreve, W. M. Swolfs, & E. Engin, *Plaxis 3D 2011* (ss. 104-376). The Netherlands: Plaxis bv.

Burland, J. B. (1998, December 9). *The enigma of the leaning tower of Pisa.* George Bush Presidential Conference Centre, College Station, Texas, USA.

Burland, J. B., & Viggiani, C. (1994, 3). Observazioni sul compartamento della Torre di Pisa. *Rivista Italiana di Geotecnica* , ss. 179-200.

Burland, J. B., Jamiolkowski, M. B., & Viggiani, C. (2009, July 01). Leaning Tower of Pisa: Behaviour after Stabilization Operations . *International Journal of Geoengineering Case Histories* , ss. 156-169.

Burland, J., Jamiolkowski, M., & Viggiani, C. (1998). Stabilizing the leaning tower of Pisa. *Bulletin of engineering geology and the environment, vol. 57, no. 1* , 91-99.

Burland, J., Jamiolkowski, M., & Viggiani, C. (2003, October). The stabilization of the leaning tower of Pisa. *SOILS AND FOUNDATIONS, Vol 43, NO. 5* , ss. 63-80.

Leoni, M., & Vermeer, P. A. (2002). *3D creep analysis of the Leaning Tower of Pisa.* Stuttgart: Institute of Geotechnical Engineering Stuttgart.

Leoni, M., & Vermeer, P. A. (2006). *3D creep analysis of the Leaning Tower of Pisa.* Stuttgart: Institute of Geotechnical Engineering Stuttgart.

Leoni, M., Karstunen, M., & Vermeer, P. A. (2006). Anisotropic creep model for soft soils. *Gèotechnique vol. 53, No. 3* , ss. 215-226.

Leroueil, S. (2001). Some fundamental aspects of soft clay behavior and practical implications. I L. e. al, *Soft soil engineering* (ss. 37-53). The Netherlands: Swets & Zeitlinger.

Neher, H. P., Wehnert, M., & Bonnier, P. (u.d.). *An evaluation of soft soil models based on trail embankments.* Hentet mars 25, 2012 fra http://www.unistuttgart.de/igs/content/publications/60.pdf

Nordal, S. (2011). *TBA4116 Geotechnical Engineering, Advanced Cource.* Trondheim: Norwegian University of Science and Technology, Geotechnical division.

Potts, D. (1993). *Calibrazione di un modello geotecnico agli elementi finiti e valutazione degli effetti indotti a seguito di alcuni interventi di consolidamento della torre di pisa.* London: G C G computing, Geotechnical analysts.

Smart, A. (2010, July 28). *Solving the 800-year mystery of Pisa's Leaning Tower.* Hentet April 23, 2012 fra http://www.telegraph.co.uk/culture/art/architecture/7907298/Solving-the-800-year-mystery-of-Pisas-Leaning-Tower.html

Squeglia, N., & Viggiani, C. (2005). Gli interventi di stabilizzazione definitiva. I V. e. al, *LA TORRE DI PISA. Gli studi e gli interventi che hanno consentito la stabilizzazione della Torre di Pisa* (ss. 155-178). Bollettino d'arte, Ministero per i Beni e le Attività Culturali.

Towerofpisa.info. (2012). *Tower of Pisa - historical facts.* Hentet march monday, 2012 fra http://www.towerofpisa.info/Tower-of-Pisa-historical-facts.html

Vermeer, P. A., & Neher, H. P. (1999). *A soft soil model that accounts for creep.* Rotterdam: Balkema.

Vermeer, P. A., & van Langen, H. (1989). Soil collapse computations with finite elements. *Archive of Applied Mechanics Vol. 59* , ss. 221-236.

Viaggi, 6. (u.d.). *Pisa, et la Piazza dei Miracoli.* Hentet April 15, 2012 fra http://6suviaggi.com/viaggi/160/pisa-e-la-piazza-dei-miracoli/

APPENDIX

Appendix A

1. Schematically overview of boreholes for the preliminary under-excavation
2. Schematically overview of boreholes for the final under-excavation

Appendix B

1. Soil parameters for the Soft Soil Creep Model and the Mohr Coulomb model
2. Description of available soil parameters in the user-defined ACM

Appendix C

1. List giving the location of each borehole with requested radius and volume strain - used for testing
2. List giving the location of each borehole with requested radius and volume strain- used for the final tower model

Appendix D

1. Procedure implemented in the ACM code to locate gauss points

Appendix E

1. Elements applied volume strain displayed with different mesh refinements – 41 intersecting tubes
2. Elements applied volume strain displayed with different mesh refinements – 41 tubes with original tube size
3. Elements applied volume strain displayed with different mesh refinements – 1 tube

Appendix F

1. Soil layering and the location of boreholes for the final tower model
2. Phases

Appendix G

1. Excess pore pressure and vertical effective stresses – phase 12
2. Horizontal effective stresses, σ'_{yy} and σ'_{xx} – phase 12
3. Total vertical displacements and incremental displacements for phase 12
4. Total volumetric strain and incremental volumetric strain for phase 12
5. Total displacement considering each analyzed phase, color scale and arrows

Appendix A

1. Schematically overview of boreholes for the preliminary under excavation
2. Schematically overview of boreholes for the final under excavation

Schematically overview of boreholes for the preliminary under-excavation

Distanza	PERFORAZIONE											
from ÷ to	6W	5W	4W	3W	2W	1W	1E	2E	3E	4E	5E	6E
13.4÷13.9					6 2 **20**	14 1 **14**	14 1 **14**					
13.9÷14.4					6 2 **20**	14 1 **14**	14 1 **14**					
14.4÷14.9					14 1 **14**	14 1 **14**	13 1 **13**					
14.9÷15.4					14 1 **14**	14 1 **14**	13 1 **13**					
15.4÷15.9	6 3 **29** 0.8	3 2 **16** 0.7	14 1 **14** 1.2	10 3 **35** 1.0	12 3 **40** 1.2	1 5 **32** 0.6	10 3 **34** 1.0	13 3 **36** 1.1	14 1 **14** 1.2	13 1 **13** 1.1	5 3 **24** 0.7	9 2 **20** 0.9
15.9÷16.4	6 3 **29** 0.8	3 2 **16** 0.7	14 1 **14** 1.2	10 3 **35** 1.0	12 3 **40** 1.2	1 5 **32** 0.6	10 3 **34** 1.0	13 3 **36** 1.1	14 1 **14** 1.2	13 1 **13** 1.1	5 3 **24** 0.7	9 2 **20** 0.9
16.4÷16.9	5 16 **126** 0.7	5 15 **96** 0.6	7 14 **120** 0.8	3 13 **94** 0.6	8 16 **131** 0.7	7 12 **82** 0.6	3 13 **89** 0.6	5 14 **133** 0.8	5 11 **87** 0.7	4 14 **102** 0.6	7 15 **115** 0.7	5 15 **114** 0.7
16.9÷17.4	5 15 **120** 0.7	5 16 **102** 0.6	7 15 **128** 0.8	3 12 **80** 0.6	7 18 **117** 0.6	7 11 **68** 0.5	3 12 **66** 0.5	0 16 **110** 0.6	5 12 **94** 0.7	4 15 **106** 0.6	7 15 **111** 0.7	5 16 **106** 0.6
17.4÷17.9	5 15 **121** 0.7	7 16 **109** 0.6	8 15 **128** 0.8	7 12 **95** 0.7	7 20 **139** 0.6	8 11 **88** 0.7	2 12 **82** 0.6	0 18 **133** 0.7	5 12 **103** 0.8	4 15 **113** 0.7	8 15 **116** 0.7	5 16 **116** 0.6
17.9÷18.4	4 11 **81** 0.7	7 14 **99** 0.6	8 12 **98** 0.7	7 12 **93** 0.7	8 20 **136** 0.6	3 11 **82** 0.7	4 11 **67** 0.5	0 19 **126** 0.6	5 12 **93** 0.7	4 12 **85** 0.6	8 14 **106** 0.7	7 13 **100** 0.7
18.4÷18.9	4 6 **48** 0.7	8 7 **68** 0.9	8 7 **60** 0.8	8 7 **64** 0.8	7 11 **89** 0.7	3 6 **47** 0.7	4 6 **39** 0.6	5 12 **83** 0.6	5 7 **54** 0.7	4 7 **45** 0.6	10 7 **67** 0.8	7 6 **42** 0.6
18.9÷19.4	4 3 **21** 0.6	8 4 **33** 0.7	8 4 **36** 0.8	8 4 **40** 0.9	10 7 **62** 0.8	4 3 **21** 0.6	9 3 **24** 0.7	3 7 **48** 0.6	5 4 **28** 0.6	5 4 **25** 0.6	10 4 **33** 0.7	8 3 **25** 0.7
19.4÷19.9					9 2 **18** 0.8			9 2 **18** 0.8				
Tot. per foro	**573**	**537**	**597**	**535**	**771**	**449**	**434**	**722**	**485**	**499**	**595**	**541**

Volume Totale **6.910** **m³**

Aggiornato al 4/6/1999 ore 16.30

LEGENDA: A B C D

A: final extraction (dm^3), **B**: number of extractions, **C**: volume extracted, **D**: efficiency

(D=C/B/Total volume) (Squeglia 2006)

Schematically overview of boreholes for the final under-excavation

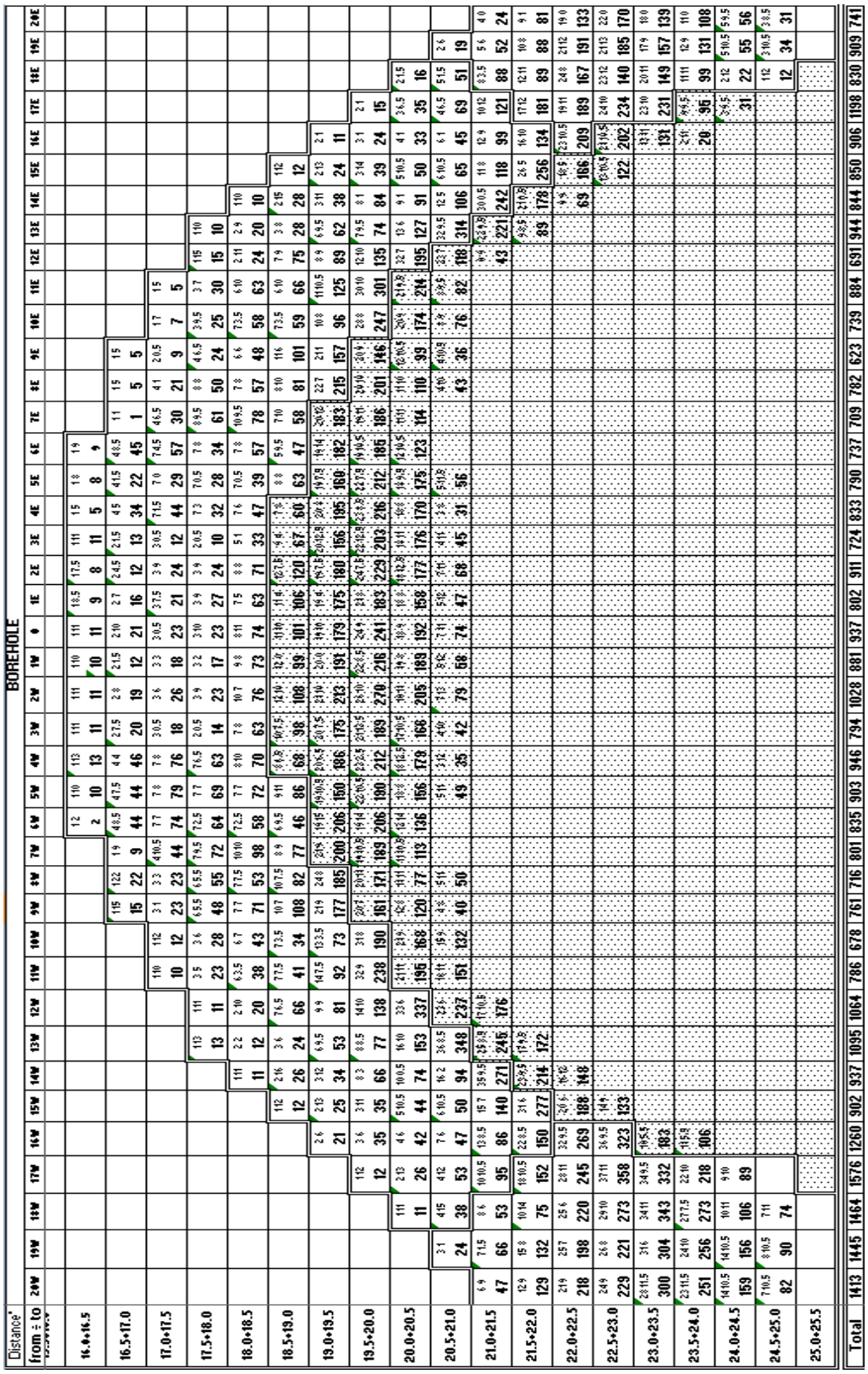

x - y
z

x: number of extractions, **y**: last extraction (dm^3), **z**: total extraction (dm^3)

Version from 6/06/2001 (Squeglia 2006). (*)Upper edge of the white tubes (end of perforation) is taken as reference for the distances

Appendix B

1. Soil parameters for the Soft Soil Creep Model and the Mohr Coulomb model
2. Description of available soil parameters in the user-defined ACM

Soil parameters for the Soft Soil Creep Model and the Mohr Coulomb model

SSCM Layer	**ϒ*** *(kN/m^3)*	**λ** *(-)*	**κ*** *(-)*	**μ*** *(-)*	**ν'** *(-)*	**ϕ** *(deg.)*	**POP** *(kN/m^2)*	**k** *(10^{-10} m/s)*
A1N	19.1	0.045	0.0045	0.0015	0.15	34.0	140	10000
A1S	19.1	0.085	0.0085	0.00283	0.15	34.0	140	10
B1	17.3	0.15	0.015	0.005	0.15	26.0	70	5
B2	17.8	0.12	0.012	0.004	0.15	26.0	50	5
B3	16.7	0.15	0.015	0.005	0.15	26.0	50	5
B4	20.0	0.07	0.007	0.0023	0.15	28.0	130	2
B5	20.0	0.07	0.007	0.0023	0.15	28.0	200	2
B7a	19.6	0.1	0.01	0.0033	0.15	27.0	70	5
B7b	17.8	0.12	0.012	0.004	0.15	27.0	70	5
B8/B9/B10	19.0	0.1	0.01	0.0033	0.15	25.0	70	3

MCM Layer	**ϒ*** *(kN/m^3)*	**E** *(kPa)*	**ν'** *(kPa)*	**ϕ** *(deg.)*	**c'** *(kPa)*	**ϑΨ** *(deg.)*	**k** *(10^{-10} m/s)*
MG	18.0	7000	0.33	34.0	20.0	0.0	100000
A2	18.2	13700	0.33	34.0	0.0	0.0	100000
B6	19.1	11600	0.33	34.0	0.0	0.0	100000

Description of available soil parameters in the user-defined ACM

Parameter	Description	*Parameter*	Description
ϕ	Friction angle	a	Destructuration factor
c'	Cohesion	b	Destructuration factor
Ψ	Dilatency angle	χ_0	Destructuration factor
λ^*	Modified compression index	ω	Rate of rotation
κ^*	Modified swelling index	ω_d	Rotation parameter
v'	Effective Poisson's ratio	ϕ_{MC}	Friction angle (Mohr Coulomb)
μ^*	Modified creep index	K_0^{NC}	Initial earth pressure coefficiant
τ	Referance time	G_0^{ref}	Reference shear modulus at very small strain ($\varepsilon<10^{-6}$)
OCR	Over-consolidation ratio	$\gamma_{0.7}$	Shear strain for a secant shear modulus, $G_s = 0.772G_0$
POP	Pre-overburden pressure	σ_{02}	Vertical stress used as input for soil test analyses

Appendix C

1. List giving the location of each borehole with requested radius and volume strain. Used for testing
2. List giving the location of each borehole with requested radius and volume strain. Used for the final tower model

List giving the location of each borehole with requested radius and volume strain - used for testing

A_X	A_Y	A_Z	B_X	B_Y	B_Z	r_{tube}	$r_{elastic}$	ε_V
19.7	10.0	-4.2	23.5	10.0	-5.6	0.346	0.346	0.5
19.3	-9.5	-4.0	23.5	-9.5	-5.6	0.330	0.330	0.5
18.8	-9.0	-3.8	23.5	-9.0	-5.6	0.315	0.315	0.5
18.3	-8.5	-3.7	23.0	-8.5	-5.4	0.327	0.327	0.5
17.9	-8.0	-3.5	22.6	-8.0	-5.2	0.292	0.292	0.5
17.4	-7.5	-3.3	21.6	-7.5	-4.9	0.261	0.261	0.5
16.9	-7.0	-3.2	21.1	-7.0	-4.7	0.266	0.266	0.5
16.4	-6.5	-3.0	20.7	-6.5	-4.5	0.287	0.287	0.5
16.4	-6.0	-3.0	20.2	-6.0	-4.4	0.300	0.300	0.5
16.0	-5.5	-2.8	19.7	-5.5	-4.2	0.258	0.258	0.5
16.0	-5.0	-2.8	19.7	-5.0	-4.2	0.240	0.240	0.5
15.5	-4.5	-2.6	19.7	-4.5	-4.2	0.239	0.239	0.5
15.5	-4.0	-2.6	19.7	-4.0	-4.2	0.232	0.232	0.5
15.5	-3.5	-2.6	19.3	-3.5	-4.0	0.260	0.260	0.5
15.0	-3.0	-2.5	19.3	-3.0	-4.0	0.251	0.251	0.5
15.0	-2.5	-2.5	19.7	-2.5	-4.2	0.247	0.247	0.5
15.0	-2.0	-2.5	19.7	-2.0	-4.2	0.253	0.253	0.5
15.0	-1.5	-2.5	19.7	-1.5	-4.2	0.232	0.232	0.5
15.0	-1.0	-2.5	19.7	-1.0	-4.2	0.264	0.264	0.5
15.0	-0.5	-2.5	19.7	-0.5	-4.2	0.244	0.244	0.5
15.0	0.0	-2.5	19.7	0.0	-4.2	0.252	0.252	0.5
15.0	0.5	-2.5	19.7	0.5	-4.2	0.233	0.233	0.5
15.0	1.0	-2.5	19.7	1.0	-4.2	0.248	0.248	0.5
15.0	1.5	-2.5	19.7	1.5	-4.2	0.221	0.221	0.5
15.0	2.0	-2.5	19.7	2.0	-4.2	0.238	0.238	0.5
15.0	2.5	-2.5	19.7	2.5	-4.2	0.231	0.231	0.5
15.0	3.0	-2.5	19.3	3.0	-4.0	0.236	0.236	0.5
15.5	3.5	-2.6	19.3	3.5	-4.0	0.245	0.245	0.5
15.5	4.0	-2.6	19.7	4.0	-4.2	0.243	0.243	0.5

List giving the location of each borehole with requested radius and volume strain - used for testing

15.5	4.5	-2.6	19.7	4.5	-4.2	0.217	0.217	0.5
16.0	5.0	-2.8	19.7	5.0	-4.2	0.250	0.250	0.5
16.0	5.5	-2.8	19.7	5.5	-4.2	0.274	0.274	0.5
16.4	6.0	-3.0	20.2	6.0	-4.4	0.242	0.242	0.5
16.4	6.5	-3.0	20.7	6.5	-4.5	0.267	0.267	0.5
16.9	7.0	-3.2	21.1	7.0	-4.7	0.252	0.252	0.5
17.4	7.5	-3.3	21.6	7.5	-4.9	0.253	0.253	0.5
17.9	8.0	-3.5	22.6	8.0	-5.2	0.248	0.248	0.5
18.3	8.5	-3.7	23.0	8.5	-5.4	0.285	0.285	0.5
18.8	9.0	-3.8	23.5	9.0	-5.6	0.237	0.237	0.5
19.3	9.5	-4.0	23.5	9.5	-5.6	0.262	0.262	0.5
19.7	10.0	-4.2	23.5	10.0	-5.6	0.251	0.251	0.5

List giving the location of each borehole with requested radius and volume strain - used for the final tower model

A_{x0}	A_{y0}	A_{z0}	B_Y	B_X	B_Z	r_{tube}	$r_{elastic}$	ε_V
-10.0	-19.7	-2.2	-10.0	-23.5	-3.6	0.474	0.346	0.5
-9.5	-19.3	-2.0	-9.5	-23.5	-3.6	0.452	0.330	0.5
-9.0	-18.8	-1.8	-9.0	-23.5	-3.6	0.432	0.315	0.5
-8.5	-18.3	-1.7	-8.5	-23.0	-3.4	0.448	0.327	0.5
-8.0	-17.9	-1.5	-8.0	-22.6	-3.2	0.401	0.292	0.5
-7.5	-17.4	-1.3	-7.5	-21.6	-2.9	0.357	0.261	0.5
-7.0	-16.9	-1.2	-7.0	-21.1	-2.7	0.364	0.266	0.5
-6.5	-16.4	-1.0	-6.5	-20.7	-2.5	0.394	0.287	0.5
-6.0	-16.4	-1.0	-6.0	-20.2	-2.4	0.412	0.300	0.5
-5.5	-16.0	-0.8	-5.5	-19.7	-2.2	0.354	0.258	0.5
-5.0	-16.0	-0.8	-5.0	-19.7	-2.2	0.328	0.240	0.5
-4.5	-15.5	-0.6	-4.5	-19.7	-2.2	0.328	0.239	0.5
-4.0	-15.5	-0.6	-4.0	-19.7	-2.2	0.318	0.232	0.5
-3.5	-15.5	-0.6	-3.5	-19.3	-2.0	0.357	0.260	0.5
-3.0	-15.0	-0.5	-3.0	-19.3	-2.0	0.344	0.251	0.5
-2.5	-15.0	-0.5	-2.5	-19.7	-2.2	0.339	0.247	0.5
-2.0	-15.0	-0.5	-2.0	-19.7	-2.2	0.347	0.253	0.5
-1.5	-15.0	-0.5	-1.5	-19.7	-2.2	0.318	0.232	0.5
-1.0	-15.0	-0.5	-1.0	-19.7	-2.2	0.362	0.264	0.5
-0.5	-15.0	-0.5	-0.5	-19.7	-2.2	0.335	0.244	0.5
0.0	-15.0	-0.5	0.0	-19.7	-2.2	0.345	0.252	0.5
0.5	-15.0	-0.5	0.5	-19.7	-2.2	0.320	0.233	0.5
1.0	-15.0	-0.5	1.0	-19.7	-2.2	0.341	0.248	0.5
1.5	-15.0	-0.5	1.5	-19.7	-2.2	0.304	0.221	0.5
2.0	-15.0	-0.5	2.0	-19.7	-2.2	0.326	0.238	0.5
2.5	-15.0	-0.5	2.5	-19.7	-2.2	0.317	0.231	0.5
3.0	-15.0	-0.5	3.0	-19.3	-2.0	0.323	0.236	0.5
3.5	-15.5	-0.6	3.5	-19.3	-2.0	0.336	0.245	0.5
4.0	-15.5	-0.6	4.0	-19.7	-2.2	0.333	0.243	0.5

List giving the location of each borehole with requested radius and volume strain - used for the final tower model

4.5	-15.5	-0.6	4.5	-19.7	-2.2	0.297	0.217	0.5
5.0	-16.0	-0.8	5.0	-19.7	-2.2	0.343	0.250	0.5
5.5	-16.0	-0.8	5.5	-19.7	-2.2	0.375	0.274	0.5
6.0	-16.4	-1.0	6.0	-20.2	-2.4	0.332	0.242	0.5
6.5	-16.4	-1.0	6.5	-20.7	-2.5	0.365	0.267	0.5
7.0	-16.9	-1.2	7.0	-21.1	-2.7	0.346	0.252	0.5
7.5	-17.4	-1.3	7.5	-21.6	-2.9	0.347	0.253	0.5
8.0	-17.9	-1.5	8.0	-22.6	-3.2	0.340	0.248	0.5
8.5	-18.3	-1.7	8.5	-23.0	-3.4	0.391	0.285	0.5
9.0	-18.8	-1.8	9.0	-23.5	-3.6	0.325	0.237	0.5
9.5	-19.3	-2.0	9.5	-23.5	-3.6	0.359	0.262	0.5
10.0	-19.7	-2.2	10.0	-23.5	-3.6	0.343	0.251	0.5

Appendix D

1. Procedure implemented in the ACM code to locate gauss points that are inside a tube

Procedure implemented in the ACM code to locate gauss points

The segment A-B represents the excavation length and forms a vector $\vec{a}$.

Another vector $\vec{b}$ is made between point B and a regarded gauss point C.

$$\vec{a} = [B_x - A_x \quad B_y - A_y \quad B_z - A_z]$$

$$\vec{b} = [C_x - B_x \quad C_y - B_y \quad C_z - B_z]$$

$$|\vec{a}| = \sqrt{(B_x - A_x)^2 + (B_y - A_y)^2 + (B_y - A_y)^2}$$

$$|\vec{b}| = \sqrt{(C_x - B_x)^2 + (C_y - B_y)^2 + (C_y - B_y)^2}$$

$$\cos\theta = \frac{\vec{a} \cdot \vec{b}}{|\vec{b}| * |\vec{a}|}$$

$$\vec{a} \bullet \vec{b} = (B_x - A_x * C_x - B_x) + (B_y - A_y * C_y - B_y) + (B_z - A_z * C_z - B_z)$$

A. If $\vec{a} \bullet \vec{b} = 0$, then $\vec{a}$ and $\vec{b}$ are orthogonal and Θ = 90°
B. Then the distance from $\vec{a}$ (the centerline of the tube) to point C, l = $|\vec{b}|$ and point C is inside the area for soil extraction if l is less than the radius of the excavation tube.
C. If $\vec{a} \bullet \vec{b} > 0$, then the angle, θ between the two vectors is < 90 deg.
D. Then l = $|\vec{b}|$*sin θ, and point C is inside the area of soil extraction if l is less than the radius of the excavation tube and if $|\vec{b}|*\cos\theta \leq |\vec{a}|$.
E. If θ = 0 meaning $\vec{a} \| \vec{b}$ then check if $|\vec{b}| \leq |\vec{a}|$. If it is longer it is out of the area of soil extraction.
F. If $\vec{a} \bullet \vec{b} < 0$, then the angle, θ between the two vectors is > 90 deg. Then the node is outside the area of soil extraction.

Summarized the routine does the following:

it checks

IF $\vec{a} \bullet \vec{b} \geq 0$

Procedure implemented in the ACM code to locate gauss points

AND $|\vec{b}|*\sin\theta \leq r_{tube}$

AND $|\vec{b}|*\cos\theta \leq |\vec{a}|$.

THEN the gauss point is inside the area for soil extraction, it is made elastic and volume strain is assigned. If the point is not found to be inside the area for soil extraction the ACM model is applied the stress point.

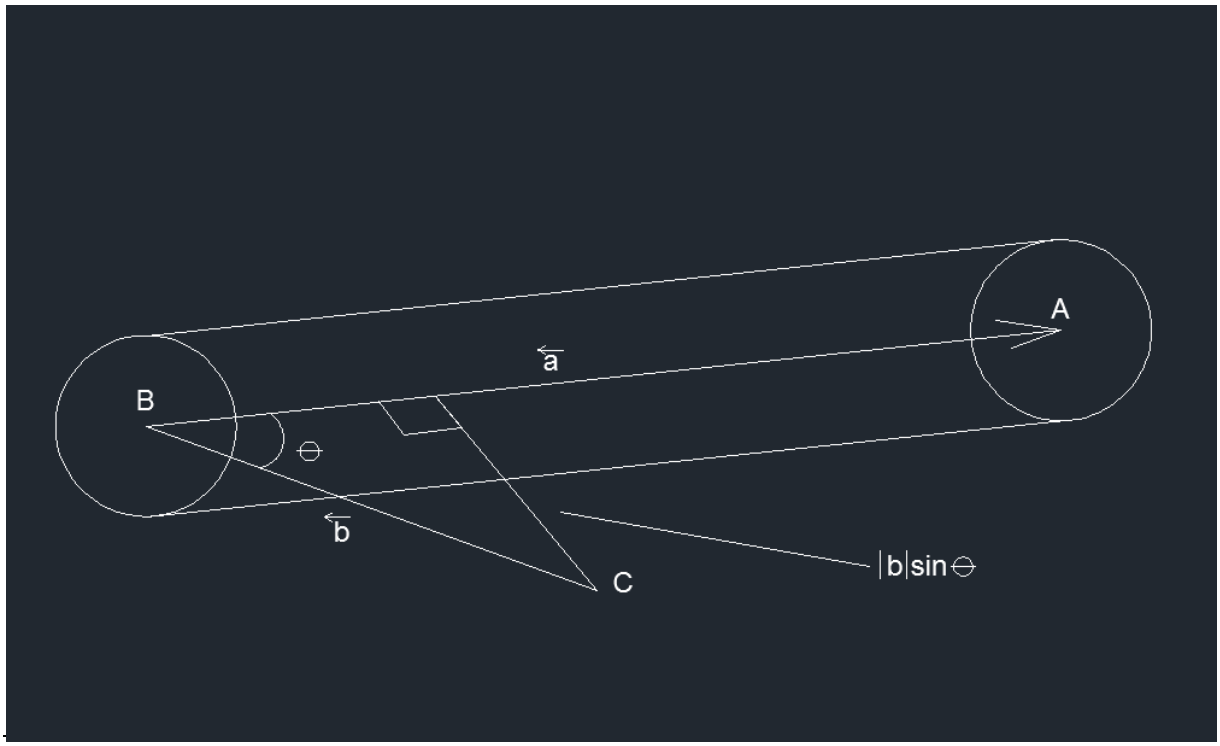

Appendix E

1. Elements applied volume strain displayed with different mesh refinements – 41 intersecting tubes
2. Elements applied volume strain displayed with different mesh refinements – 41 tubes with original tube size
3. Elements applied volume strain displayed with different mesh refinements – 1 tube

Elements applied volume strain displayed with different mesh refinements - 41 intersecting tubes

Number of soil elements:
109694
Number of nodes:
157128
Average element size:
0,2188 m

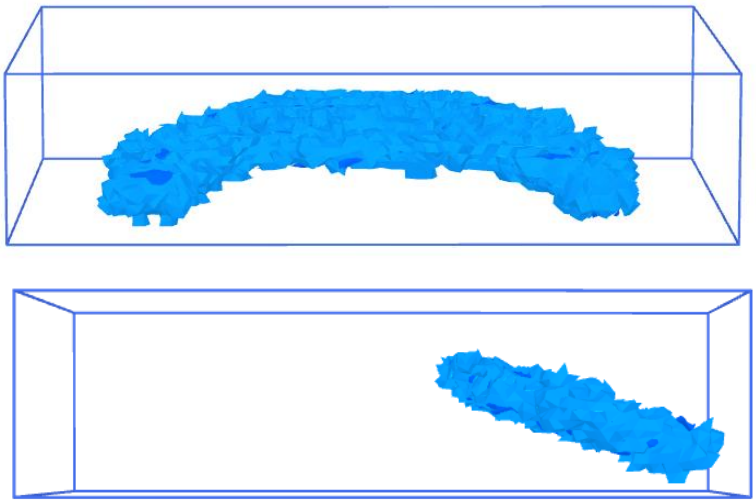

Number of soil elements:
44246
Number of nodes:
64812
Average element size:
0.3445 m

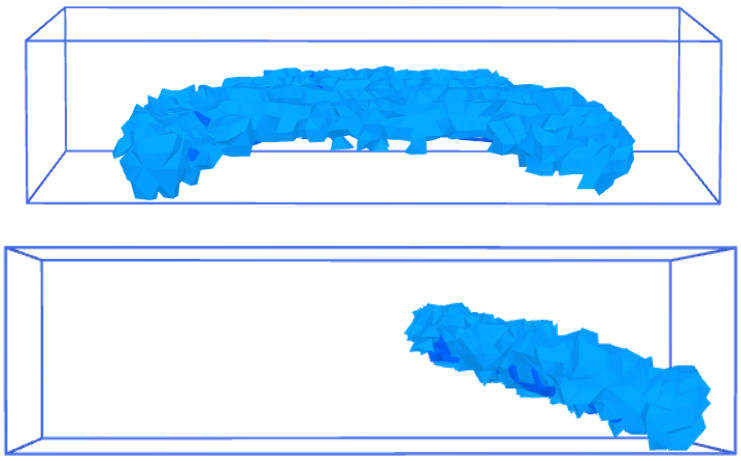

Number of soil elements:
16493
Number of nodes:
24989
Average element size:
0,5642 m

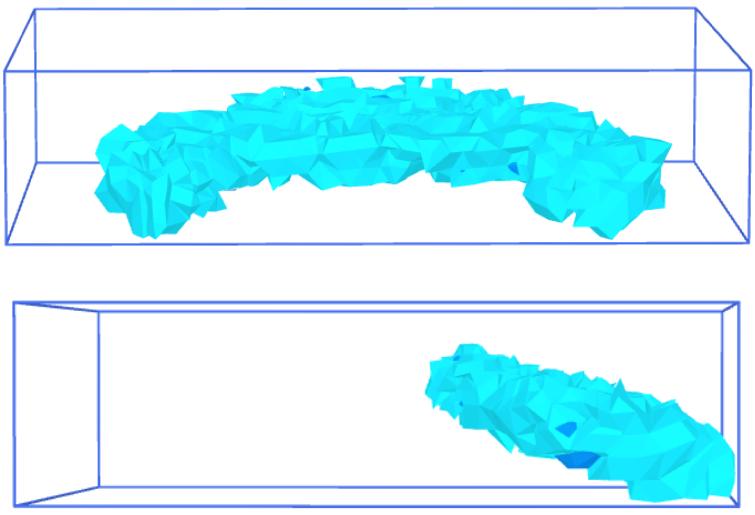

Elements applied volume strain displayed with different mesh refinements - 41 intersecting tubes

---

Number of soil elements:

5035

Number of nodes:

8030

Average element size:

1,021 m

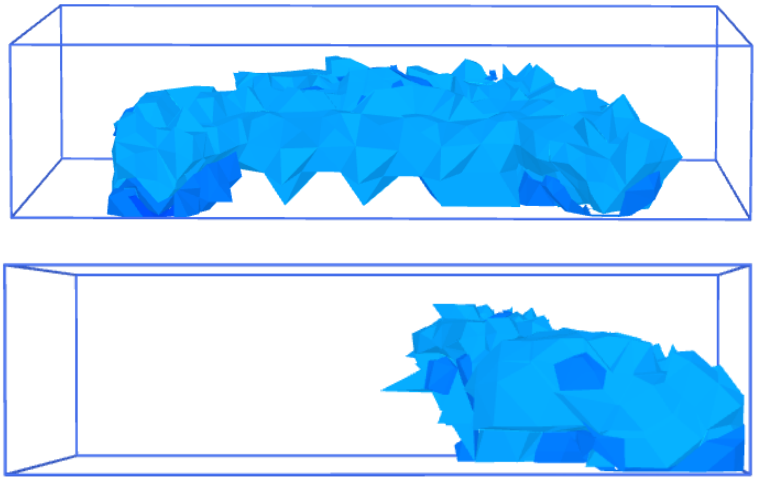

Number of soil elements:

2317

Number of nodes:

3877

Average element size:

1,51 m

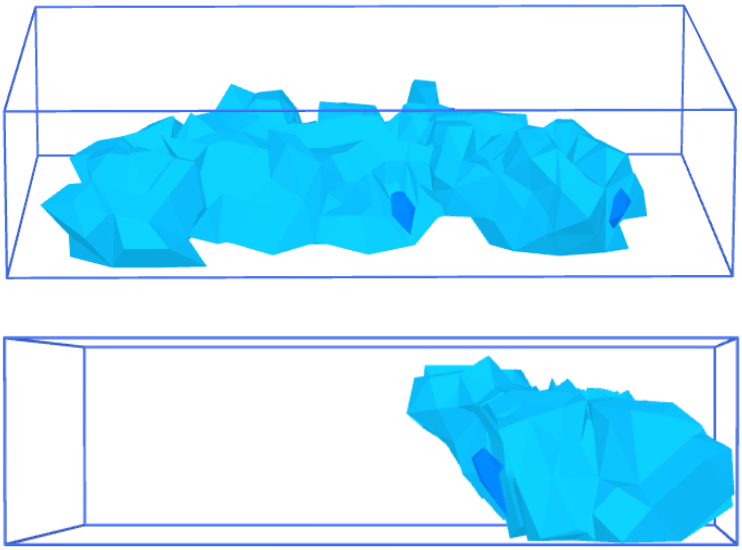

Elements applied volume strain displayed with different mesh refinements - 41 tubes with original tube size

---

Number of soil elements:
109694
Number of nodes:
157128
Average element size:
0,2188 m

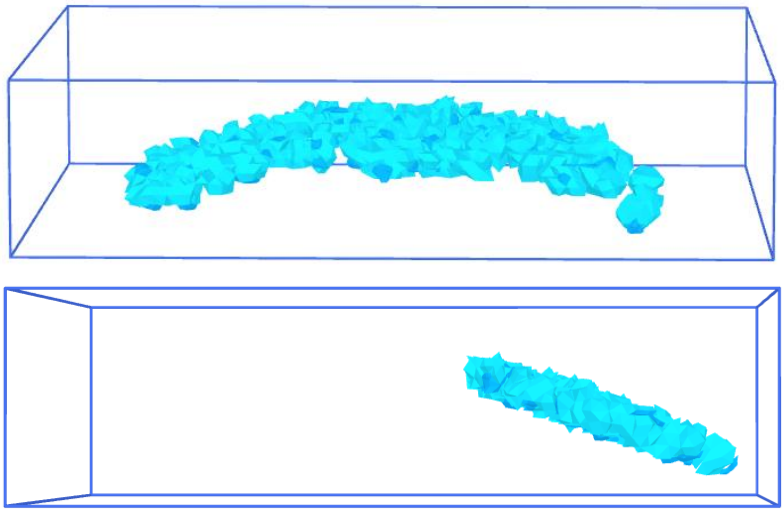

Number of soil elements:
44246
Number of nodes:
64812
Average element size:
0.3445

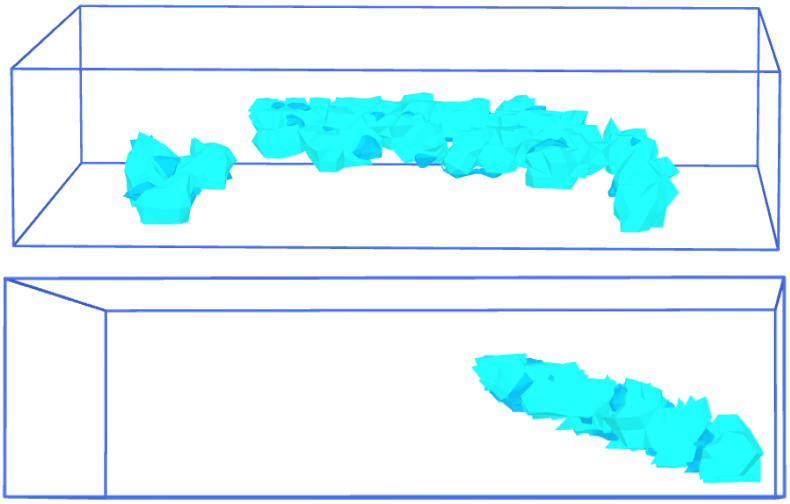

Elements applied volume strain displayed with different mesh refinements - 41 tubes with original tube size

---

Number of soil elements:
16493
Number of nodes:
24989

Average element size:
0,5642 **m**

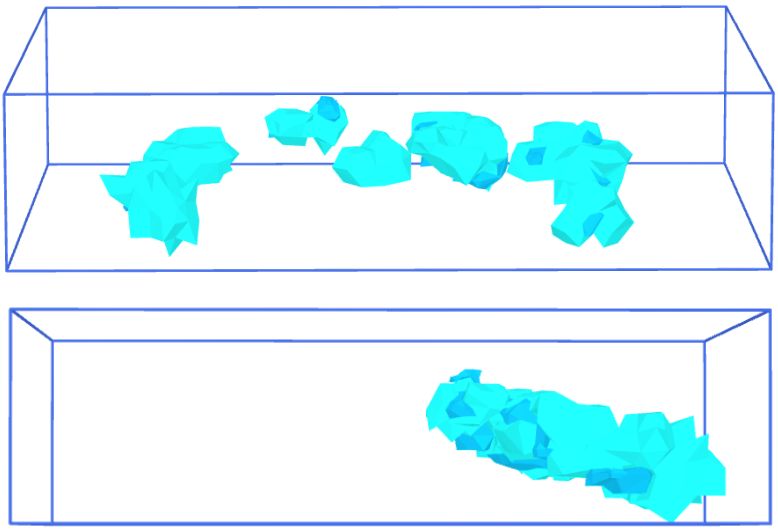

Number of soil elements:
5035
Number of nodes:
8030
Average element size:
1.021 m

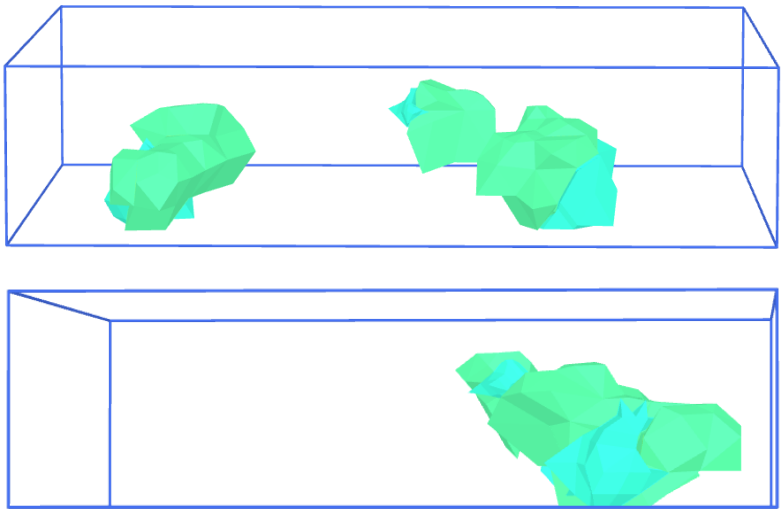

Elements applied volume strain displayed with different mesh refinements - 41 tubes with original tube size

---

Number of soil elements:

2317

Number of nodes:

3877

Average element size:

1,51 m

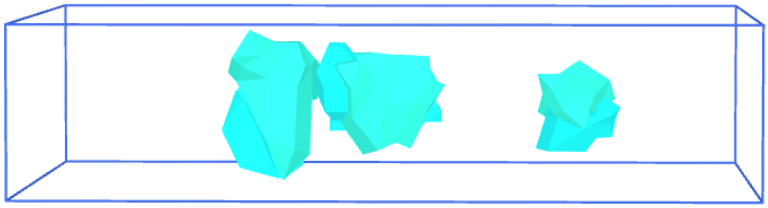

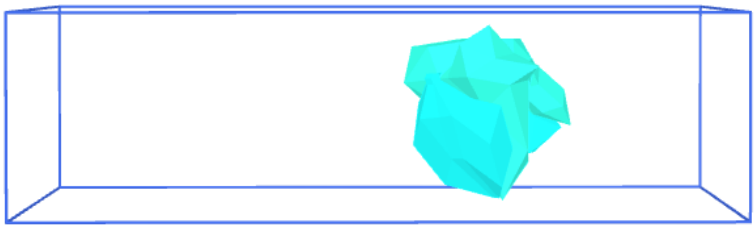

Elements applied volume strain displayed with different mesh refinements - 1 tube

Number of soil elements:
109694
Number of nodes:
157128
Average element size:
0,2188 m

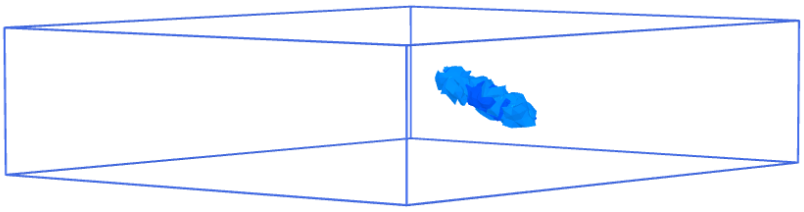

Number of soil elements:
44246
Number of nodes:
64812
Average element size:
0.3445 m

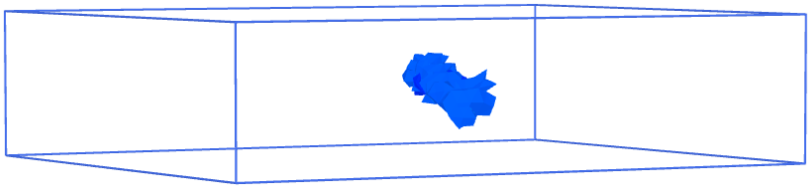

Number of soil elements:
16493
Number of nodes:
24989
Average element size:
0,5642 m

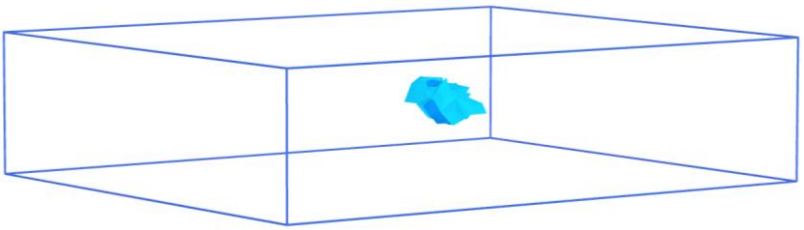

Number of soil elements:
5035
Number of nodes:
8030
Average element size:
1.021 m

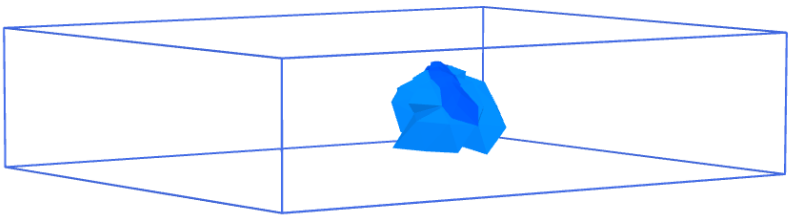

Number of soil elements:
2317
Number of nodes:
3877
Average element size:
1,51 m

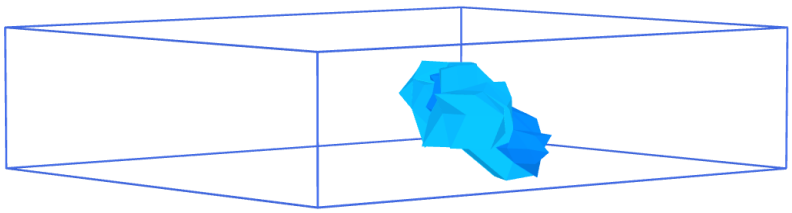

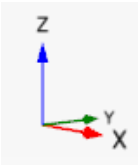

Appendix F

1. Soil layering and the location of boreholes for the final tower model

2. Phases

Soil layering and the location of boreholes for the final tower model

Layers		Borehole 1		Borehole 2		Borehole 3		Borehole 4	
Nr.	*Material*	*Top*	*Bottom*	*Top*	*Bottom*	*Top*	*Bottom*	*Top*	*Bottom*
1	MG	3,0	0,0	3,0	0,0	3,0	0,0	3,0	0,0
2	A1S	0,0	0,0	0,0	-3,0	0,0	-5,2	0,0	-5,2
3	A1N	0,0	-5,2	-3,0	-5,2	-5,2	-5,2	-5,2	-5,2
4	A2	-5,2	-7,4	-5,2	-7,4	-5,2	-7,4	-5,2	-7,4
5	B1	-7,4	-10,9	-7,4	-10,9	-7,4	-10,9	-7,4	-10,9
6	B2	-10,9	-12,9	-10,9	-12,9	-10,9	-12,9	-10,9	-12,9
7	B3	-12,9	-17,8	-12,9	-17,8	-12,9	-17,8	-12,9	-17,8
8	B4	-17,8	-19,0	-17,8	-19,0	-17,8	-19,0	-17,8	-19,0
9	B5	-19,0	-22,0	-19,0	-22,0	-19,0	-22,0	-19,0	-22,0
10	B6	-22,0	-24,4	-22,0	-24,4	-22,0	-24,4	-22,0	-24,4
11	B7a	-24,4	-25,0	-24,4	-25,0	-24,4	-25,0	-24,4	-25,0
12	B7b	-25,0	-29,0	-25,0	-29,0	-25,0	-29,0	-25,0	-29,0
13	B8/B9/ B10	-29,0	-37,0	-29,0	-37,0	-29,0	-37,0	-29,0	-37,0

Boreholes	x-position	y-position
1	0	-25
2	0	15
3	25	0
4	-20	0

Phases

Name	Calculation type	Loading input	Time interval	Control parameters
[InitialPhase]:Initial phase	K0-procedure	Ultimate time	0,00 days	Updated mesh
[Phase _1]:Nil	Drained	Ultimate time	0,00 days	Updated mesh Reset displ.
[Phase_2]:Foundation	Consolidation	Ultimate time	365 days	Updated mesh Reset displ.
[Phase _3]:Ord1	Consolidation	Ultimate time	31,76 days	Updated mesh
[Phase _4]Ord2	Consolidation	Ultimate time	365 days	Updated mesh
[Phase _5]: Ord3	Consolidation	Ultimate time	365 days	Updated mesh
[Phase _6]: Pause1	Consolidation	Ultimate time	34335 days	Updated mesh
[Phase _7]:Ord4	Consolidation	Ultimate time	548 days	Updated mesh
[Phase _8]:Ord5	Consolidation	Ultimate time	548 days	Updated mesh
[Phase _9]:Ord6	Consolidation	Ultimate time	548 days	Updated mesh
[Phase_10]:Ord7	Consolidation	Ultimate time	548 days	Updated mesh
[Phase_11]:Pause2	Consolidation	Ultimate time	29956 days	Updated mesh
[Phase_12]:BellChamber	Consolidation	Ultimate time	52 days	Updated mesh

Phases

[Phase_13]:Cons_BellChamber	Consolidation	Ultimate time	3600 days	Updated mesh
[Phase _14]:Pause3	Consolidation	Ultimate time	170940 days	Updated mesh
[Phase _15]:Catino excavation	Consolidation	Ultimate time	608 days	Updated mesh
[Phase _16]:2nd Catino excavation and Conglomerate	Consolidation	Ultimate time	34440 days	Updated mesh
[Phase _17]:Water table change and foundation grouting	Consolidation	Ultimate time	21635 days	Updated mesh
[Phase _18]:Counterweights 1st part	Consolidation	Ultimate time	905 days	Updated mesh
[Phase _19]:Micro piles	Plastic	Ultimate time	34 days	Updated mesh
[Phase _20]:Counterweights 2nd part	Plastic	Ultimate time	15 days	Updated mesh
[Phase _21]:Micro piles	Consolidation	Ultimate time	1350 days	Updated mesh
[Phase _22]:Soil extraction – preliminary and final	Consolidation	Ultimate time	627 days	Updated mesh
[Phase _23]:Future creep	Consolidation	Ultimate time	36500 days	Updated mesh

Appendix G

1. Excess pore pressure and vertical effective stresses – phase 12
2. Horizontal effective stresses, σ'_{yy} and σ'_{xx} – phase 12
3. Total vertical displacements and incremental displacements for phase 12
4. Total volumetric strain and incremental volumetric strain for phase 12
5. Total displacement considering each analyzed phase, color scale and arrows

Excess pore pressure and vertical effective stresses – phase 12

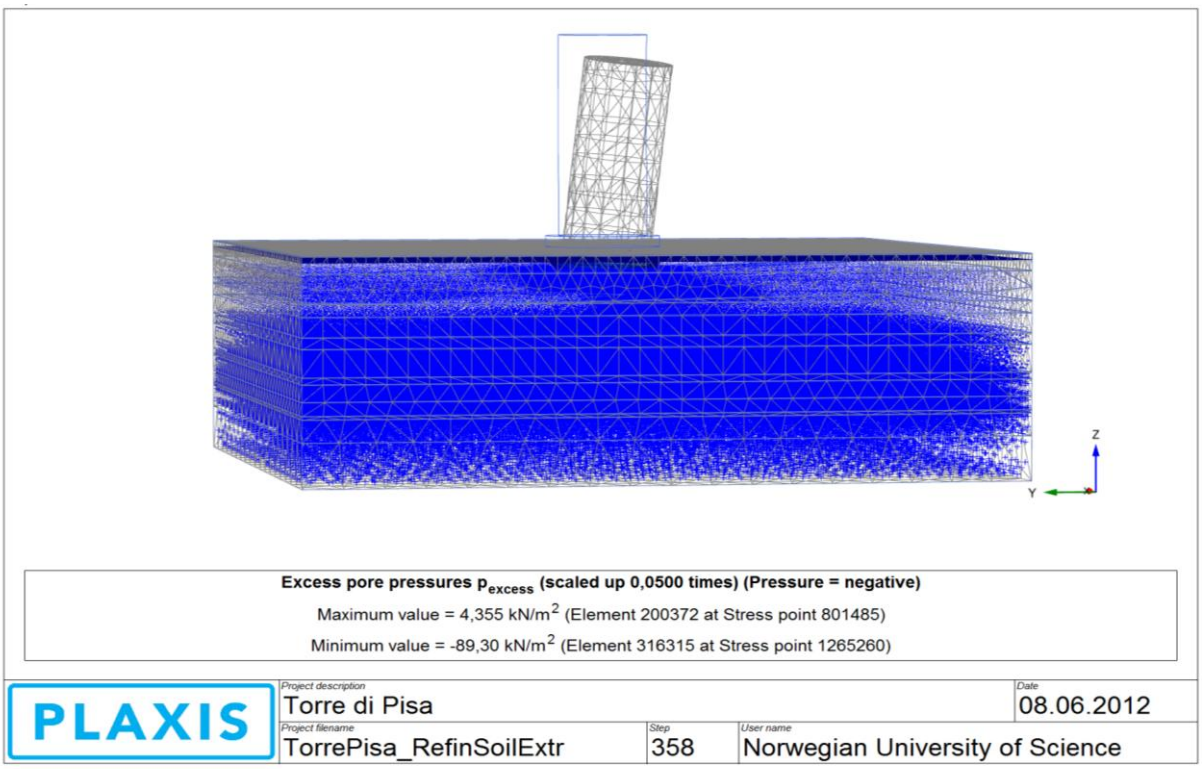

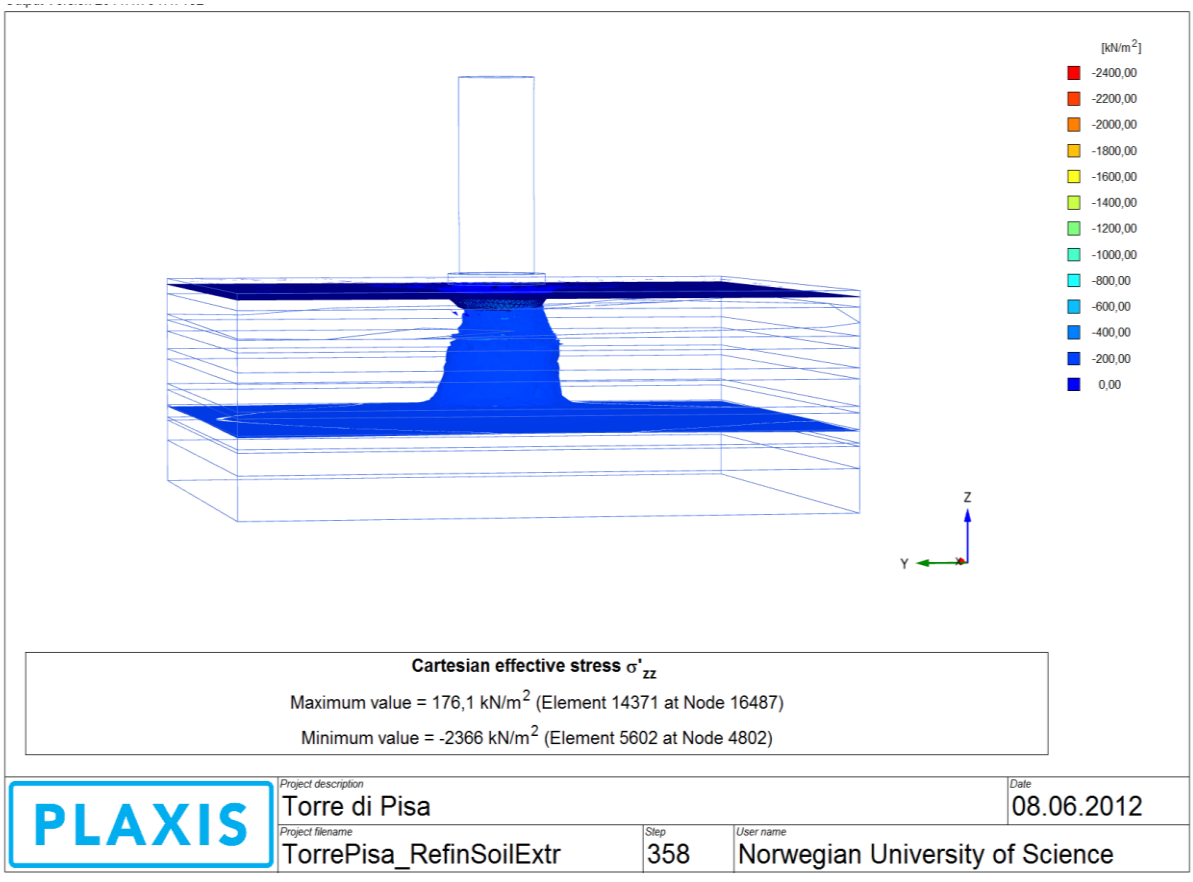

Horizontal effective stresses, σ'_{yy} and σ'_{xx} – phase 12

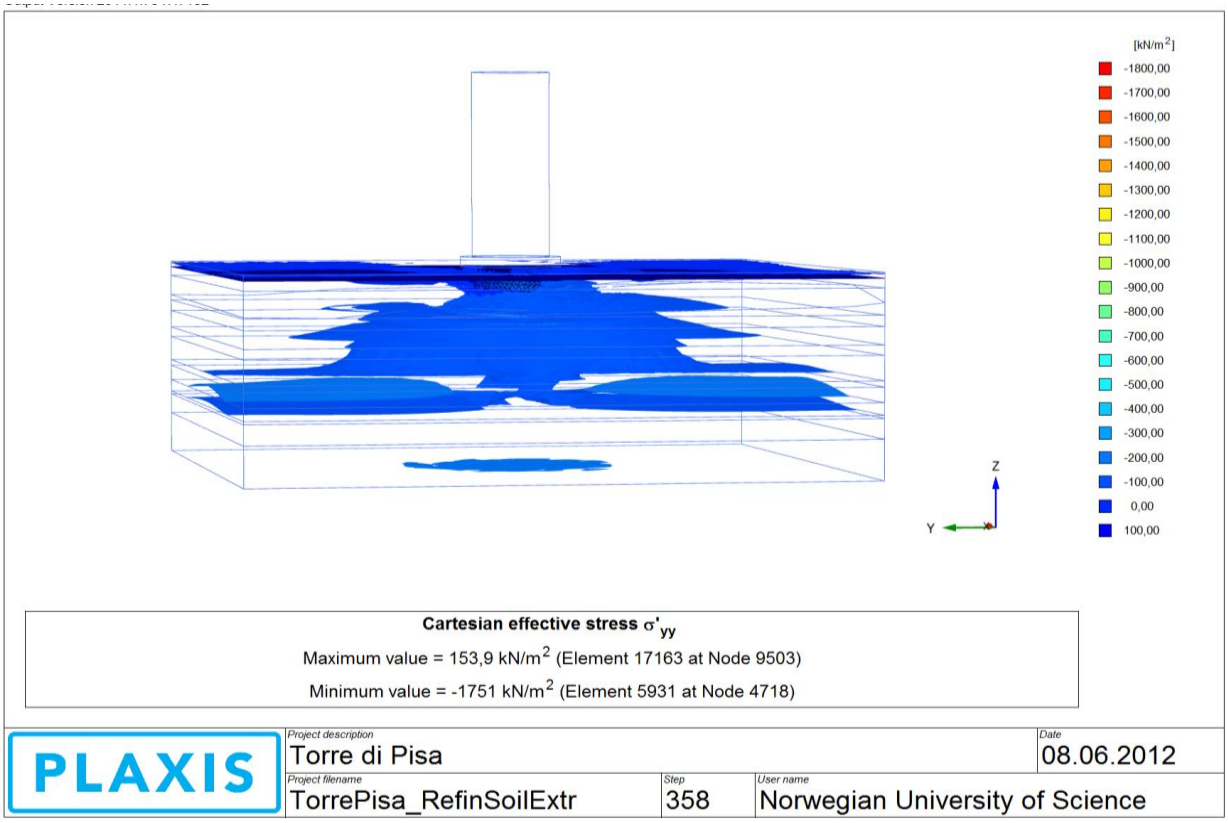

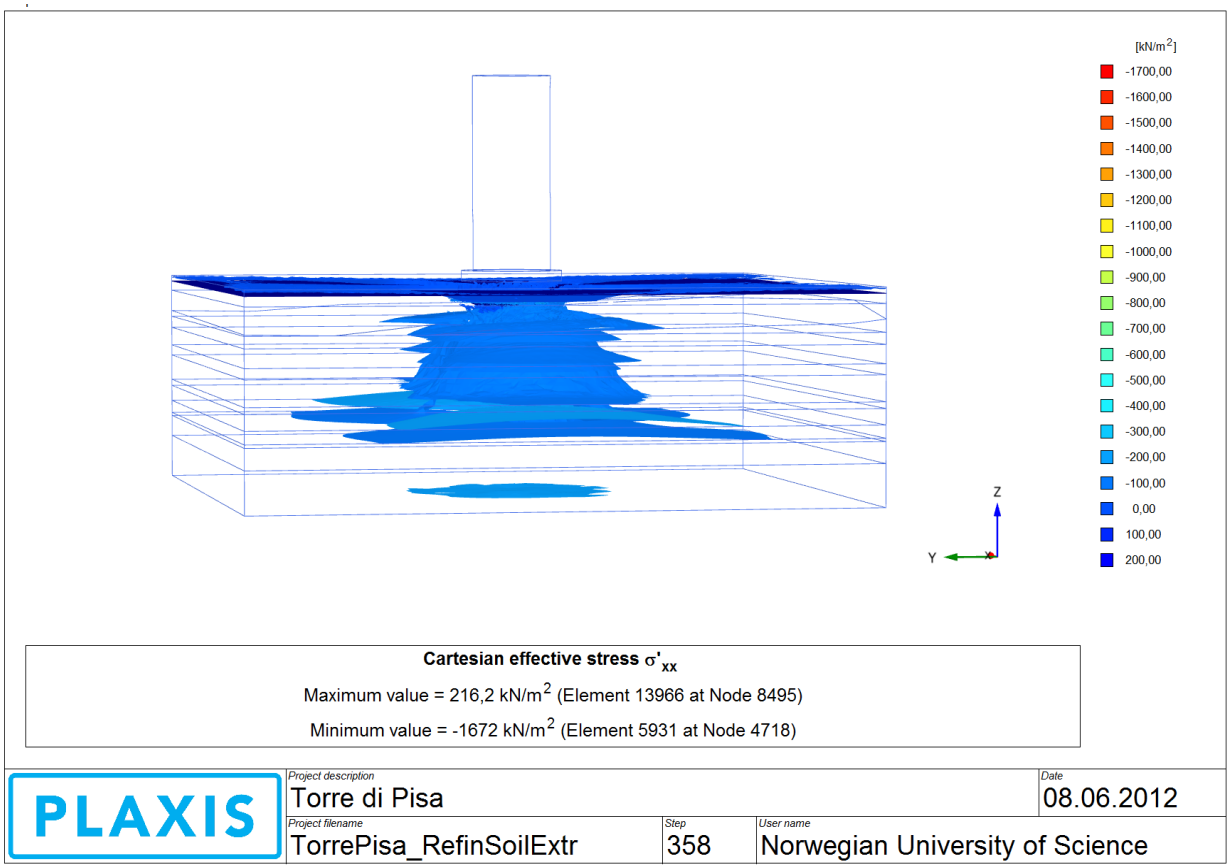

1. *Total volumetric strain and incremental volumetric strain for phase 12*

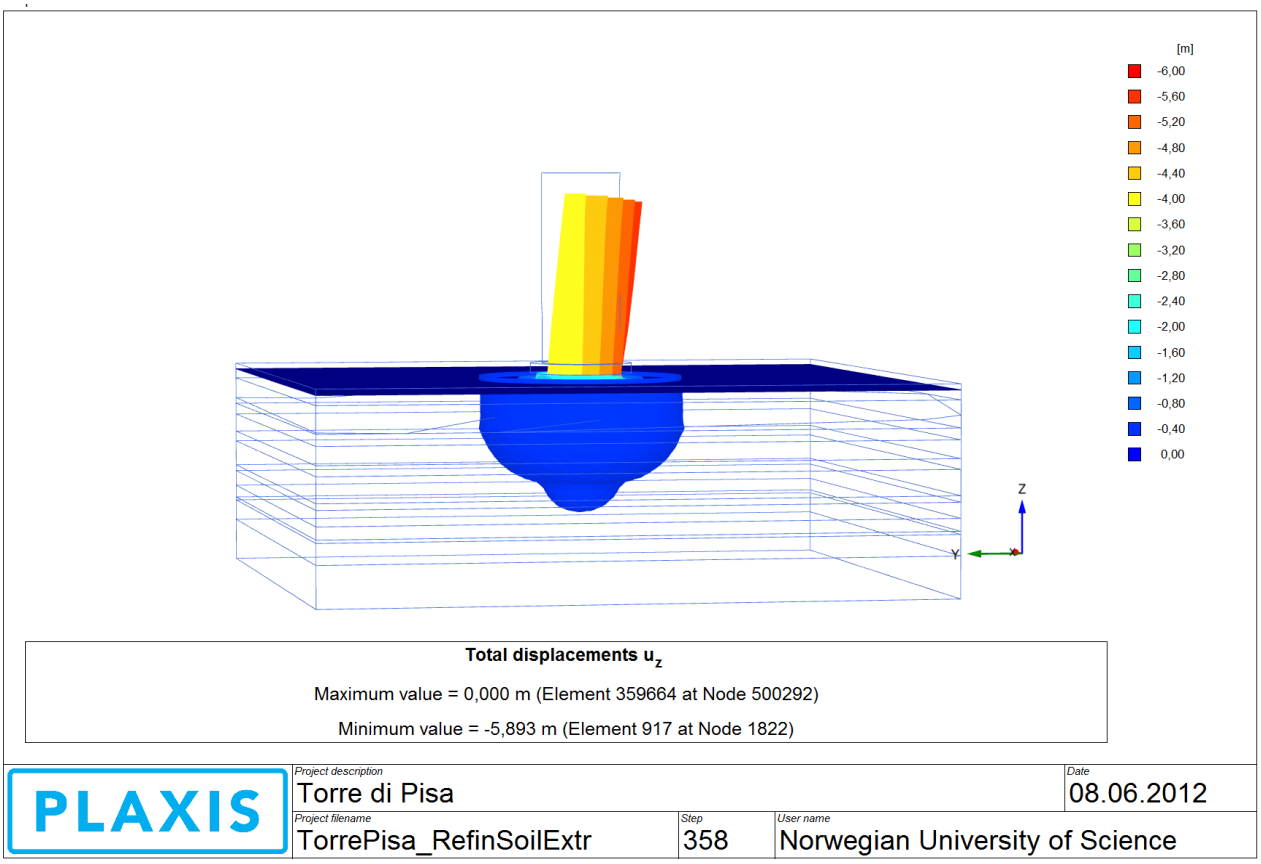

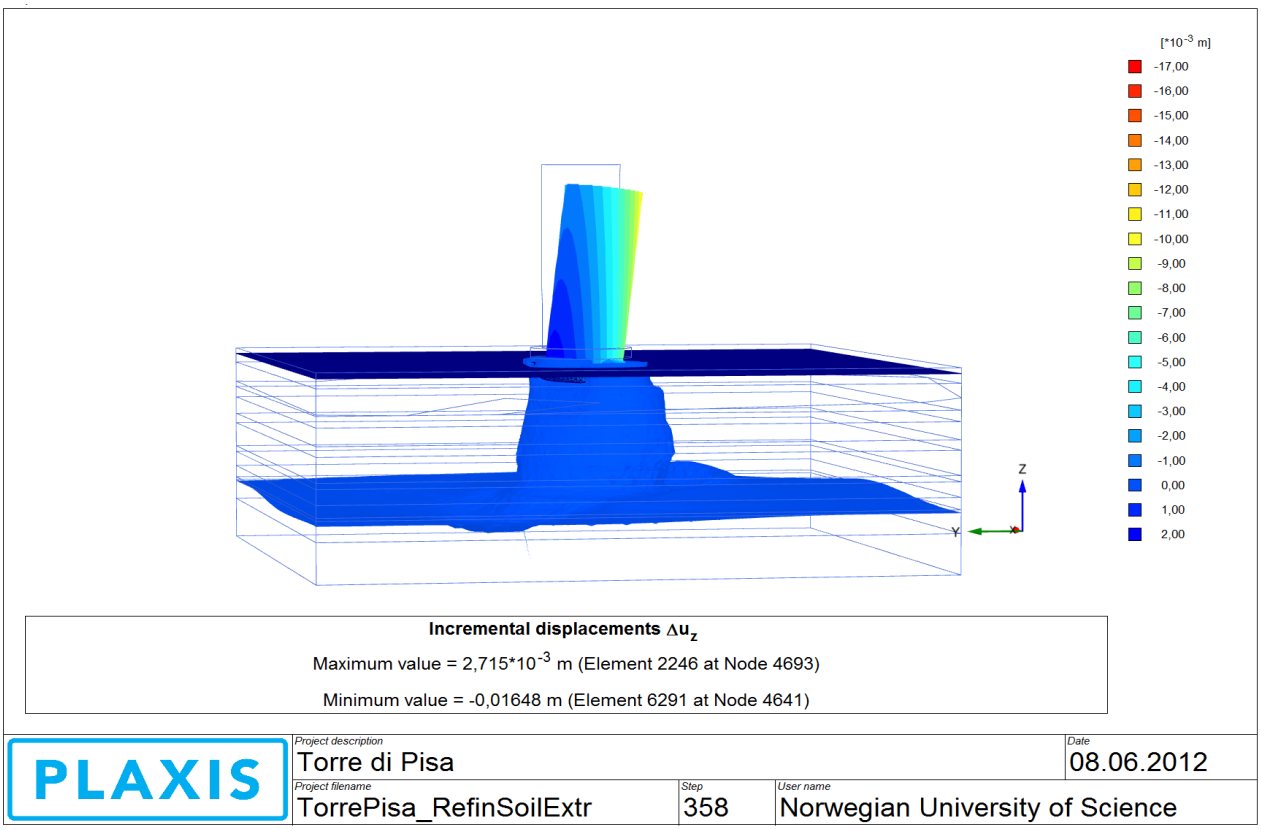

Total displacement considering each analyzed phase, color scale and arrows

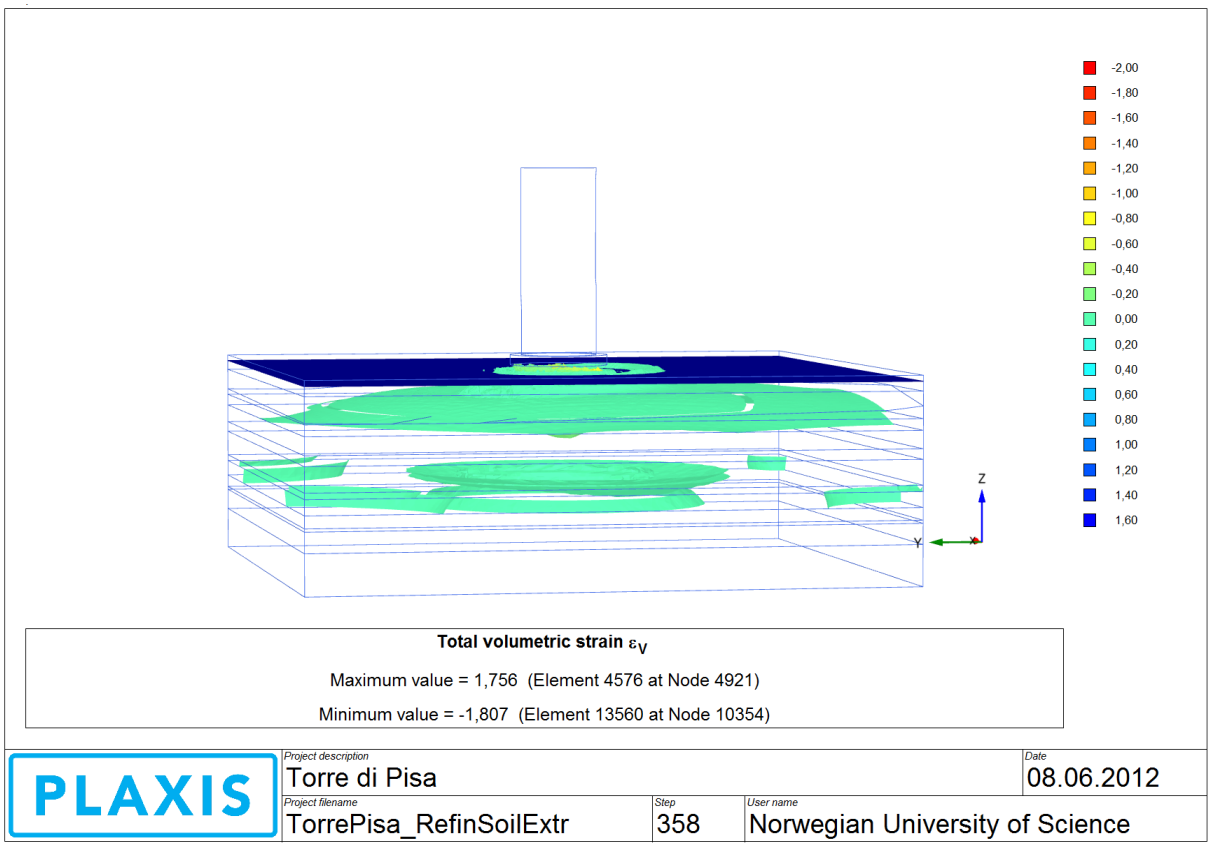

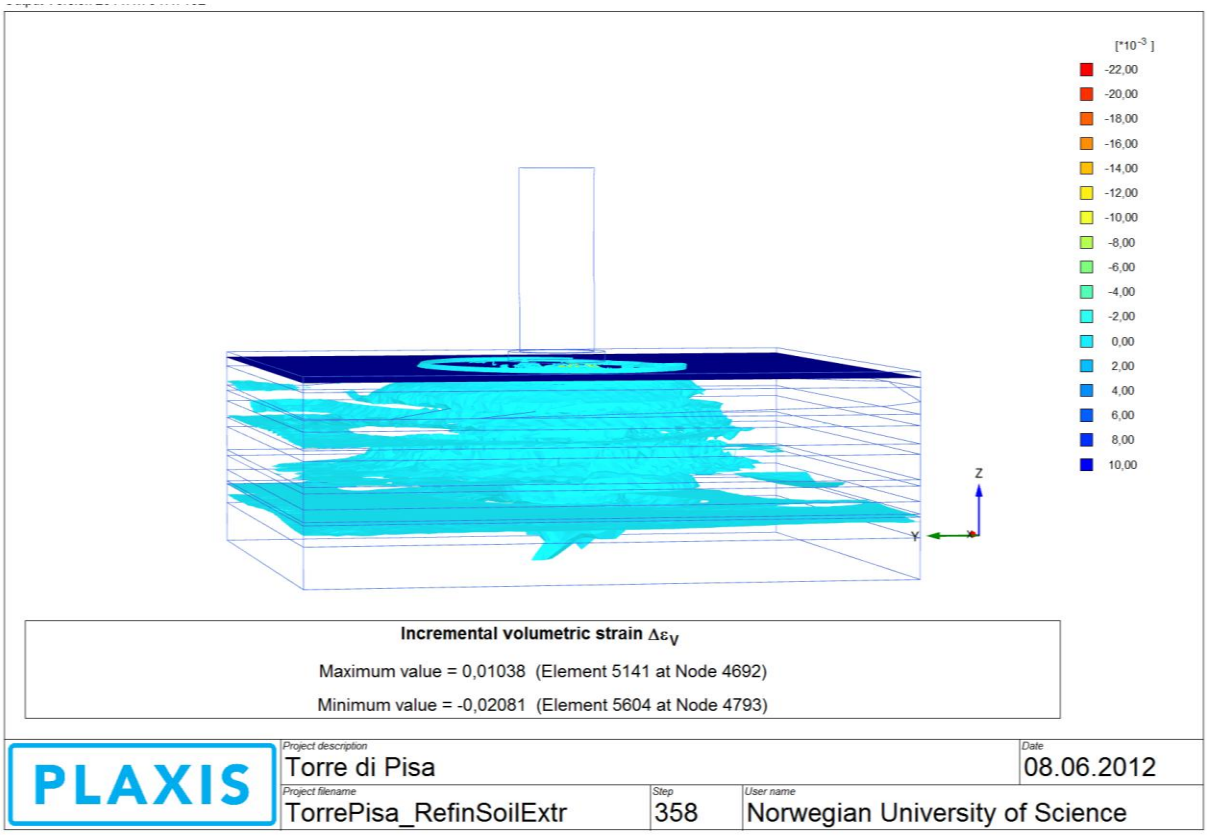

Total displacement considering each analyzed phase, color scale and arrows

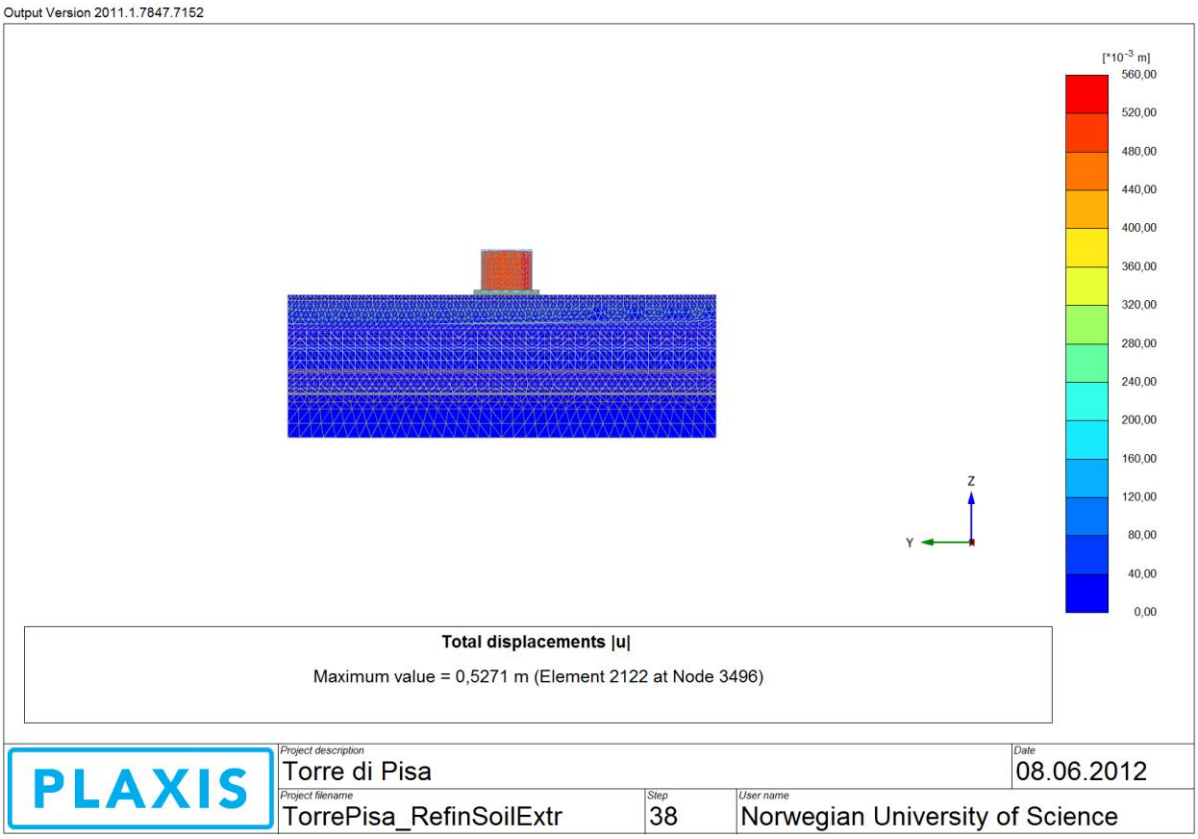

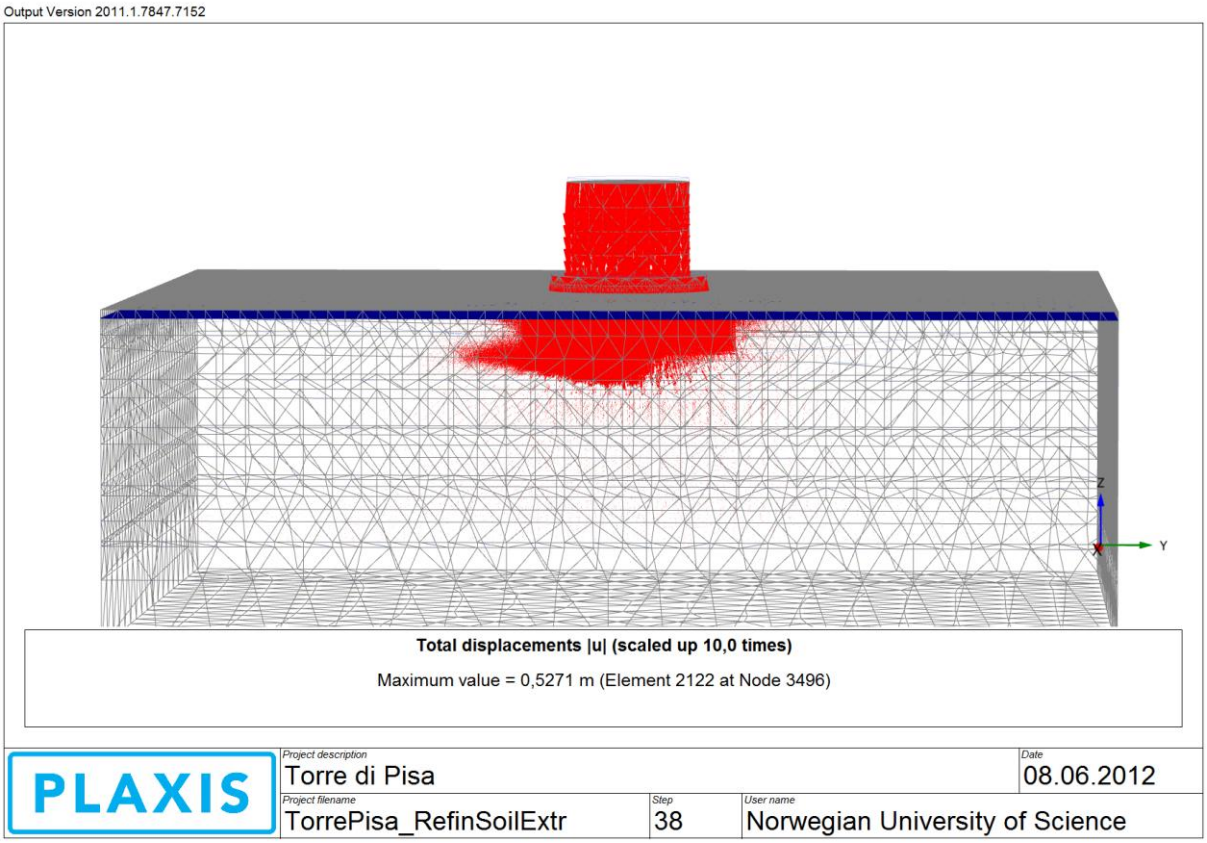

Total displacement considering each analyzed phase, color scale and arrows

Output Version 2011.1.7847.7152

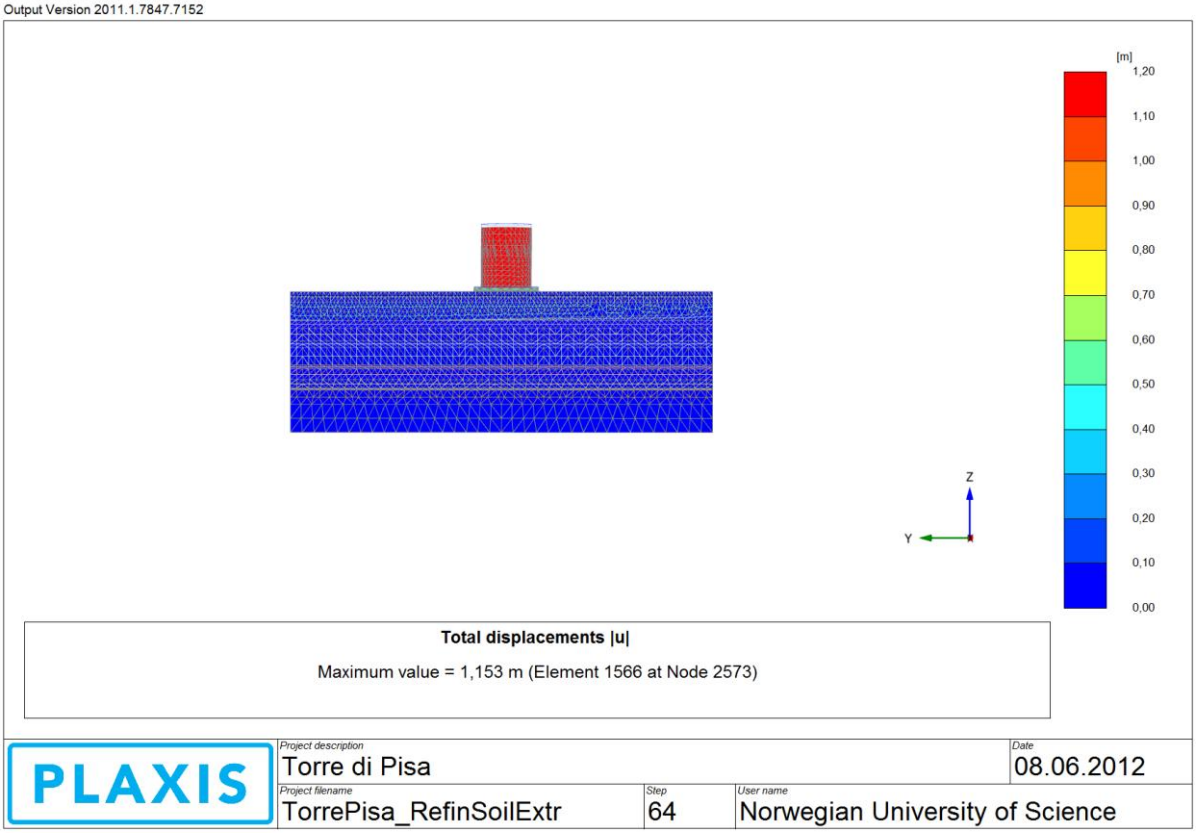

Output Version 2011.1.7847.7152

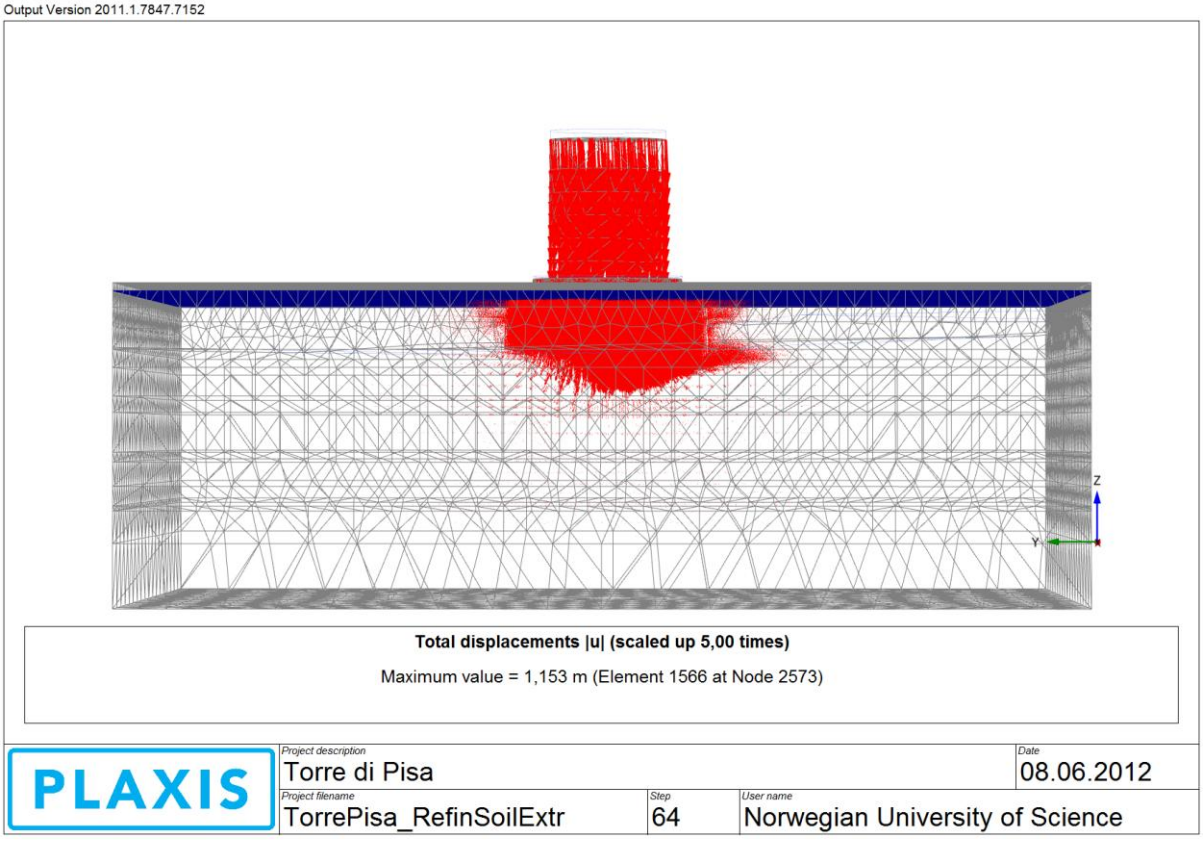

Total displacement considering each analyzed phase, color scale and arrows

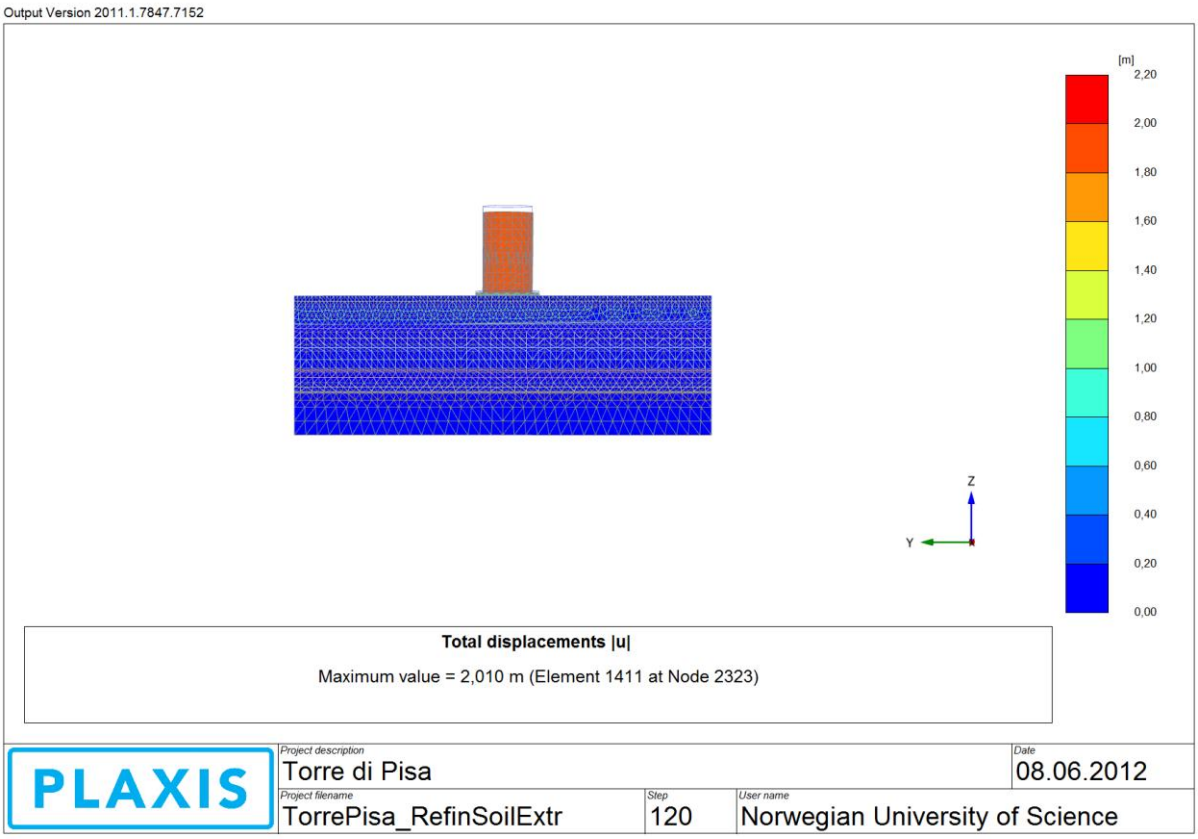

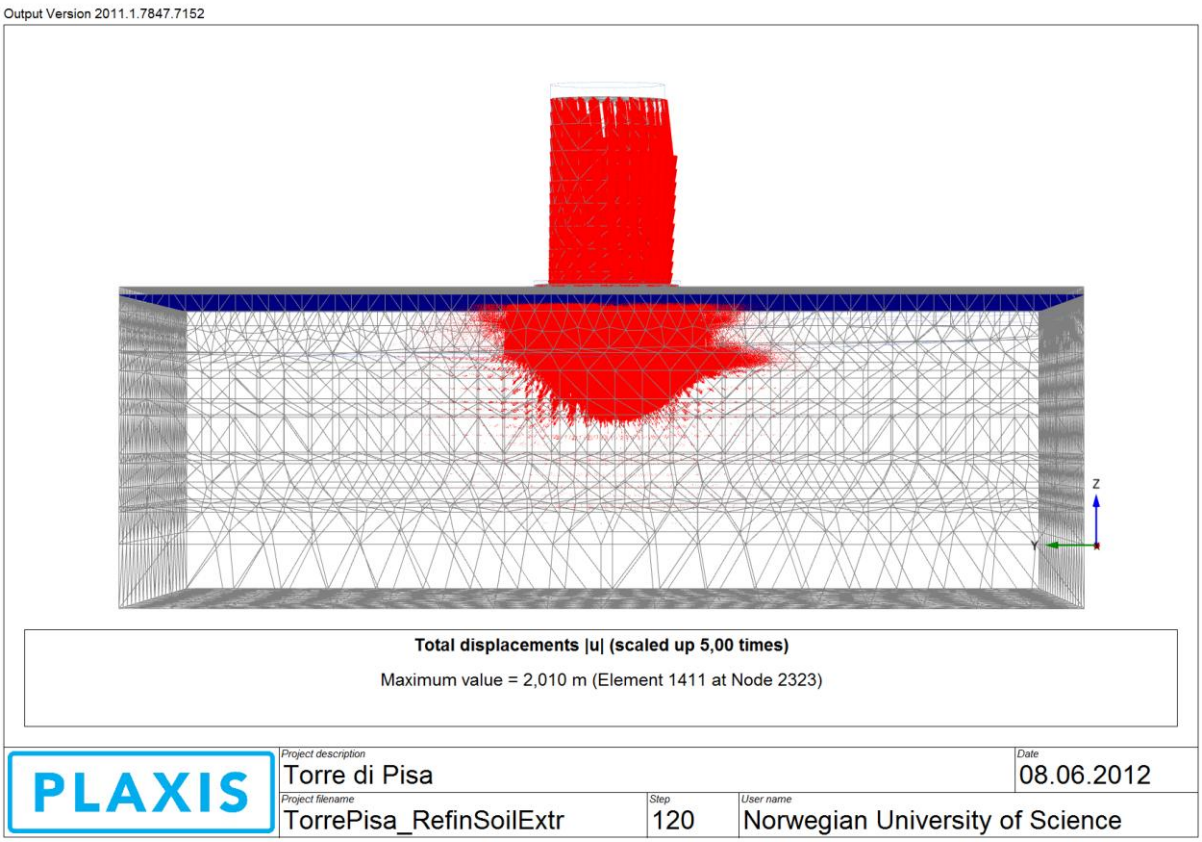

Total displacement considering each analyzed phase, color scale and arrows

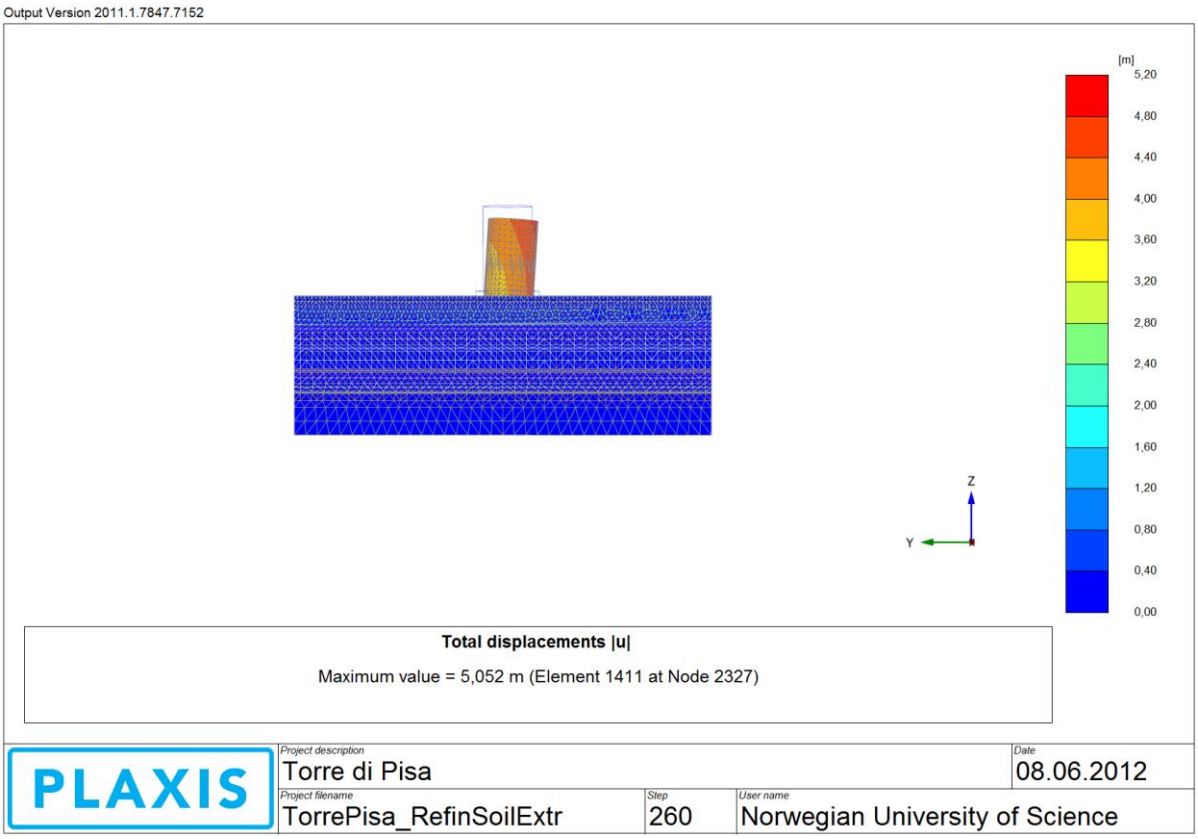

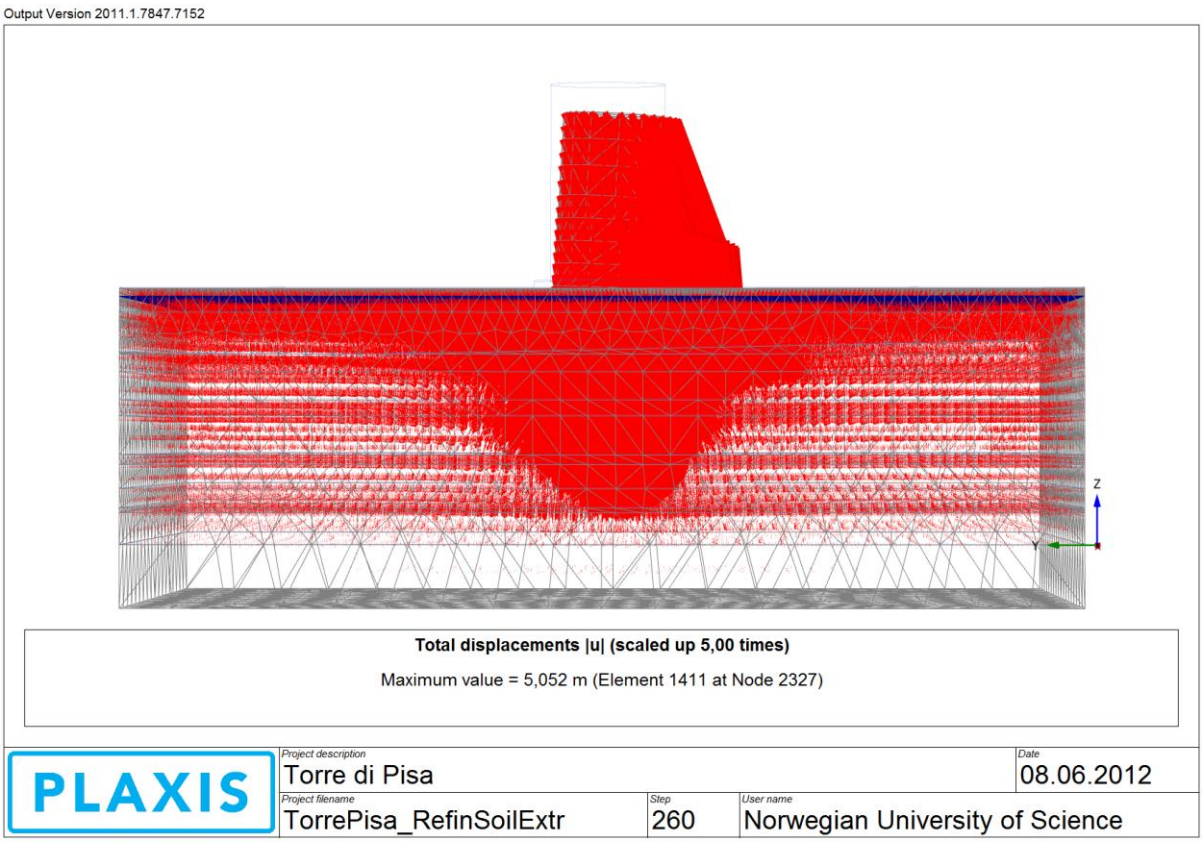

Total displacement considering each analyzed phase, color scale and arrows

Output Version 2011.1.7847.7152

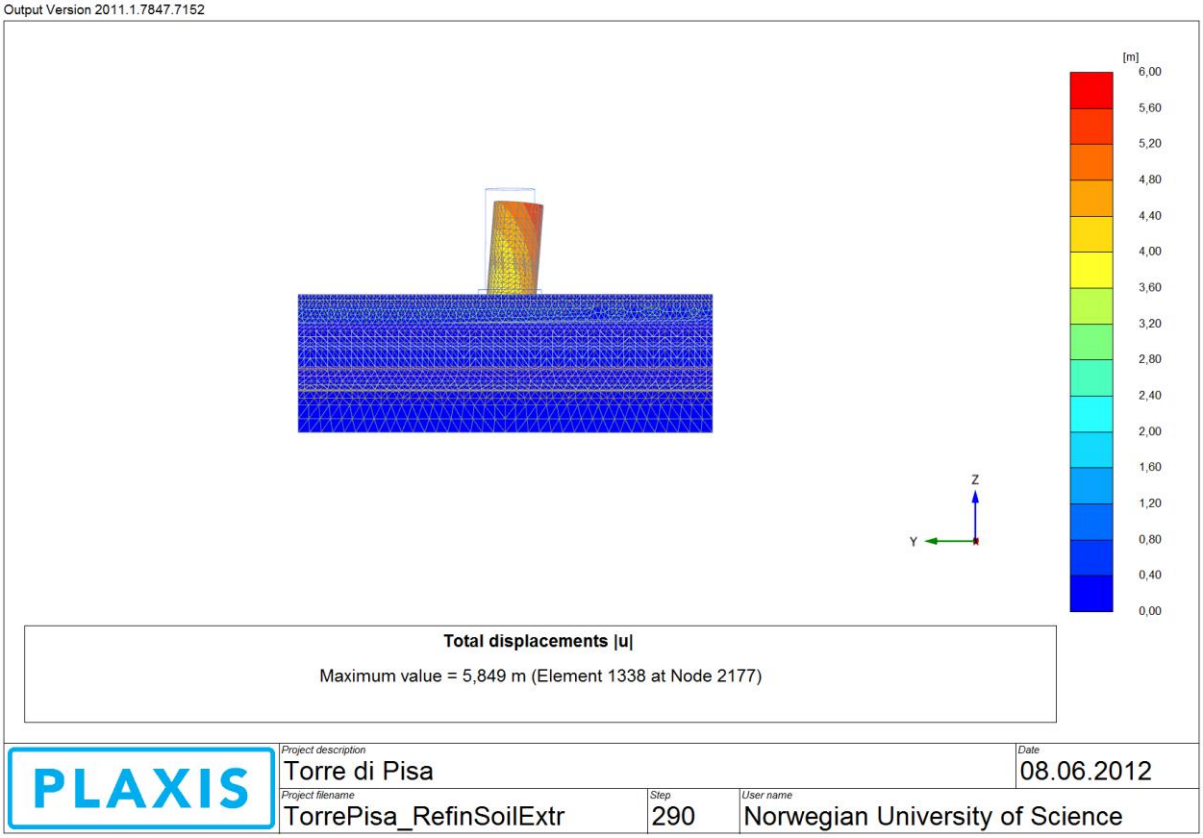

Output Version 2011.1.7847.7152

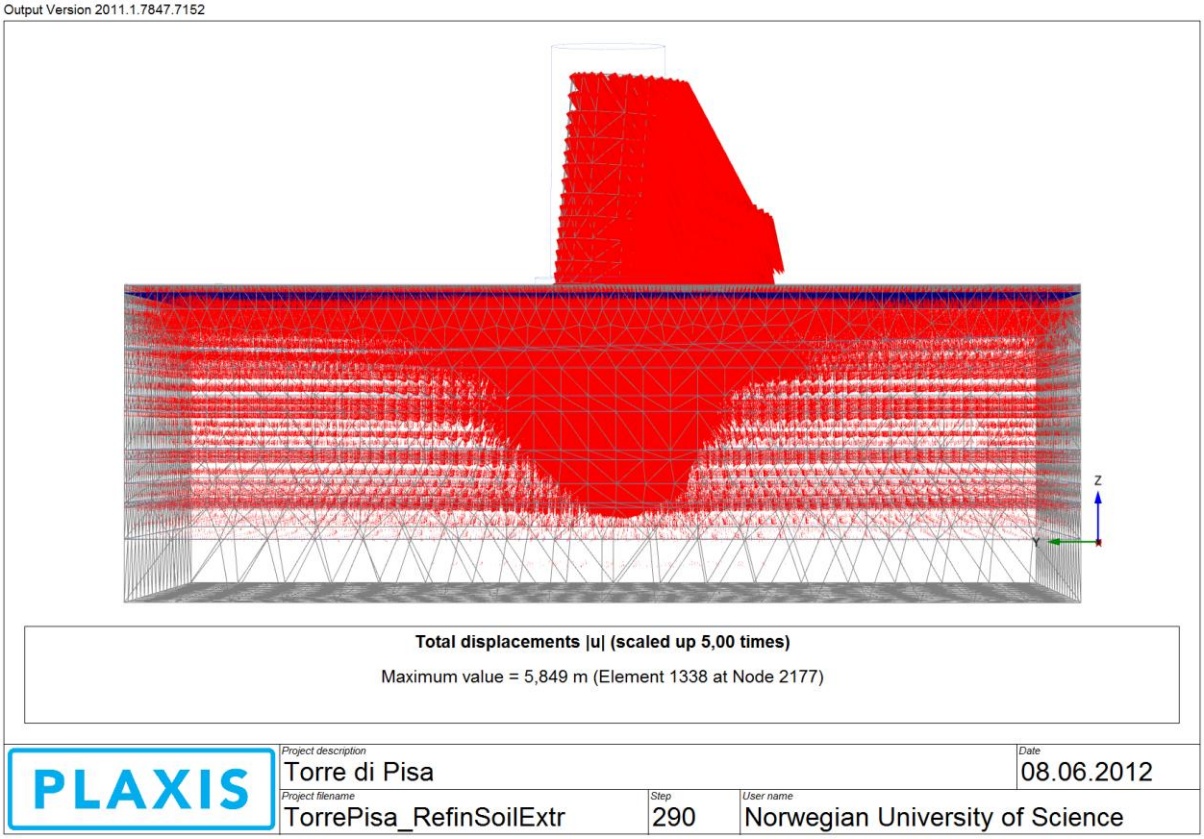

Total displacement considering each analyzed phase, color scale and arrows

Output Version 2011.1.7847.7152

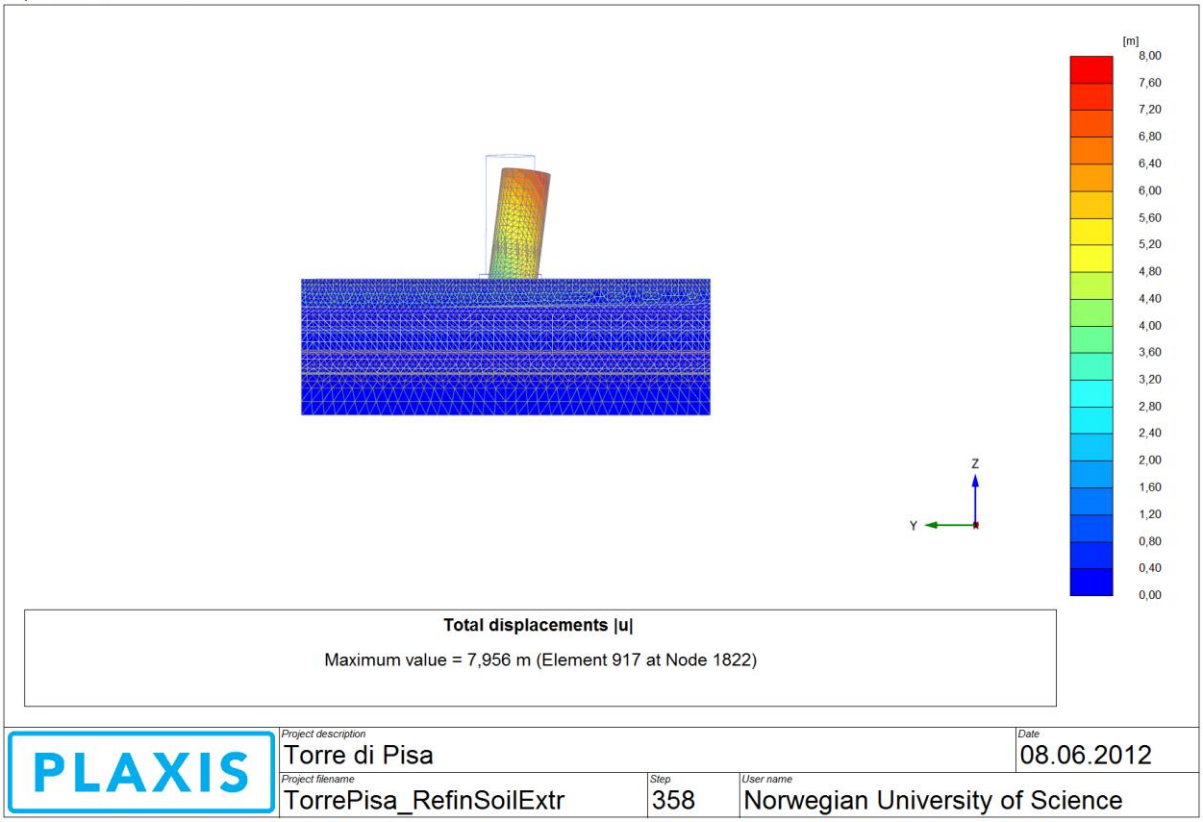

Output Version 2011.1.7847.7152